Extending the Satellite PMC Data Record with OMPS

Matthew DeLand, Nick Gorkavyi

Science Systems and Applications, Inc. (SSAI)

STAR JPSS Science Team Meeting
College Park, MD 24-28 August 2015

Ozone Mapping and Profiler Suite (OMPS)

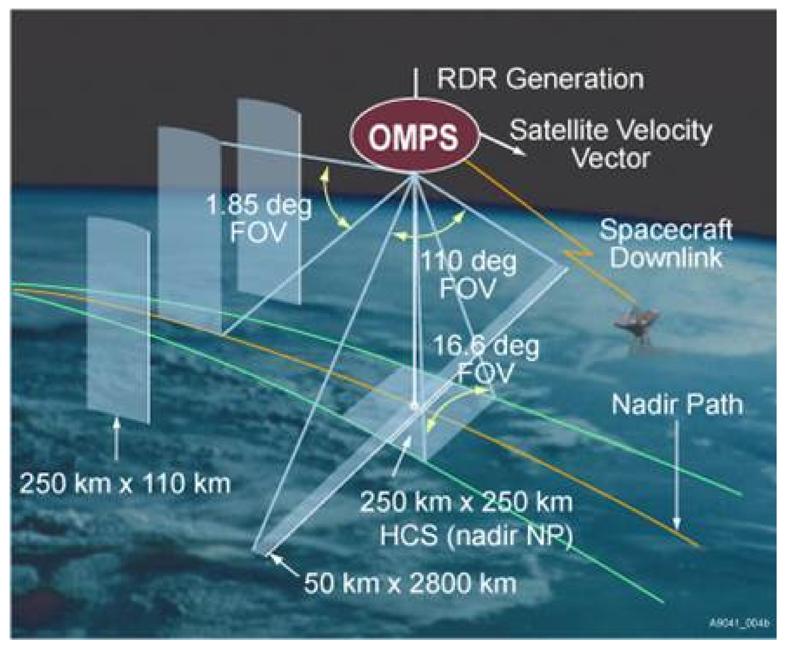

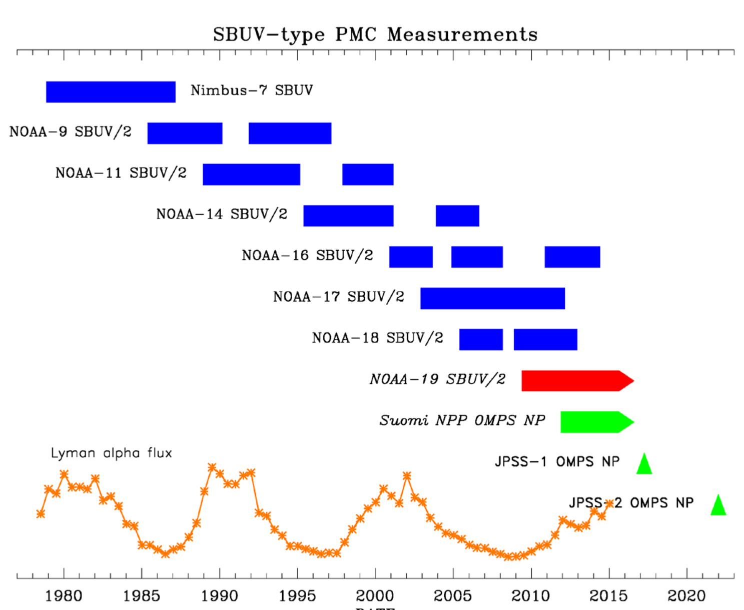

- OMPS instruments are designed to continue long-term monitoring of ozone. Launched on Suomi National Polar-orbiting Partnership (NPP) satellite on 28 October 2011. All sensors use hyperspectral CCDs.
- **Nadir Mapper (NM)** measures total ozone using backscattered UV. 2800 km swath, 50 km x 50 km pixels (adjustable), spectral range = 300-380 nm.
- **Nadir Profiler (NP)** measures stratospheric profile ozone using backscattered UV. 250 km x 250 km footprint, spectral range = 250-310 nm.
- **Limb Profiler (LP)** measures profile ozone and aerosols using limb scattering in UV/VIS/IR. Altitude coverage = 0-80 km, spectral range = 290-1000 nm.

Nadir Profiler (NP)

- Designed to replicate SBUV/2 functionality (similar viewing geometry and spectral range) for measuring stratospheric ozone profiles.
- Hyperspectral measurements maintain ability to use legacy SBUV PMC detection algorithm, but also allows for testing of other options (*e.g.* use more or different wavelengths).
- Current results are consistent with concurrent NOAA-19 SBUV/2 data.
- Next NP instrument on JPSS-1 satellite (planned launch in early 2017) will conduct normal operations with 50 km x 50 km pixels within current footprint → more ability to detect fine structure.
- NOAA plans to operate additional NP instruments through 2040, which would extend SBUV-type PMC record to 60+ years.

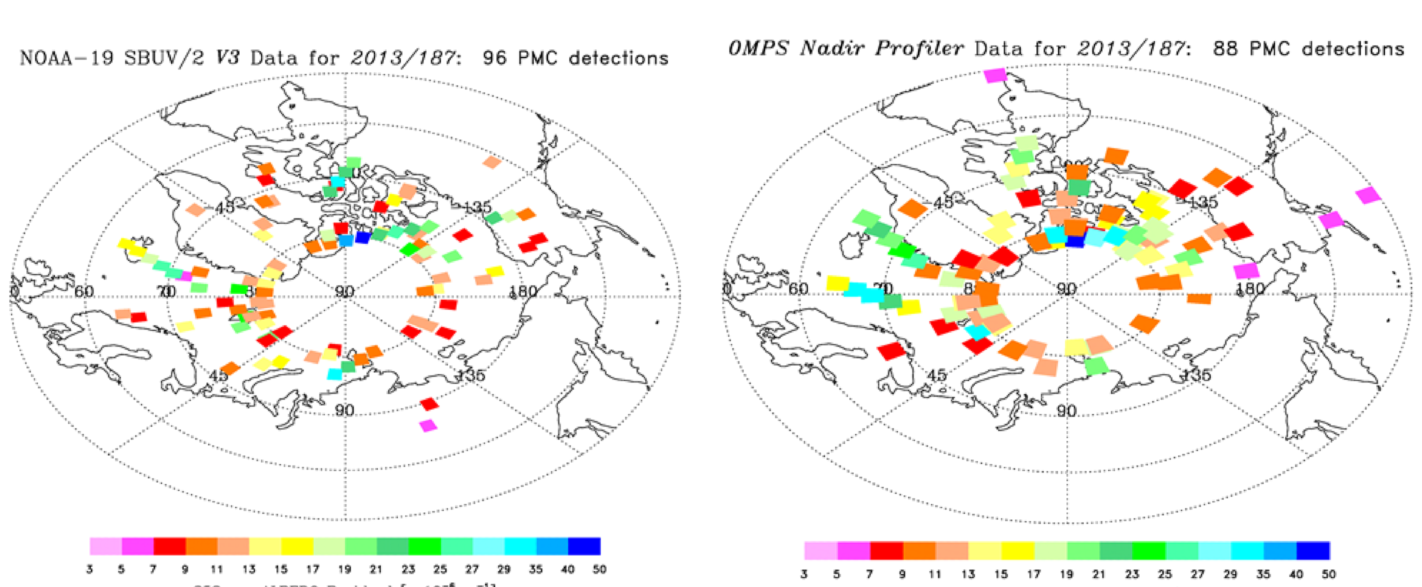

NOAA-19 SBUV/2 and S-NPP OMPS NP PMC detection results for 6 July 2013

Limb Profiler (LP)

Overview of Measurements

Polar Mesospheric Cloud

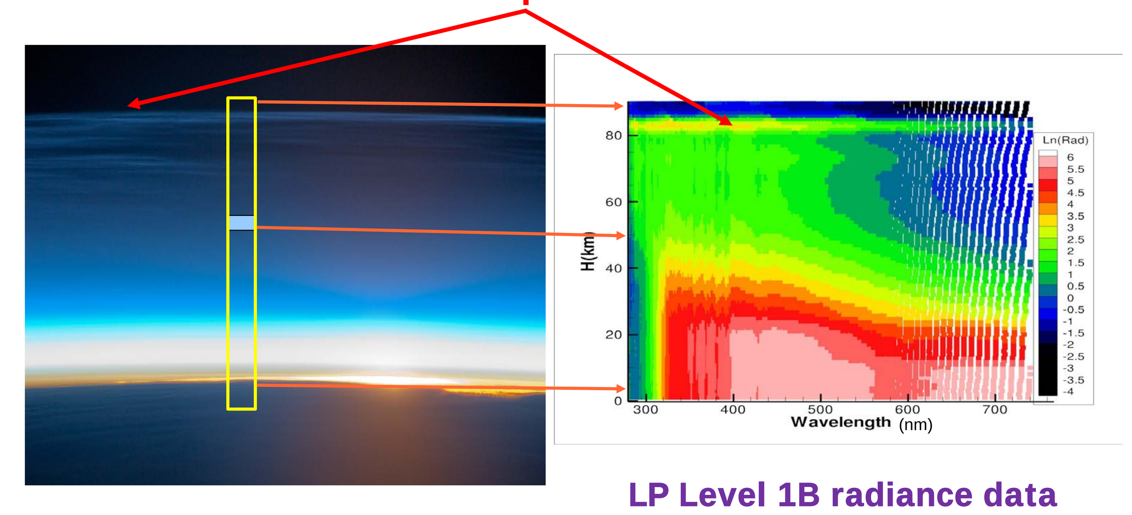

LP slit on Earth limb

LP Level 1B radiance data

- LP limb scattering measurements give snapshot of atmosphere over 0-80 km (Δz = 1 km) and 290-1000 nm ($\Delta\lambda$ = 1-30 nm) every 19 seconds (~125 km separation between profiles).
- Three parallel slits look backward, oriented along-track and 4.25° (~250 km) to each side.
- Center slit observes same atmospheric region as NP instrument approximately 7 minutes later throughout every orbit → Continuous "common volume" observations.

Operational Constraints

- Maximum altitude coverage varies between slits, along orbit, and during season. Southern Hemisphere measurements typically capture full PMC vertical extent, Northern Hemisphere measurements may not capture PMC peak (*see examples below*).
- Scattering angle covers large range along orbit (high in SH, low in NH). Ice phase function varies by factor of ~30 at UV wavelengths over LP observation range → Observed PMC signal will vary substantially between hemispheres (similar to SME and SNOE).
- SH PMC analysis is affected by South Atlantic anomaly (SAA) effects on CCD pixels, since tangent point is ~26° southward of satellite at mid-latitudes.

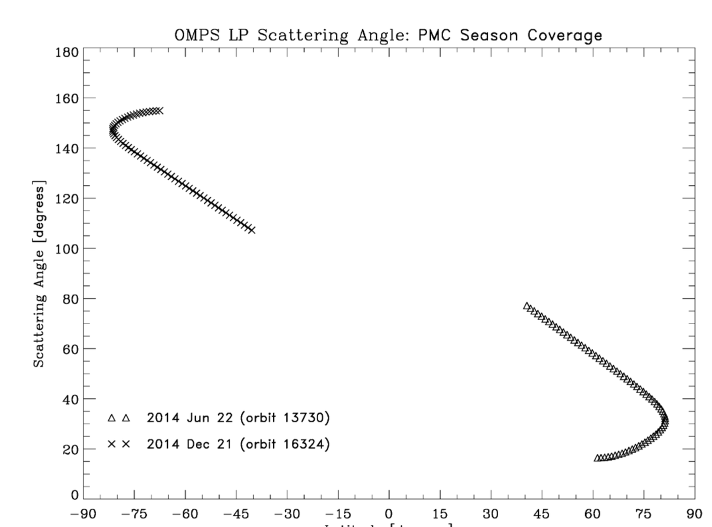

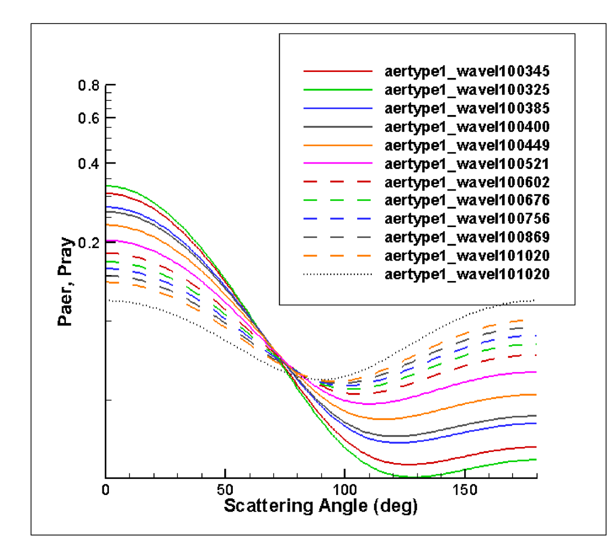

Ice phase function for 325-1020 nm (r = 45 nm, σ = 1.4)

Identification of PMCs in LP Data

- A cloud located at 80-85 km can be seen in LP radiances down to 50 km (sometimes lower) due to line-of-sight viewing effects.
- LP Level 2 ozone processing generates forward model radiance profile (no cloud) for every event, but only up to 80 km.
- Residual difference between observed and calculated radiance (> 20%, evaluated at 65 km) provides a very sensitive indicator of PMC presence.

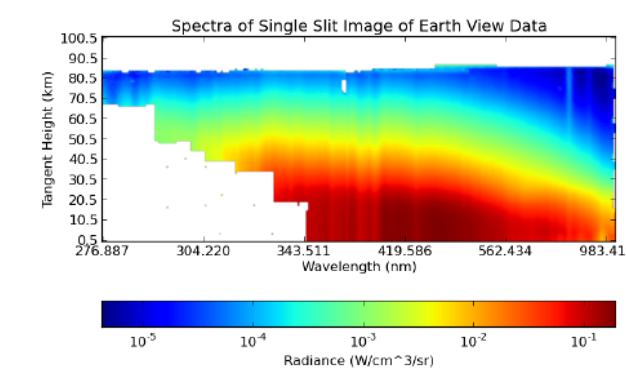

LP radiance data for single event (interpolated to regular spectral and altitude grid)

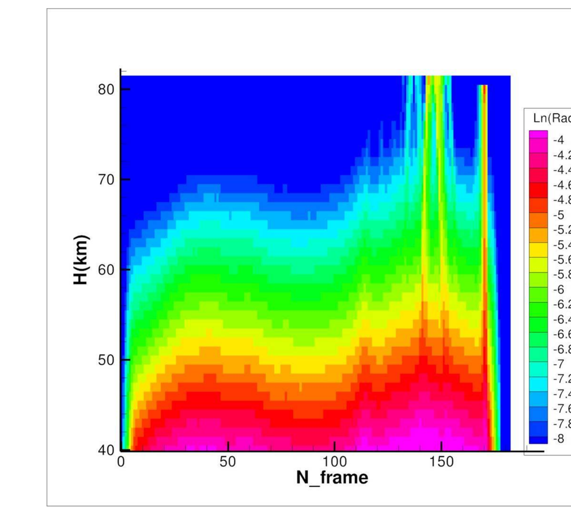

LP radiance data for single orbit at 353 nm

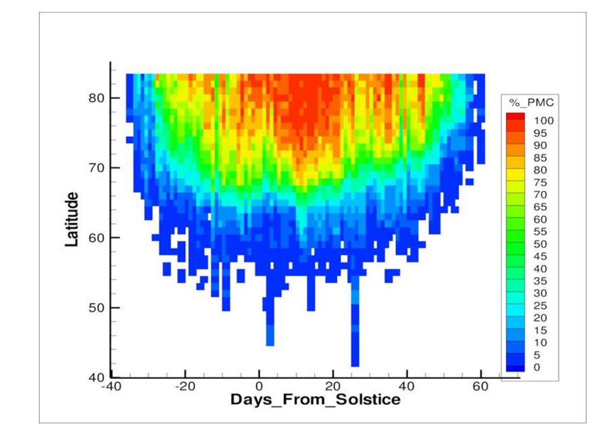

LP PMC occurrence frequency (residual test), NH 2013

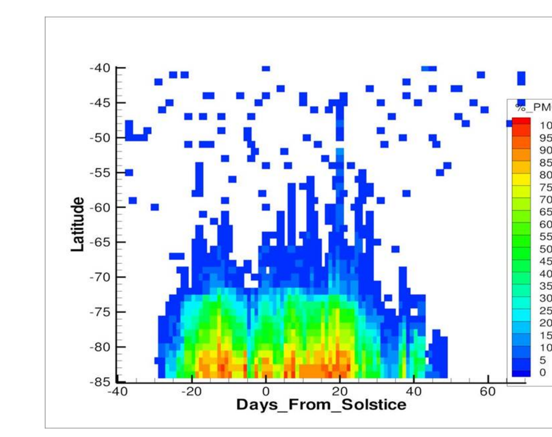

LP PMC occurrence frequency (residual test), SH 2012-2013

- Early tests based on LP radiance peak detection demonstrated consistency between LP and NP PMC observations.

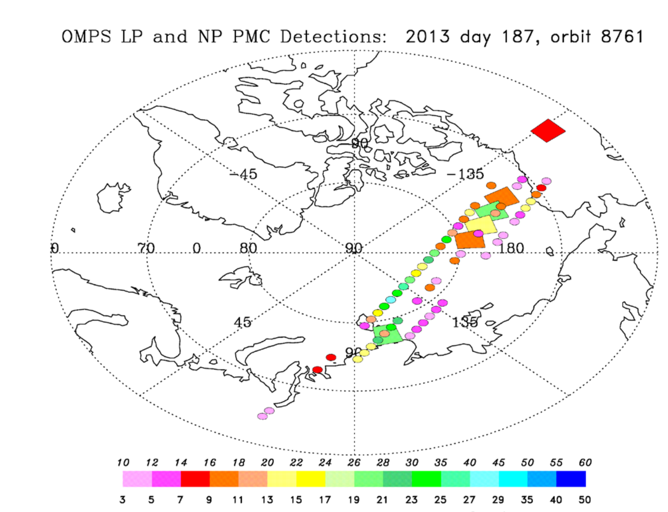

Characterization of PMCs in LP Data

- Current LP stray light correction is less accurate at high altitude, longer wavelengths → Subtracting calculated radiance is problematic for quantitative analysis.
- Determine background by averaging non-cloud observed profiles at lower latitudes, normalizing to observed profile below PMC signal.
- Calculate difference to estimate strength of PMC signal.

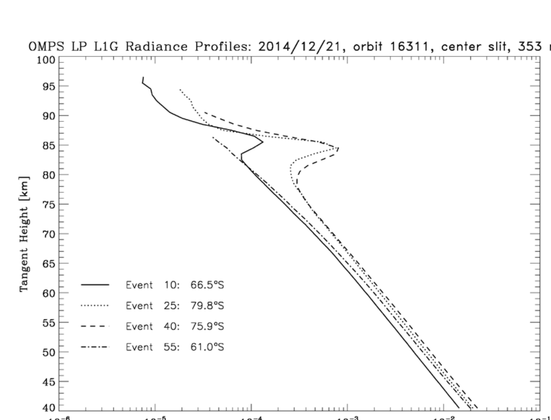

SH raw data, 353 nm, C slit

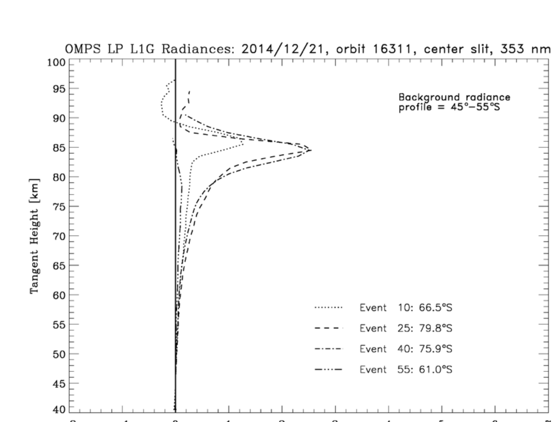

SH difference, 353 nm

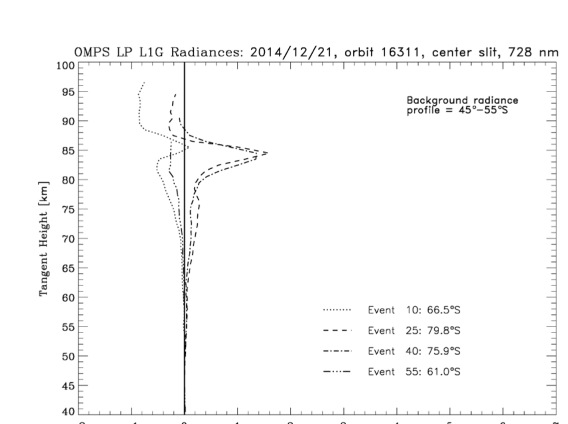

SH difference, 728 nm

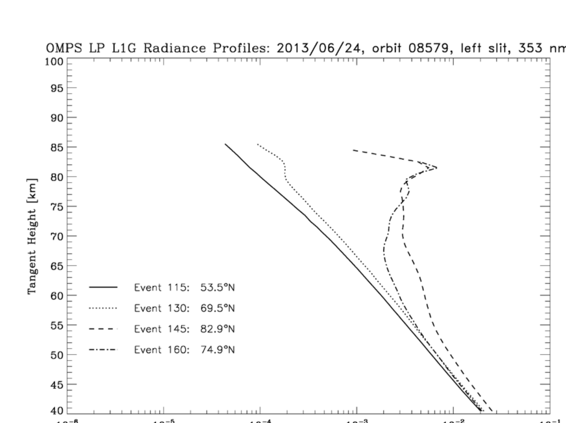

NH raw data, 353 nm, L slit

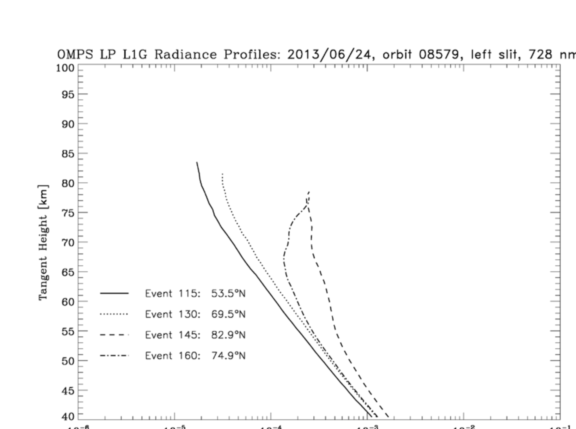

NH raw data, 353 nm, R slit

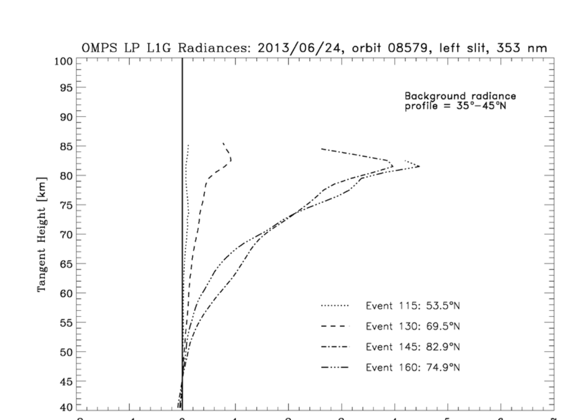

NH difference, 353 nm

Future Work (*lots!*)

- Create seasonal processing code for NP data and compare 2012-2015 results to NOAA-19 data.
- Incorporate OMPS NP data in long-term trend analysis.
- Evaluate changes in NP PMC detection results when different wavelength selections are used.
- Refine background determination and application for LP observations.
- Implement calculation of PMC peak intensity (parabolic fit?).
- Create seasonal processing code for LP data.
- Begin common volume studies.
- Note that LP instrument is not manifested on JPSS-1 satellite, but is planned for JPSS-2 satellite (launch ~2022).

Estimation of outgoing longwave radiation from Cross-track Infrared Sounder (CrIS) radiance measurements

Kexin Zhang(1), Fengying Sun(2), Mitch Goldberg(3), Thomas King(1), Quanhua Liu(4), Walter Wolf(4), Changyi Tan(1), Letitia Soulliard(1)

1I.M. Systems Group, Inc., 2INNOVIM, 3NOAA JPSS Office and 4NOAA/NESDIS/STAR

Abstract:

The purpose of this study is to provide real time *CrIS-track Infrared Sounder* (CrIS) *Outgoing Longwave Radiation* (OLR) using the hyperspectral infrared sounder radiance measurements. *Atmospheric Infrared Sounder* (AIRS) is used as the third transfer instrument, and the least-squares regression algorithm is applied to generate two sets of regression coefficient. One is between collocated Clouds and the *Earth's Radiant Energy System* (CERES) OLR on *Aqua* and pseudo channel radiance calculated from *AIRS* radiance. The other regression equation is obtained by relating the pseudo channel radiance difference between AIRS and CrIS to the individual measured CrIS radiance in each pseudo channel, which is called adjustment coefficient. CrIS OLR is estimated as weighted linear combination of CrIS adjusted 17 pseudo channel radiances. We validate CrIS OLR by using very limited available CERES NPP OLR observations over 1°X1° global grids, and we also validate it against CERES (Aqua) OLR cases over the S-NPP and Aqua *Simultaneous Nadir Overpass* (SNO) observations. The results show that the precision of CrIS OLR estimation is within 3 W/m^2, and the accuracy is within 5 W/m^2.

Algorithm Description

In this work, we use broadband radiometer CERES OLR as truth, and AIRS as the third transfer instrument. Radiance adjustment regression database between AIRS and CrIS is derived with theoretical radiative transfer model simulations given 'noaa88' and 'noaa89' sounding collections for all sky conditions. Cloud conditions were simulated by ATOV derived cloud properties. Cloud is black except for cirrus which has spectral-dependent emissivity. We degrade AIRS, CrIS radiance spectra into 17 pseudo channels, and in each pseudo channel, the CrIS pseudo channel radiance is adjusted to AIRS pseudo channel radiances. Least squares regression algorithm is applied to relate CERES (Aqua) OLR to adjusted pseudo channel radiances calculated from CrIS radiances. Eight sets of regression coefficients are trained to account for view angle dependence of CrIS radiances. CrIS OLR is estimated directly as the weighted sum of pseudo channel radiance calculated from CrIS radiances.

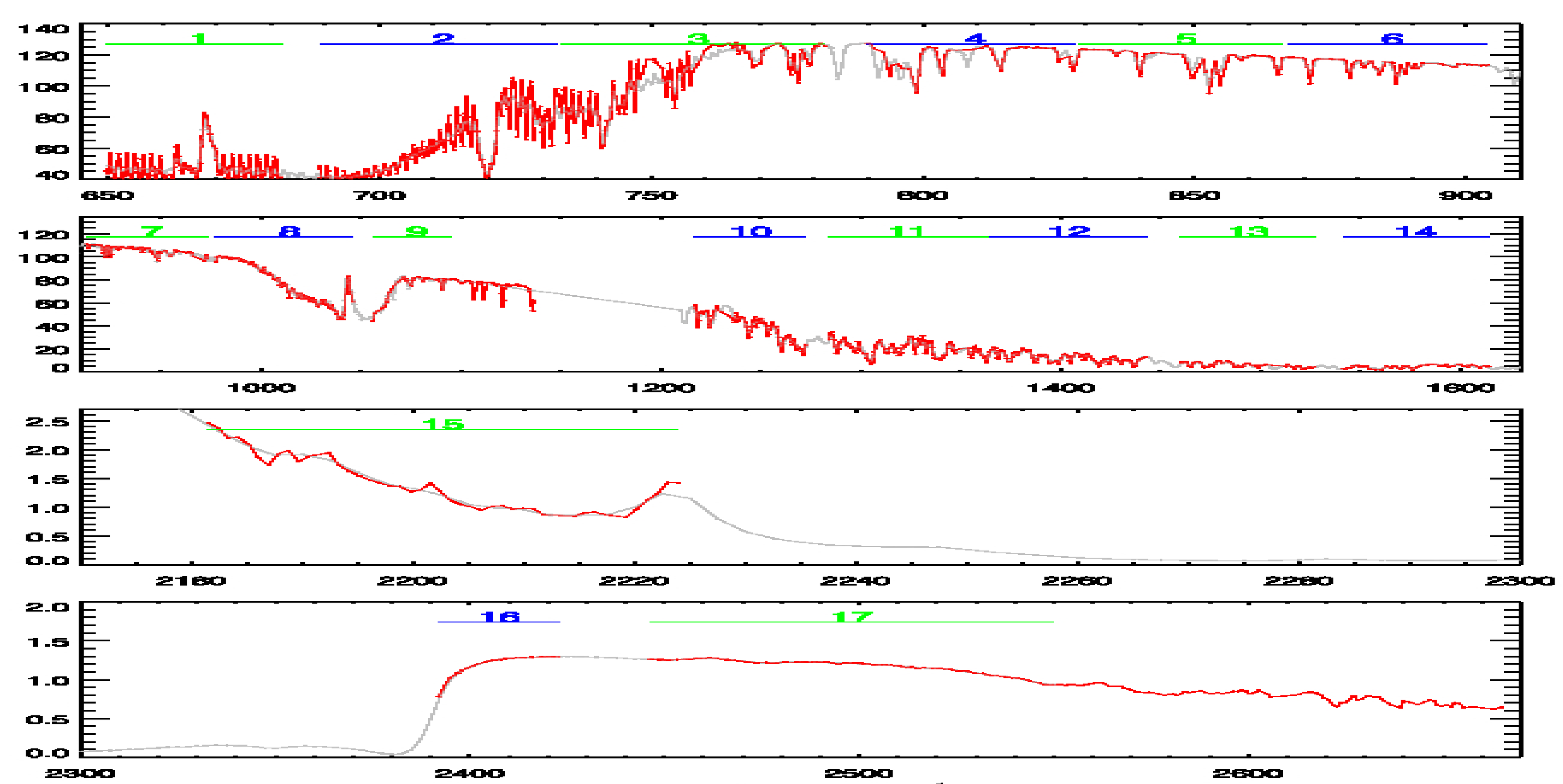

$$R(i) = \sum_{k=1}^{K} \frac{1}{\nu_{2i} - \nu_{1i}} \cdot r(k) \cdot \Delta\nu(k)$$

Convolved pseudo channel radiance for both AIRS and CrIS

$$\Delta R(i) = a_0 + \sum_{k=1}^{K} a(k) \cdot r_{CrIS}(k)$$

Pseudo channel radiance difference (between CrIS and AIRS) adjustment

$$\hat{F}_{CrIS} = b_0 + \sum_{i=1}^{17} b(i) \cdot [R(i) + \Delta R(i)]$$

Estimated CrIS OLR

Algorithm Validation

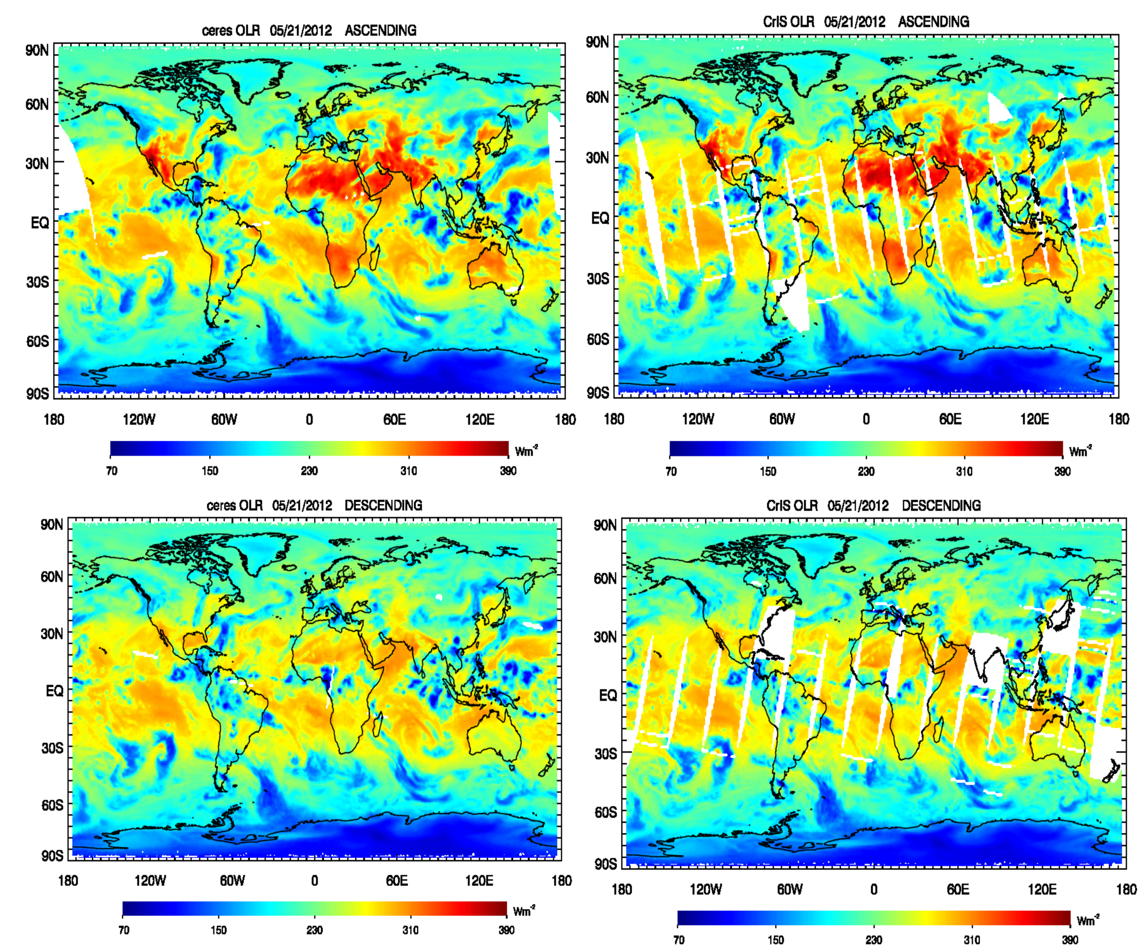

Homogeneous Scenes

We take the ratio of coefficient of variation less than 15%, and we get more homogeneous scenes and better standard deviation (right panels).

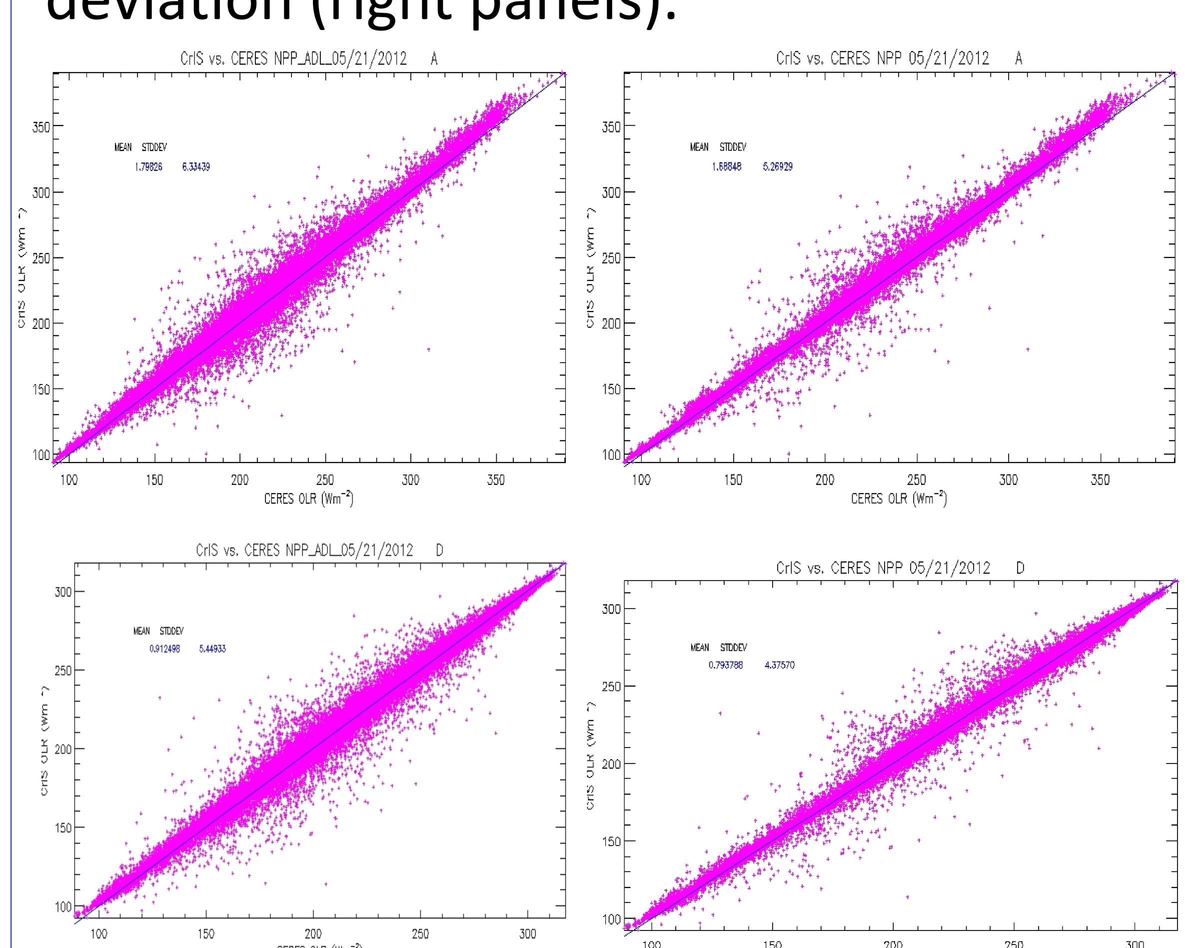

Simultaneous Nadir Overpass (SNO) observations comparison

Compare the estimated CrIS OLR with Aqua CERES OLR over the SNO observations. Take S-NPP and Aqua SNO observations from Jan. 2013 to Oct. 2013. *Average samples* for both CrIS and Aqua OLR within time difference less than 90 seconds, and distance difference less than 45 km; *Single sample pairs* with the smallest time and distance differences.

Average sample: Mean= -2.57486, std= 4.40283

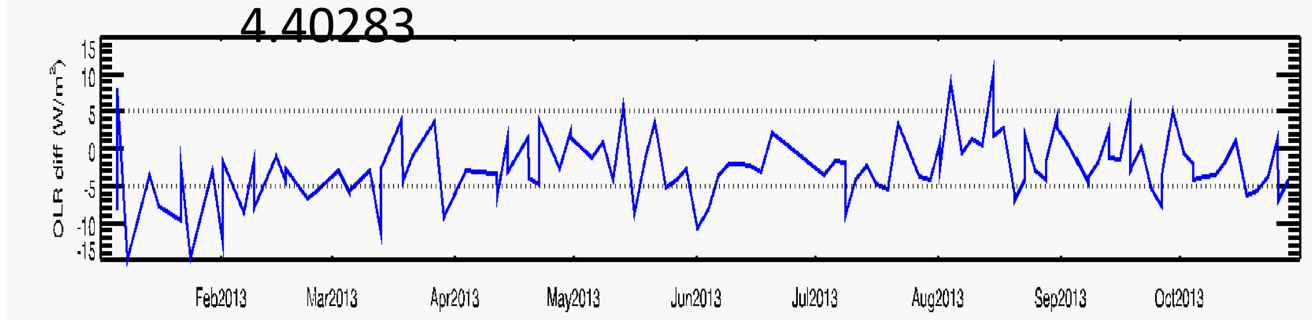

Single sample: Mean= -2.65107, std= 4.58340

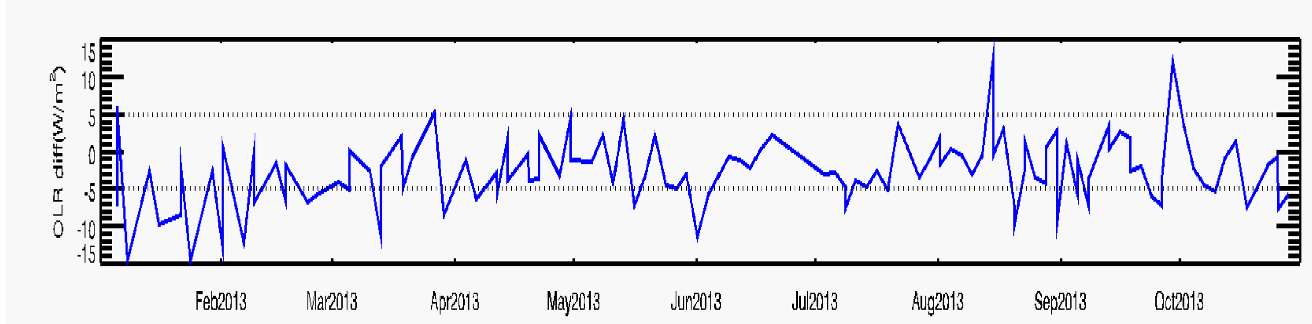

Summary

CrIS OLR was compared with simultaneous CERES NPP OLR directly over 1°X1° global grids. For CrIS homogeneous scenes , the results show that the standard deviation is within 5 w/m^2, and the bias is within 2 w/m^2.

SNO OLR comparison shows that the standard deviation between CrIS OLR and Aqua OLR are within 5 W/m2, and bias are less than 3 w/m^2.

References

[1] Sun, F., M. D. Goldberg, X. Liu, and J. J. Bates (2010a), Estimation of outgoing longwave radiation from Atmospheric Infrared Sounder radiance measurements, J. Geophys. Res., 115, D09103, doi:10.1029/2009JD012799.

Poster # 2, STAR JPSS 2015 Annual Science Team Meeting, 24-28 August, NCWCP, College Park, MD.

Corresponding Author: kexin.zhang@noaa.gov

ATMS/AMSU Snowfall Rates during the 2014-15 Winter Season

Huan Meng[1], Jun Dong[2], Cezar Kongoli[2], Nai-Yu Wang[3], Ralph Ferraro[1], Bradley Zavodsky[4], Banghua Yan[5], Limin Zhao[5]

[1] NOAA/NESDIS/STAR, [2] CICS-UMD, [3]IMSG, [4]NASA/SPoRT, [5]NOAA/NESDIS/OSPO

Introduction

SNPP ATMS and POES and MetOp AMSU/MHS take passive microwave (MW) measurements at certain high frequencies (88.2~190.31 GHz) that are sensitive to the scattering effect of snow particles and can be utilized to retrieve snowfall properties. An AMSU/MHS liquid equivalent snowfall rate (SFR) product has been produced operationally at NOAA/NESDIS since 2012. An ATMS SFR algorithm has been developed based on the AMSU/MHS SFR. The combined SFR products are generated from five satellites (NOAA-18/19, MetOp-A/-B, and SNPP), and can provide up to ten snowfall estimates at any location over global land at mid-latitudes. There are more estimates at higher latitudes.

Applications

The SFR products can be used to support weather forecasting

- fill in gaps where traditional snowfall data are not available to weather forecasters such as in mountains and remote regions where radar and weather stations are sparse or radar blockage and overshooting are common
- provide quantitative snowfall information to complement snowfall observations or estimations from other sources (stations, radar, GOES imagery data, etc.)
- to identify snowstorm extent and location of the maximum intensity within the storm
- Track storms and derive trending information (e.g., strengthening or weakening of the storm) by pairing with radar and/or GOES IR/VIS/WV images

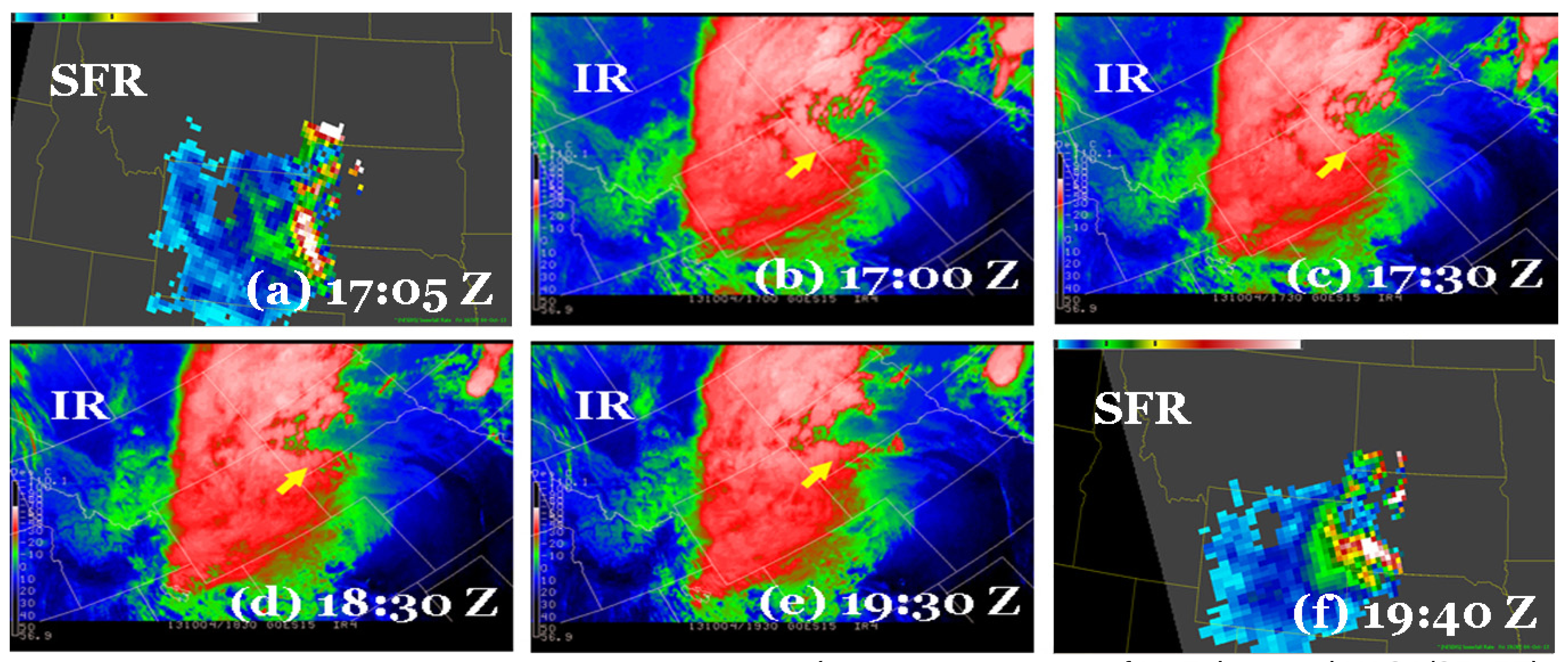

(Images are courtesy of M. Folmer and NASA/SPoRT)

Time sequence of a snowstorm in the Northern Plains. (a) and (f): the AMSU/MHS SFR product at around 17:05Z and 19:40Z, respectively; (b)-(e) GOES-15 IR images at 17:00Z, 17:30Z, 18:30Z, and 19:30Z, respectively. The yellow arrow points to the most intense snow in the IR images. The IR sequence indicates that the snow max rotated counter-clockwise and moved north between the two SFR observations. This is confirmed by the second satellite pass at 19:40Z. The snow max is in white color in the SFR images.

Product Assessment

- NASA SPoRT led ATMS/AMSU SFR assessment in the 2014-2015 winter season. Several NWS Weather Forecast Offices (WFOs) from the Eastern Region, Front Range, Alaska and the NESDIS/Satellite Analysis Branch (SAB) participated in the evaluation.
- Direct Broadcast (DB) data from CIMSS at the University of Wisconsin and GINA at the University of Alaska Fairbanks were used to reduce product latency.

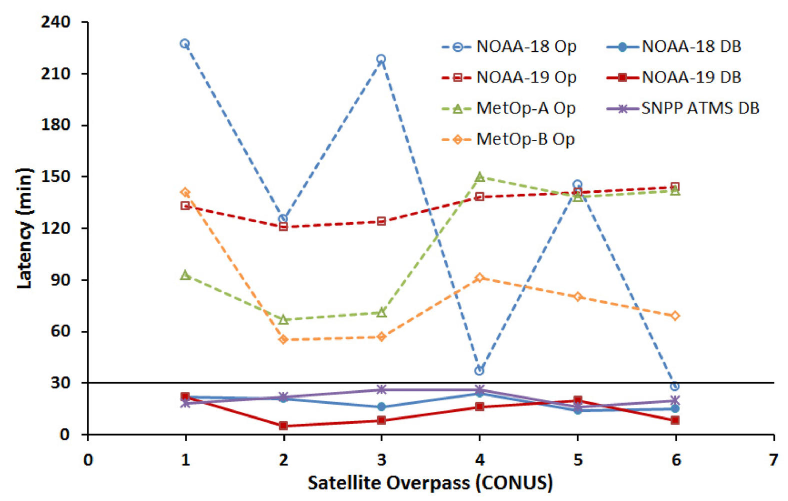

Left: Comparison of latency between operational (Op) and direct broadcast (DB) data streams from ATMS and AMSU respectively aboard SNPP, POES, and Metop satellites

Near Real-Time SFR Webpage at CICS/UMD

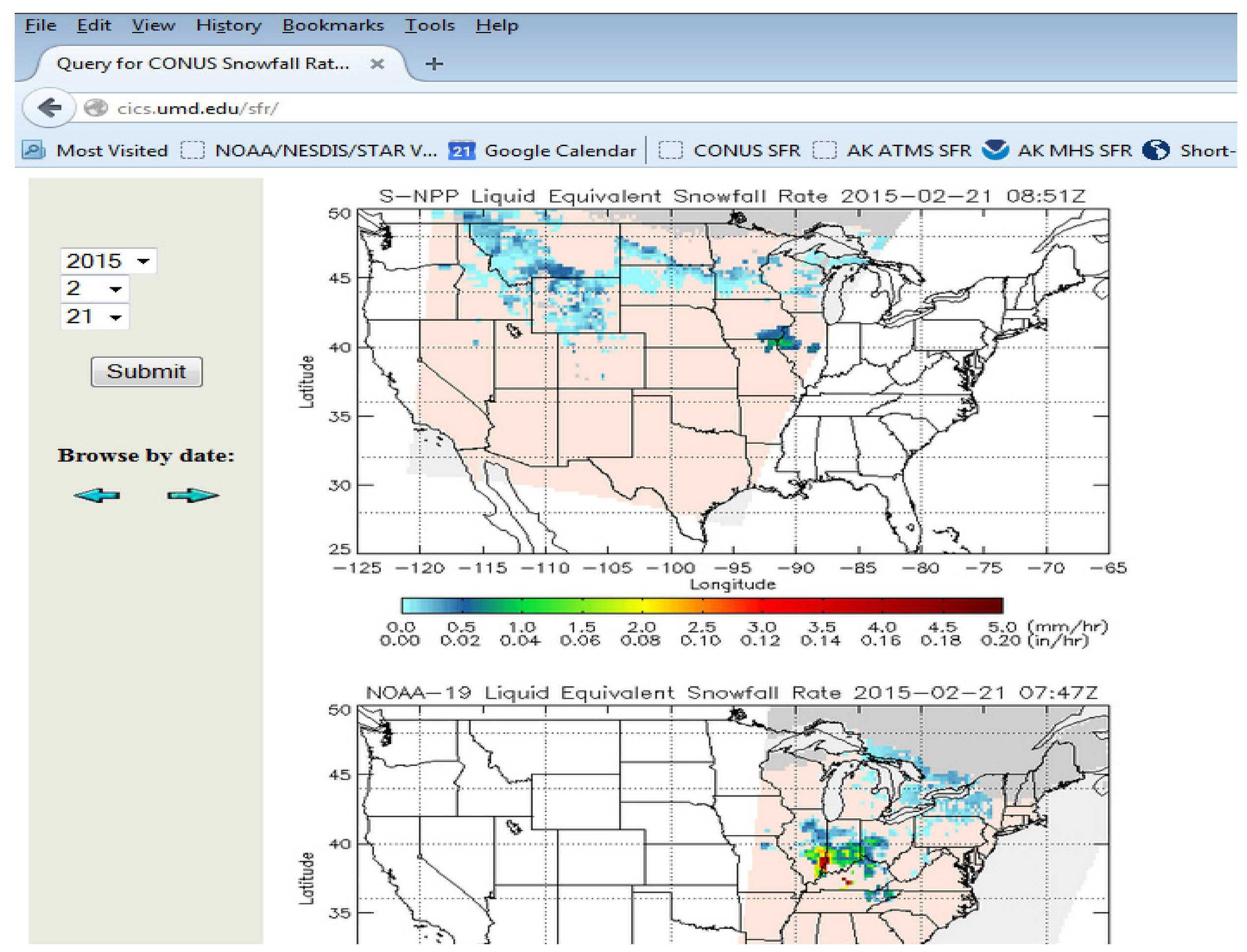

SPoRT near real-time SFR images in AWIPS II format are at http://weather.msfc.nasa.gov/sport/

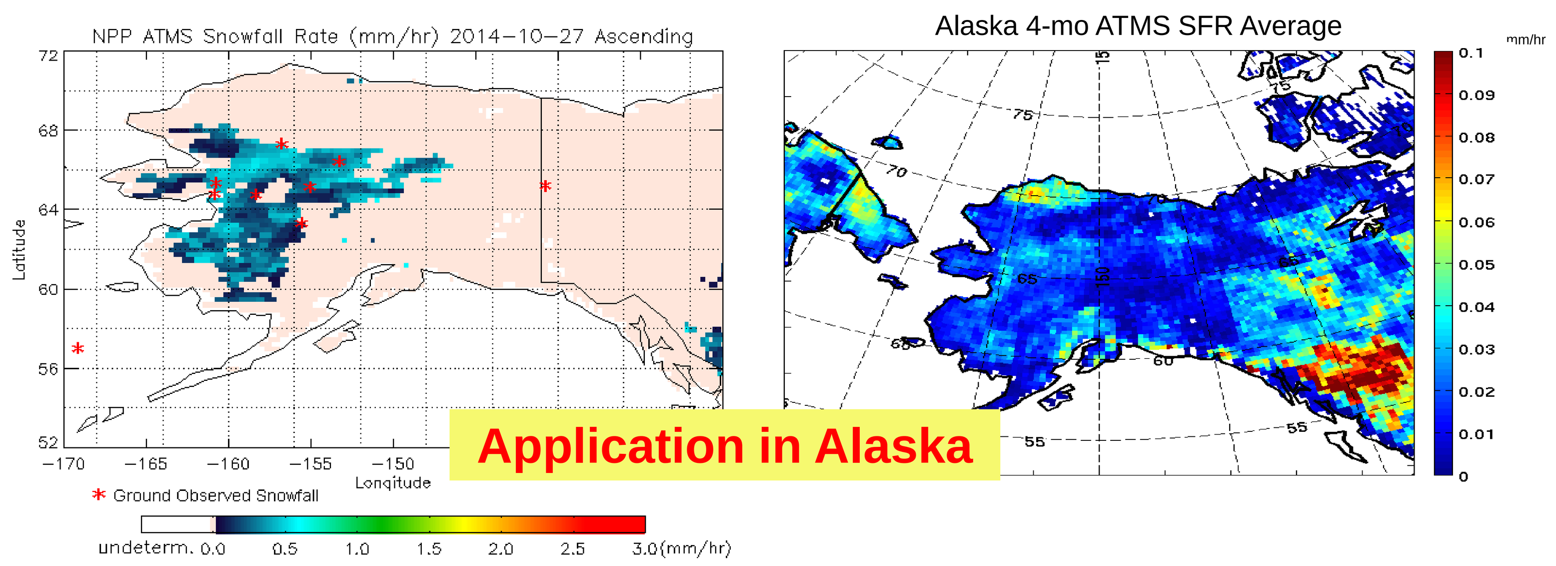

This study was partially supported by NOAA grant NA09NES4400006 (Cooperative Institute for Climate and Satellites -CICS) at the University of Maryland/ESSIC.

Cases and Feedback

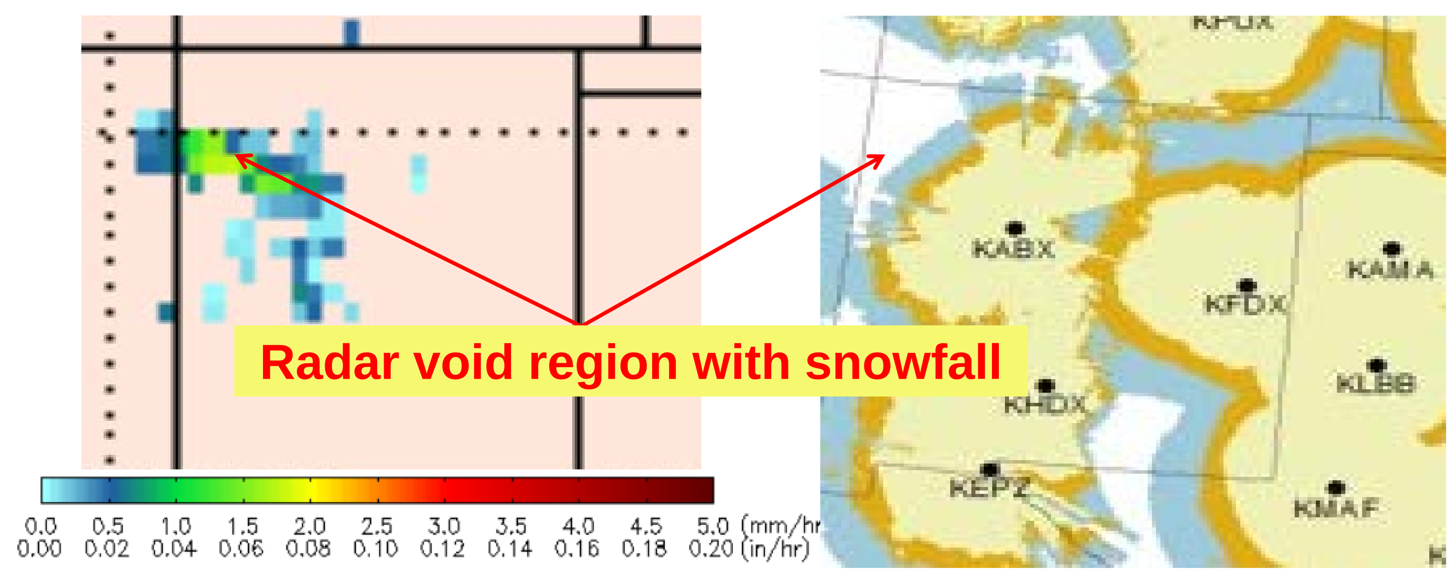

Albuquerque, NM WFO (ABQ): The 919UTC image matched the NAM12 QPF forecast very well within a data void region. From this information I was able to determine the NAM forecast was too slow with the evolution of the precip…The radar values dropped off away from the KABX radar which is expected, whereas the SFR product increased in the area of heaviest snowfall. Rates were close to the observed value at KGUP. The NM DOT web page indicated difficult driving conditions within this region.

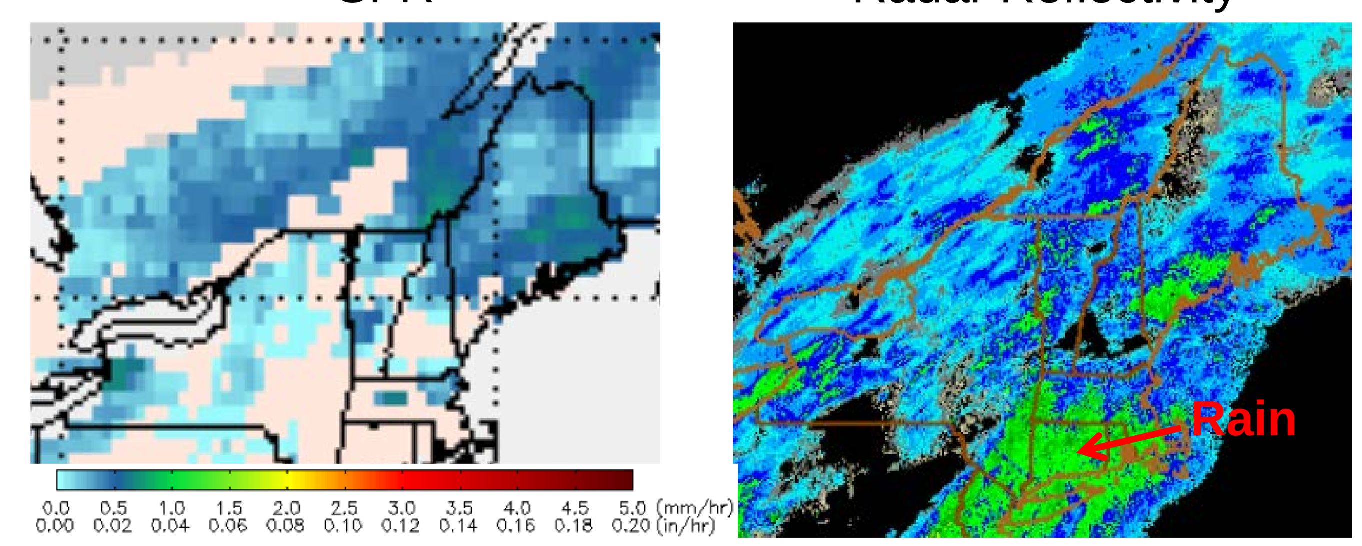

Burlington, VT WFO (BTV): Light snow was widespread across the area at that time. It (SFR) provided useful input for snowfall rates across portions of the northern Green Mountains …. Rates appeared quite reasonable. While not in our area, Sherbrooke, QE (CYSC) reported its lowest visibilities at 1800 UTC beneath the areal max of around 1.0 mm/hr in the satellite estimate at 1748 UTC. This added confidence to the accuracy of the product.

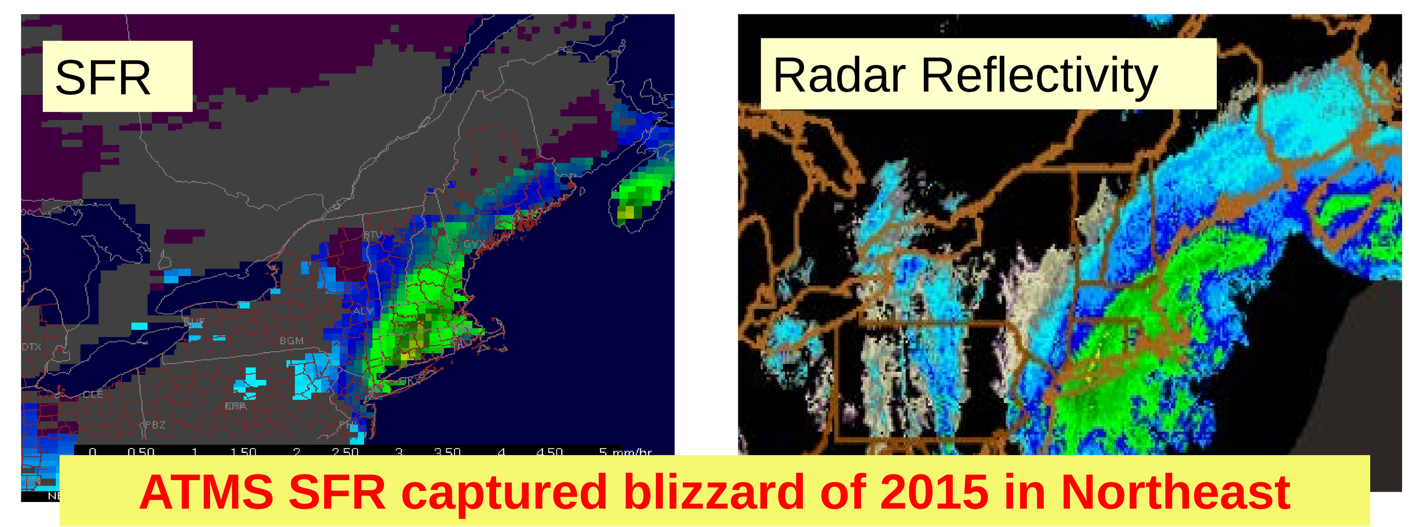

ATMS SFR captured blizzard of 2015 in Northeast

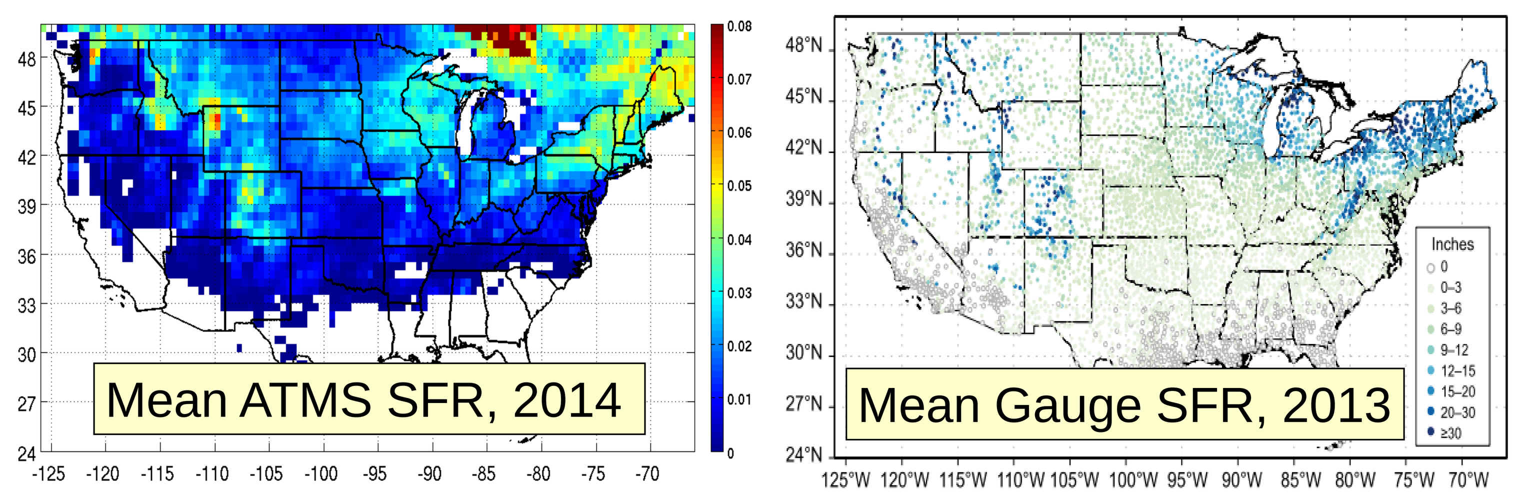

ATMS SFR Climatology

The role of the GCOS Reference Upper-air Network (GRUAN) in climate research

Greg Bodeker[1], Michael Sommer[2], Ruud Dirksen[3], Peter Thorne[4]

[1]GRUAN co-chair; Bodeker Scientific, Alexandra, New Zealand
[2]GRUAN Lead Centre; Deutscher Wetterdienst, Lindenberg, Germany
[3]Head of GRUAN Lead Centre; Deutscher Wetterdienst, Lindenberg, Germany
[4]GRUAN co-chair; Maynooth Unversity, Department of Geography, Maynooth Ireland

GRUAN data: http://www.gruan.org/data
email: gruan.lc@dwd.de or gruan.chairs@dwd.de
Web page: www.gruan.org

What is GRUAN?

The Global Climate Observing System (GCOS) Reference Upper-Air Network (GRUAN) is an international observing network, designed to meet climate requirements and to fill a major void in the current global observing system by providing reference observations. GRUAN is envisaged as a network of 30-40 sites building, where possible, on existing observational networks and capabilities (Fig. 1 and 2).

GRUAN as part of a system of systems observing architecture

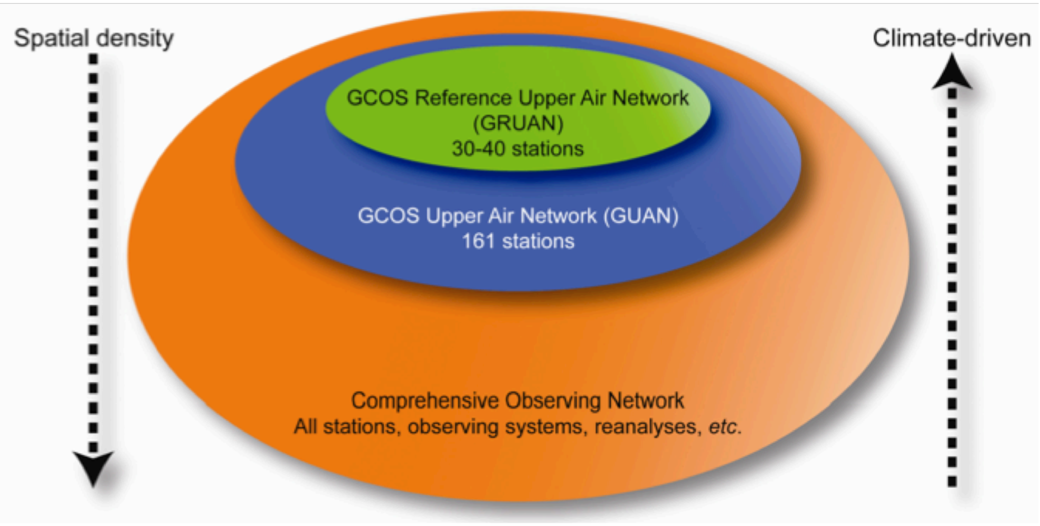

Figure 2: GRUAN is intended to serve as a reference network which consists of well instrumented and well understood sites.

GRUAN RS92 radiosonde data product

- Tailored GRUAN data processing has been developed to correct temperature, pressure, humidity, and wind profiles for all known systematic biases and to generate vertically resolved estimates of the measurement random uncertainties (Dirksen et al. 2014).
- The dominant source of RS92 measurement errors is solar radiation, which causes temperature warm biases (partially compensated by ventilation) and humidity dry biases (Fig. 5).
- Corrections for radiation-related biases, and their uncertainties, are based on the results of experiments made at the GRUAN Lead Centre.
- Availability of the GRUAN RS92 radiosonde data product is shown in Fig.4.

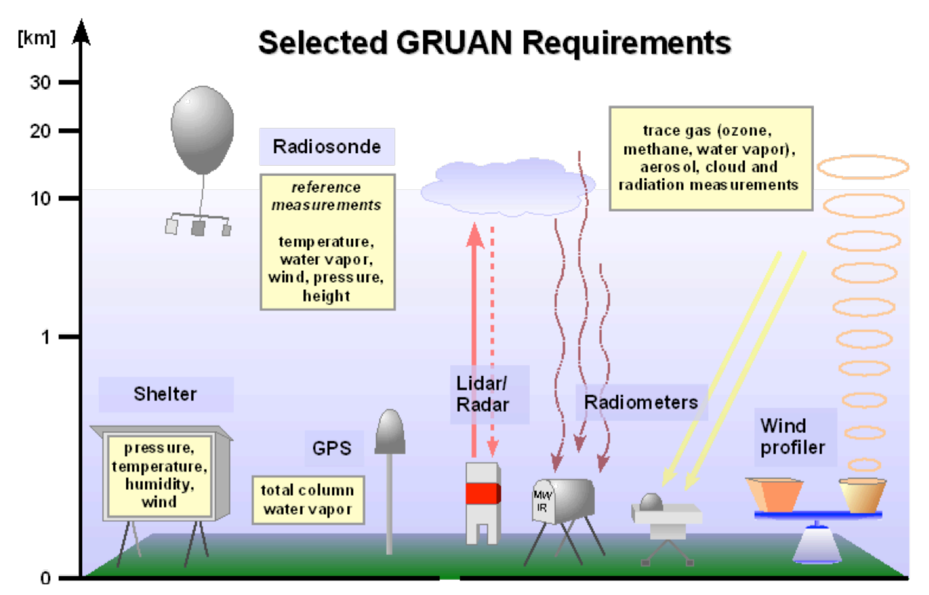

Figure 3: Schematic diagram showing some required measurements for a generic GRUAN site.

Partners

- National contributors (fundamental to success of the enterprise)
- The Global Space-based Inter-calibration System (GSICS) and the Sustained, Coordinated Processing of Environmental Satellite Data for Climate Monitoring (SCOPE-CM) Initiative
- WMO; its Commission for Instruments and Methods of Observations (CIMO); Commission on Climatology (CCI); Commission for Basic Systems (CBS); The World Climate Research Programme (WCRP)
- Existing observational networks (NDACC, ARM, GAW, BSRN, GUAN, GSN)

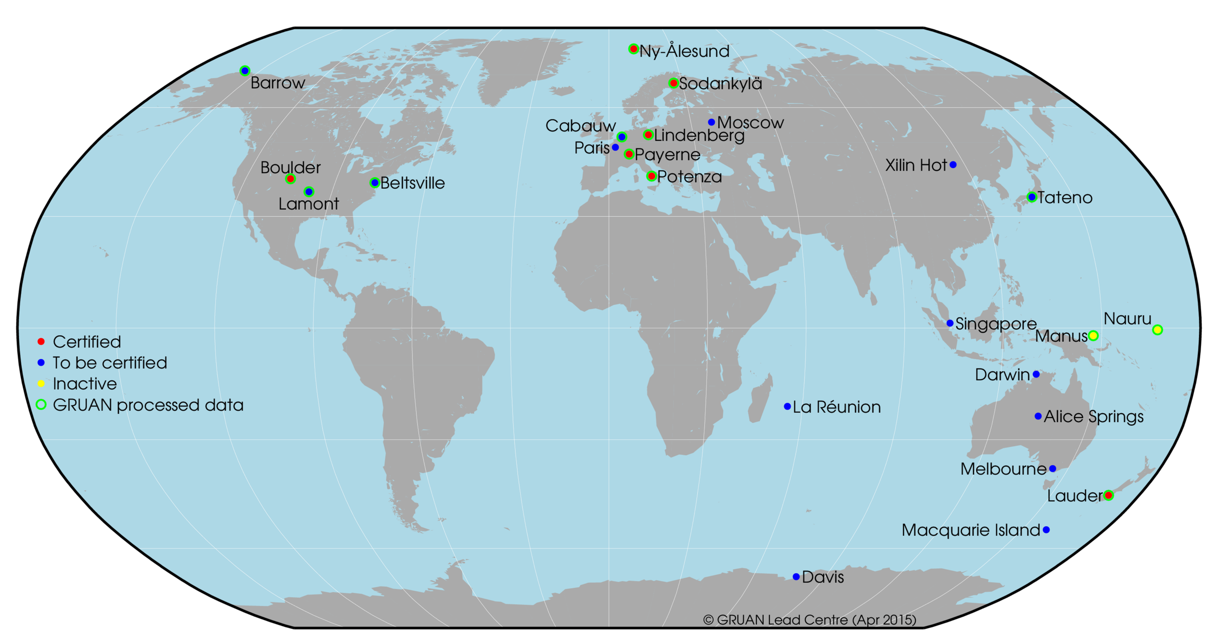

Figure 1: Current sites in GRUAN

A GRUAN reference observation

- ✓ Is traceable to an SI unit or an accepted standard
- ✓ Provides a comprehensive uncertainty analysis
- ✓ Maintains all raw data
- ✓ Includes complete meta data description
- ✓ Is documented in accessible literature
- ✓ Is validated (e.g. by intercomparison or redundant observations)

Other products in development

- Additional radiosondes: Modem. Meteolabor, Mesei.
- Water vapour profiles from high-resolution chilled-mirror frost point temperature measurements.
- Ground-based Global Navigation Satellite Systems (GNSS) total column water vapour.
- Lidar measurements of temperature, ozone and water vapour profiles
- Data products from FTS (Fourier Transform Spectroscopy) including water vapour, methane, carbon dioxide and ozone.
- Microwave radiometer (MWR) observations of temperature and water vapour profiles, total column water vapour and total cloud liquid water.

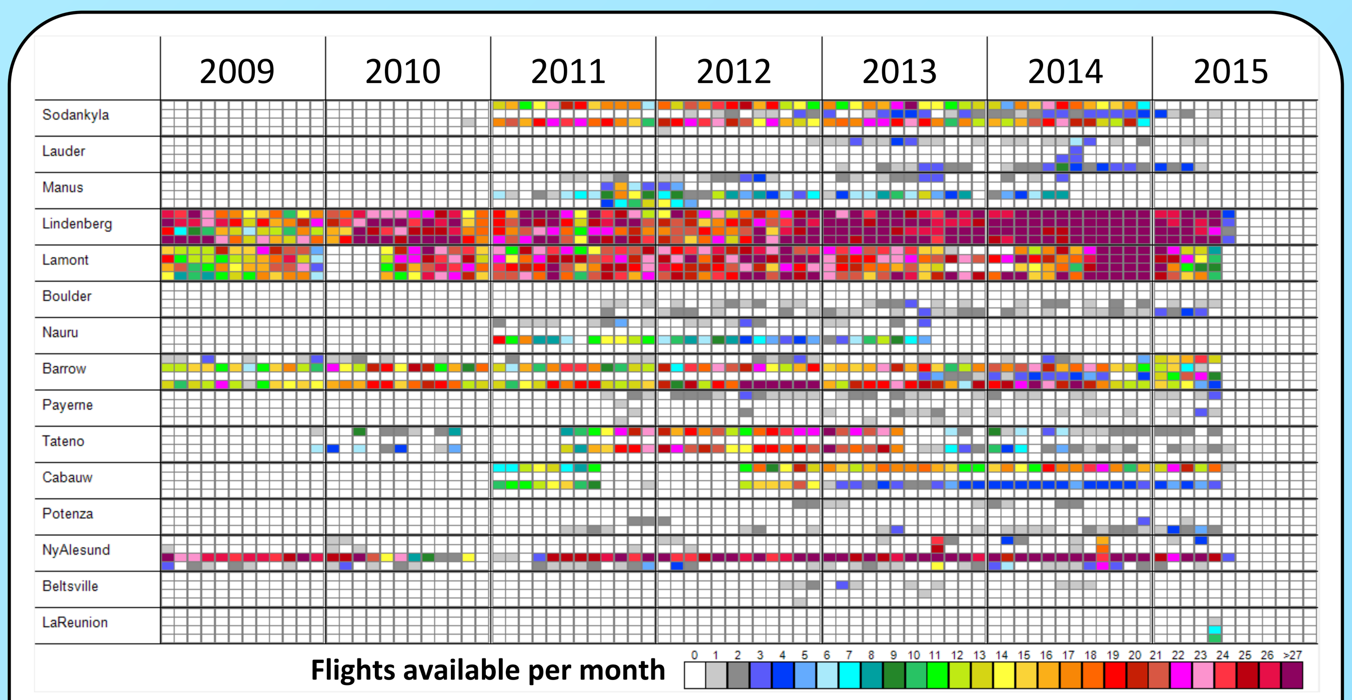

Figure 4: Availability of RS92 radiosonde data from across GRUAN. Each row for each site shows the data availability in 6 hour periods i.e. 00:00-06:00, 06:00-12:00, 12:00-18:00 and 18:00-24:00.

Getting involved in GRUAN

The primary point of contact is the Lead Centre through gruan.lc@gruan.org. Sites wishing to enter the network are encouraged to contact the Lead Centre. Scientists wishing to contribute to the network development and understanding can join one of several task teams or initiate a project under the science coordinators. Using GRUAN data benefits both GRUAN and your science. Please let us know if you undertake published work using the data and provide constructive feedback.

Research in support of GRUAN operations

- It is imperative for GRUAN's operations to be founded on research published in the peer-reviewer literature for scrutiny by the global community. Some examples:
- Solar radiation-induced biases in radiosonde measurements have been assessed in Philipona et al. (2012).
- Correction schemes developed for RS92 radiosonde data products have proven useful for developing correction methods for historical radiosonde data (Wang et al. 2013) and validating pre-flight corrections applied in the Vaisala ground-station software (Yu et al. 2015).
- Whiteman et al. (2011) investigated time to detect water vapour trends at ~200 hPa. Conclusion: at best it would take at least 12 years of daily observations at the Southern Great Plains site in northern Oklahoma.
- Fassò et al. (2014) established statistical basis for understanding extent to which collocation uncertainty is related to environmental factors.
- Madonna et al. (2014) provided criteria to quantify the value of complementary measurements and assess how measurement uncertainty is reduced by measurement complementarity.

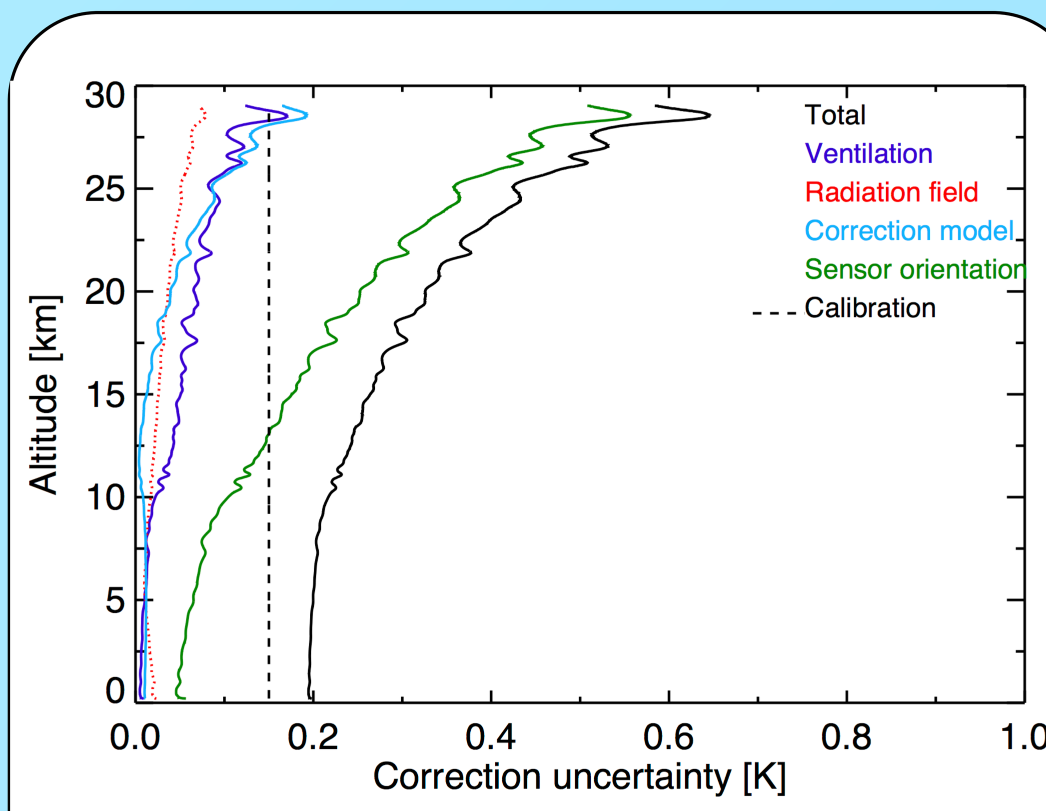

Figure 5: Contributions of the various uncertainty terms to the total uncertainty estimate of the GRUAN temperature correction for a specific sounding performed at Lindenberg on 27 September 2013 (from Dirksen et al., 2014). The total uncertainty is the geometric sum of the squared individual uncertainties. The correction model is the estimated vertically resolved error on the temperature based on the estimated actinic flux. This error is subtracted from the measured temperature profile to produce the corrected ambient temperature.

Literature

- Bodeker, G. E. et al., Reference upper-air observations for climate: From concept to reality. *Bull. Amer. Met. Soc.* In press.
- Dirksen, R.J. et al., Reference quality upper-air measurements: GRUAN data processing for the Vaisala RS92 radiosonde. *Atmos. Meas. Tech.*, 7, 4463-4490, doi: 10.5194/amt-7-4463-2014. **2014.**
- GCOS-170, The GCOS Upper-Air Reference Network (GRUAN) Manual, **2013**.
- GCOS-171, The GCOS Upper-Air Reference Network (GRUAN) Guide to Operations, **2013**.
- Immler, F.J. et al., Reference Quality Upper-Air Measurements: guidance for developing GRUAN data products. *Atmos. Meas. Tech.*, 3, 1217–1231, doi:10.5194/amt-3-1217-2010, **2010**.
- Philipona, R. et al., Solar and thermal radiation profiles and radiative forcing measured through the atmosphere. Geophys. Res. Lett., 39, L13806, doi: 10.1029/2012GL052087, **2012**.
- Wang, J. et al., Radiation dry bias correction of Vaisala RS92 humidity data and its impacts on historical radiosonde data. J. Atmos. Oceanic Technol., 30, 197-214, doi:10.1175/jtech-d-12-00113.1, **2013**.
- Whiteman, et al., The relative importance of random error and observation frequency in detecting trends in upper tropospheric water vapor. J. Geophys. Res., 116, D21118, doi: 21110.21029/22011JD016610.
- Yu, H. et al., Evaluation of humidity correction methods for Vaisala RS92 tropical sounding data. J. Atmos. Oceanic, Technol., 32, 397-411, doi:10.1175/jtech-d-14-00166.1, **2015**.

THE PREPROCESSOR OF THE NOAA UNIQUE CRIS/ATMS PROCESSING SYSTEM (NUCAPS)

Changyi Tan[1], Quanhua Liu[2], A. Gambacorta[3], Nicholas R. Nalli[1], Flavio Iturbide-Sanchez[1], Kexin Zhang[1], Michael Wilson[1], and Walter Wolf[2]

[1]I.M. Systems Group, Inc., [2]NOAA/NESDIS/STAR, and [3]Science and Technology Corporation

Abstract: The Cross-track Infrared Sounder (CrIS) and Advanced Technology Microwave Sounder (ATMS) are two critical sounding sensors onboard the Suomi National Polar-orbiting Partnership (S-NPP) satellite. The NOAA Unique CrIS/ATMS Processing System (NUCAPS) is an infrared (IR) and microwave (MW) hybrid atmospheric profile retrieval system which uses collocated CrIS and ATMS measurements. The NUCAPS algorithm uses the Stand-alone AIRS Radiative Transfer Algorithm (SARTA) forward model for IR and MIT MW forward model for MW sounding to retrieve atmospheric vertical profiles of temperature, moisture, trace gases and other geophysical parameters. From the hardware aspect, due to the ATMS oversampling, the geolocation pointings of S-NPP IR and MW sensors are mismatched. Therefore, the NUCAPS preprocessor, in software aspect, does the critical function of CrIS/ATMS footpoint collocation. The NUCAPS preprocessor is the module to match-up the two sensors of CrIS and ATMS. We proposed and implemented four versions of CrIS/ATMS footpoint match-up methods in our offline test bed, namely: 1) CrIS FOR center matchup method (NOAA operational version) --- Select the single ATMS FOV which is closest to the center of each CrIS FOR and average it with the surrounding 8 ATMS FOVs. 2) CrIS FOV matchup method --- Select 9 single ATMS FOVs which are closest to each CrIS FOV respectively and average the selected 9 ATMS FOVs. 3) Backus-Gilbert (B-G) remapping method --- Select ATMS FOVs around a CrIS FOR and multiply them with pre-calculated B-G coefficients (per scan position and per ATMS channel) to obtain the effective brightness temperature as it is measured by a single microwave antenna with the antenna gain pattern that matches the effective CrIS FOR. 4) Improved CrIS FOV matchup method --- Select 9 single ATMS FOVs which are closest to each CrIS FOV respectively and average the selected 9 ATMS FOVs. Plus, apply the ATOVS and AVHRR Preprocessing Package (AAPP) package on ATMS channels 1, 2 to resize the beam width from 5.2 degrees to 3.3 degrees.

Descriptions of CrIS/ATMS Collocation Methods

1, CrIS FOR center match-up method

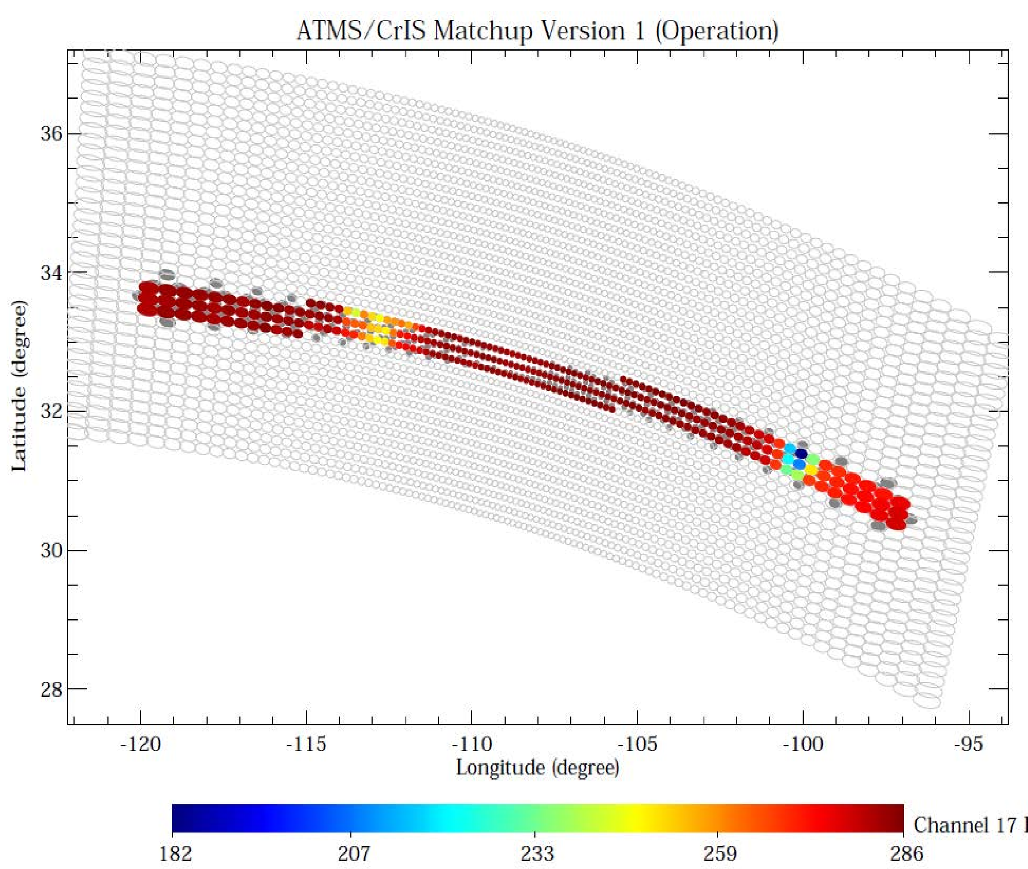

2, CrIS FOV matchup method

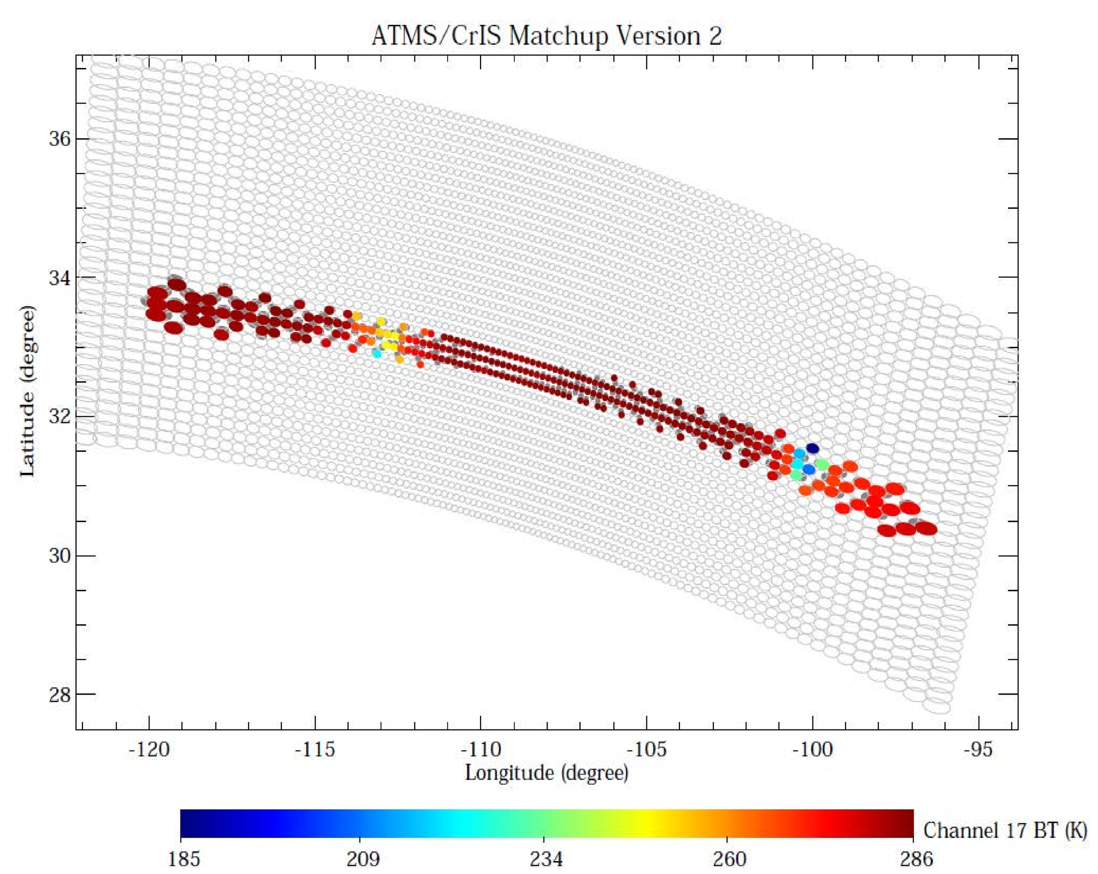

3, Backus-Gillbert (B-G) method

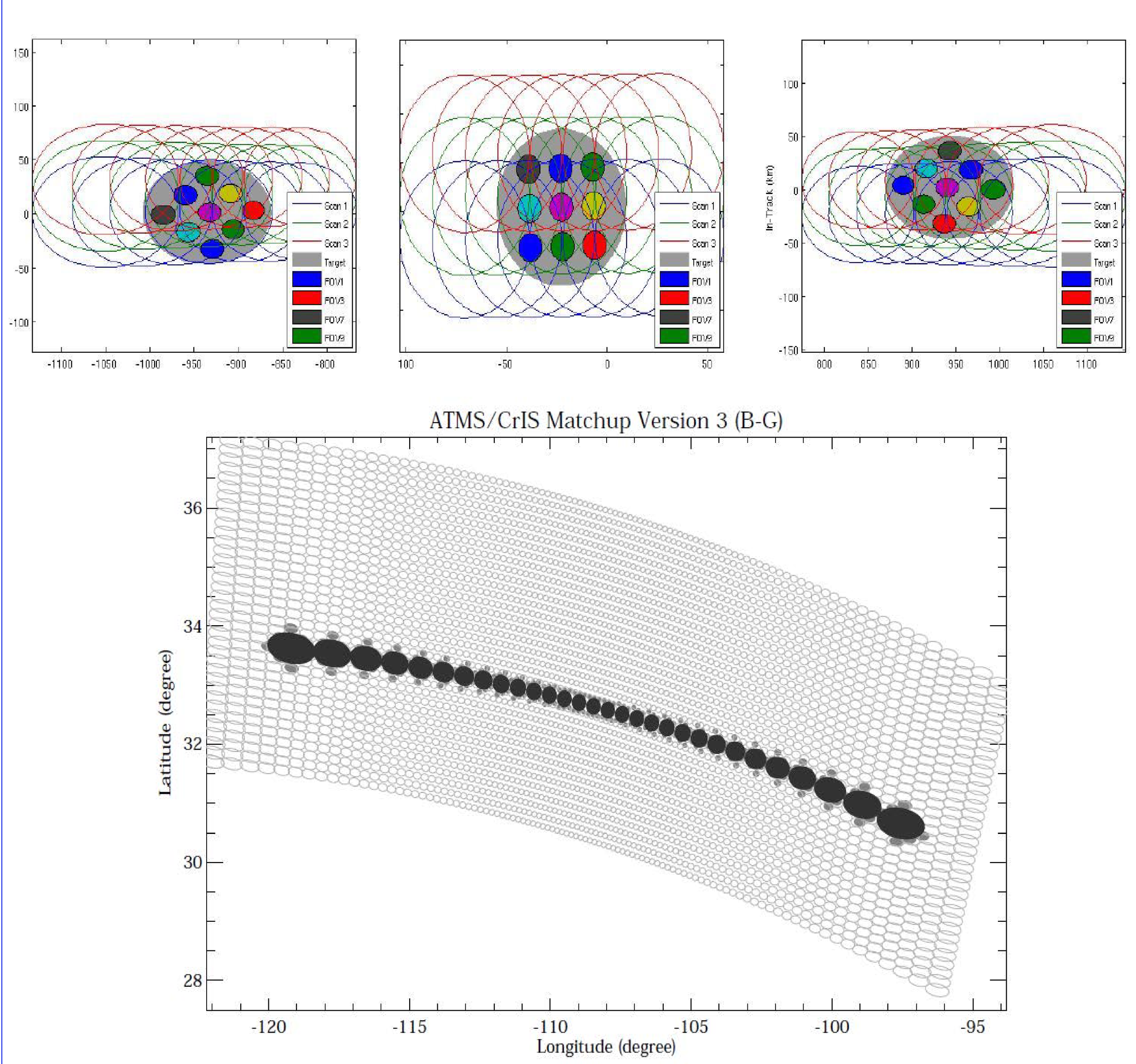

4, Improved CrIS FOV matchup method

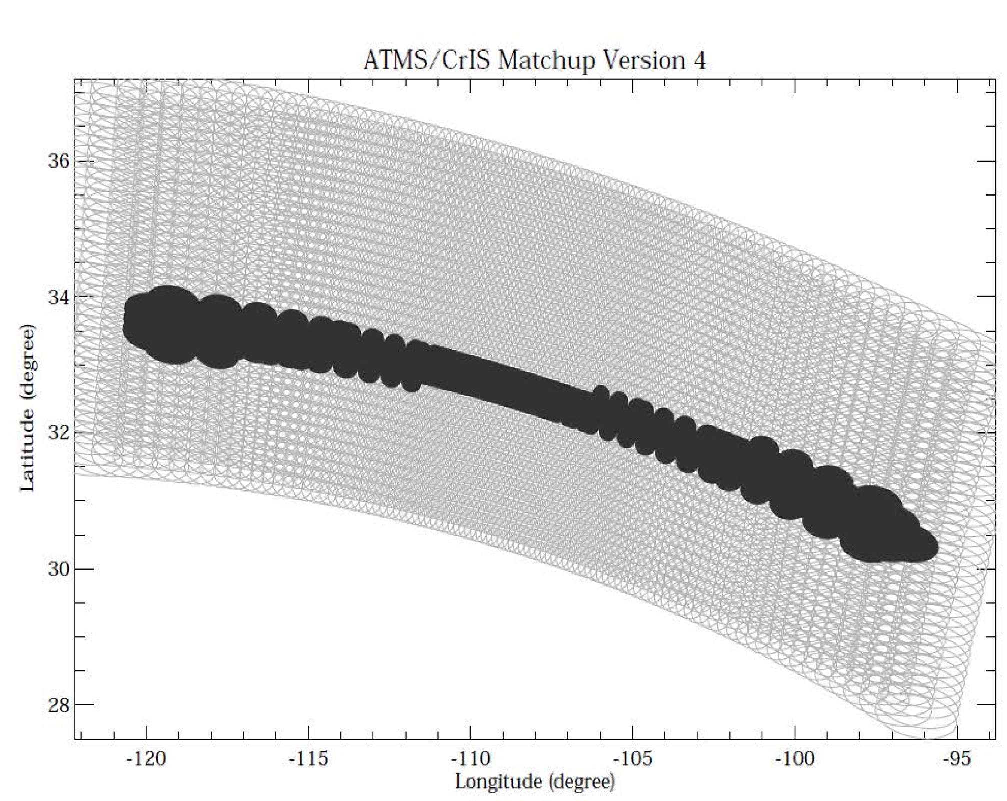

Differences between the preprocessed ATMS brightness temperatures via different preprocessors (in one given scan line).

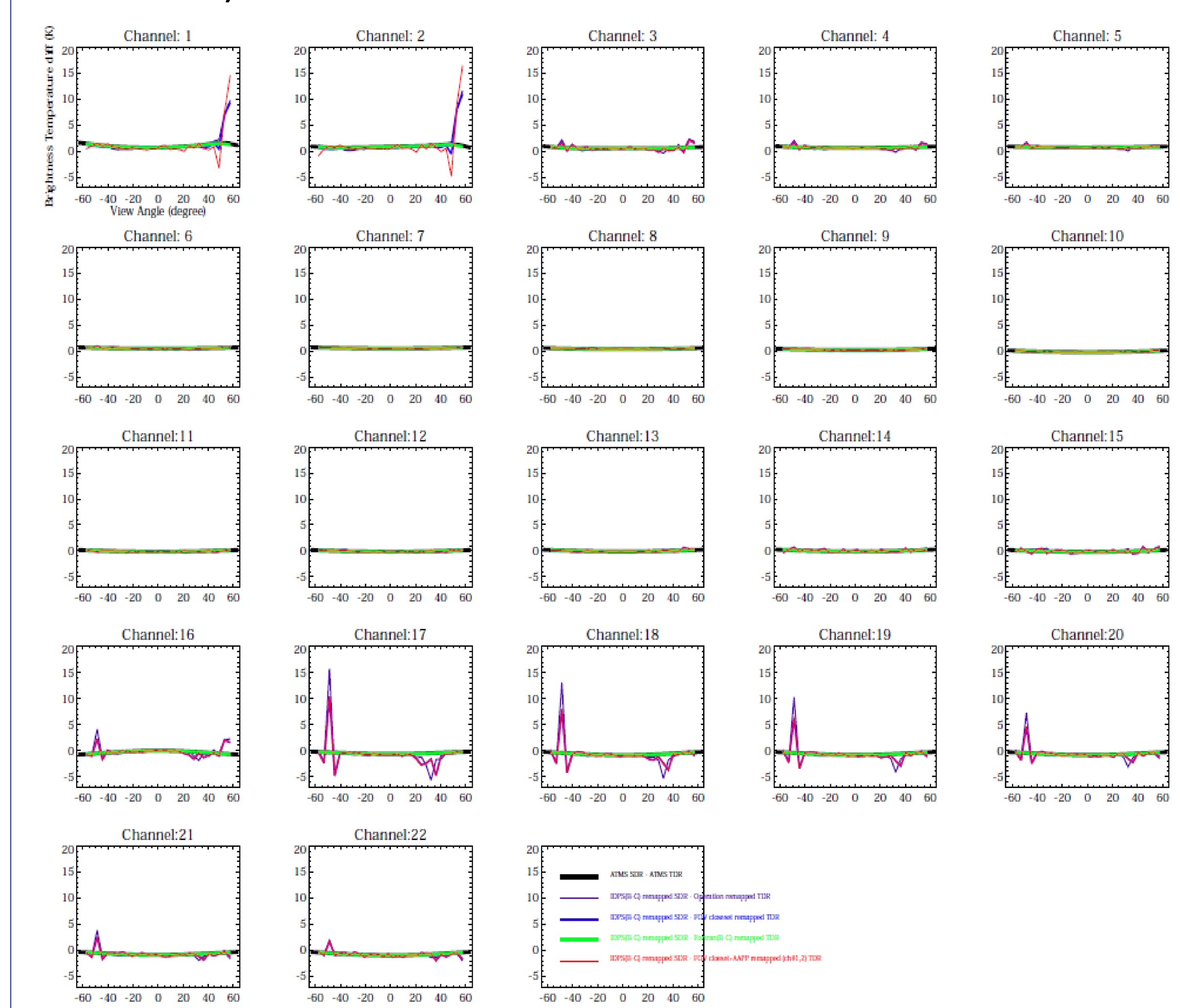

Performance Assessment (granule samples in "red" area, 5/30/2013)

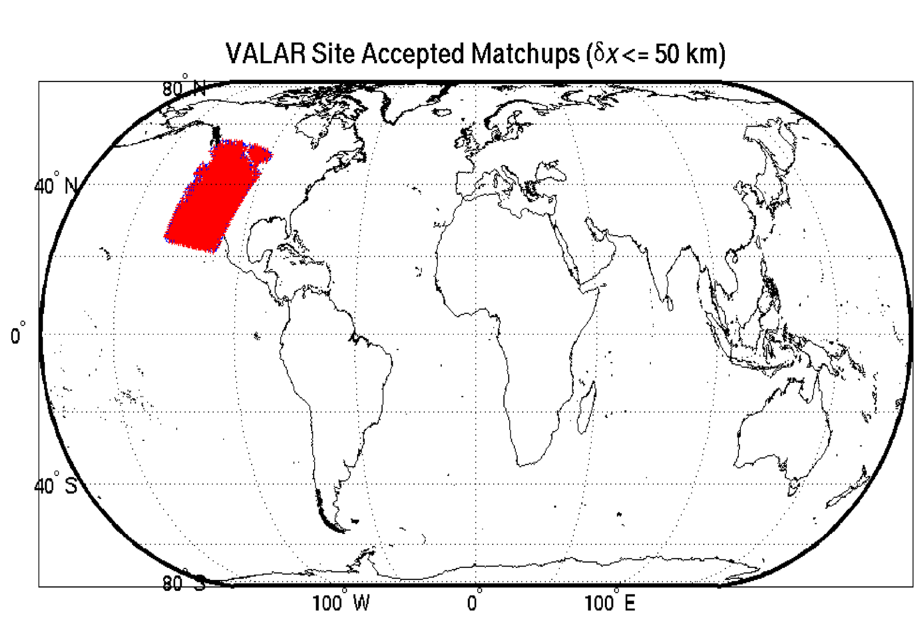

Performance Assessment

With Method 1

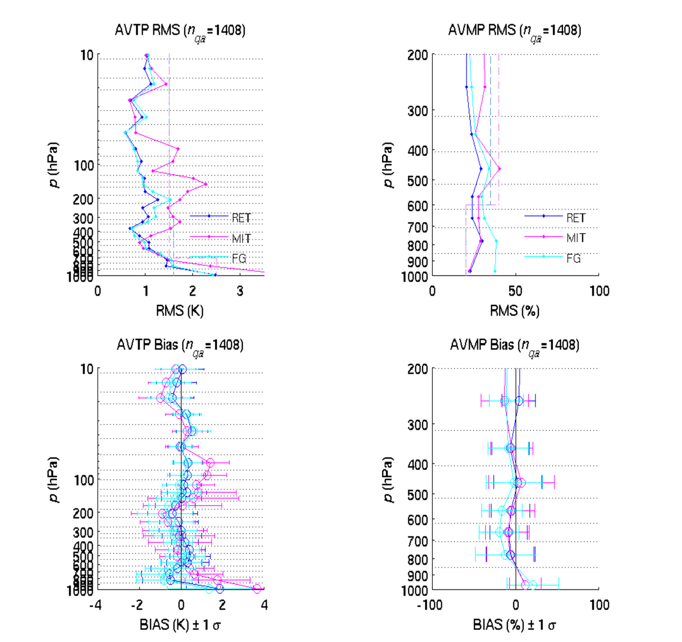

With Method 2

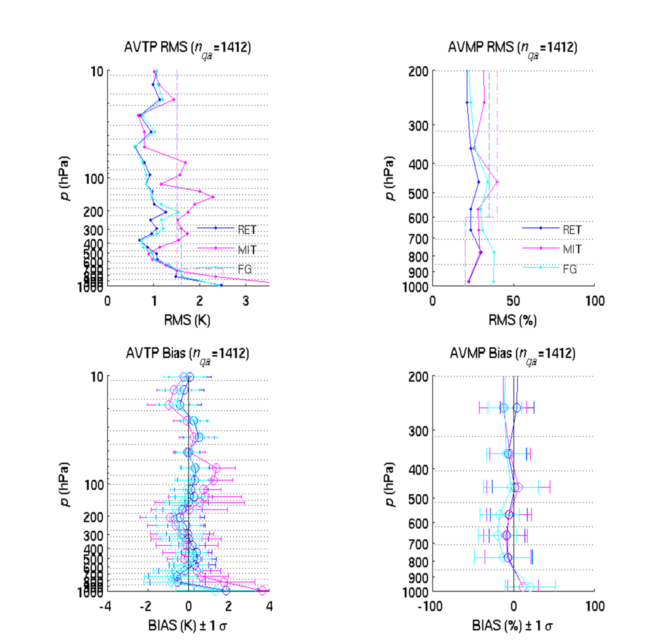

With Method 3

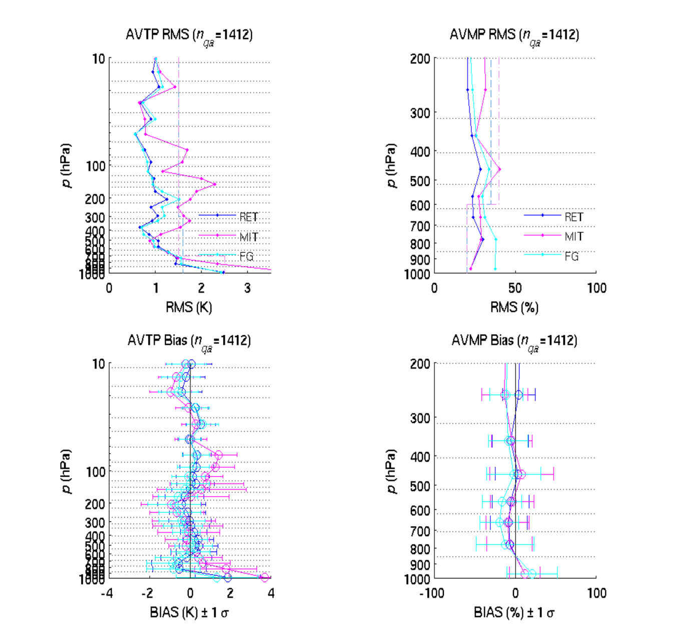

With Method 4

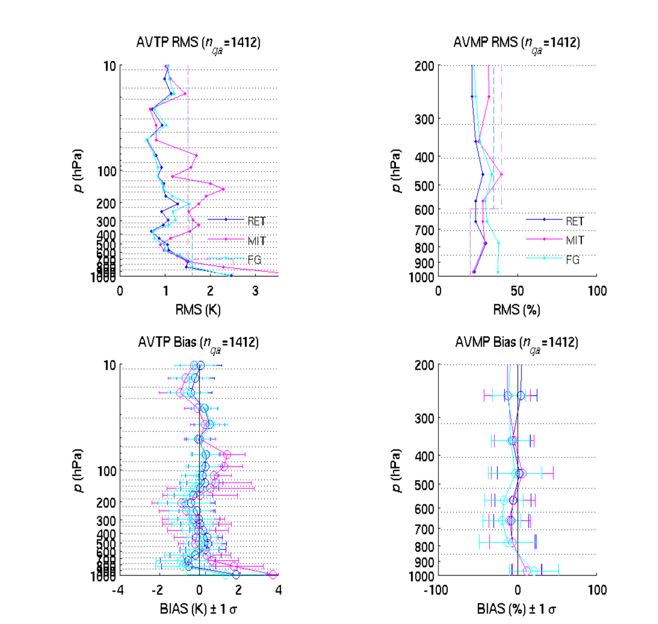

Summary

- All the four CrIS/ATMS match-up methods are computationally efficient enough to meet the real time operational requirements.
- The B-G method shows remarkable systematic corrections and positive impacts on the final retrieval products with an improved yield rate.
- We will focus on the B-G method improvements in the path forward and apply this method on the Joint Polar Satellite System (JPSS) series satellites.

References

[1] C. Barnet, M. Goldberg, L.E. Gumley, A. Gambacorta, E. Maddy, and T. King, "Implementation of the NOAA Unique CrIS/ATMS processing System (NUCAPS) within the Community Satellite Processing Package (CSPP)," *American Meteorological Society*, Atlanta GA, February 2014.

[2] A. Gambacorta, C. Barnet, W. Wolf, T. King, N. Nalli, K. Zhang, X. Xiong, E. Maddy, F. Iturbide Sanchez, C. Tan and M. Goldberg, "The NOAA Unique CrIS/ATMS Processing System (NUCAPS): algorithm description and validation results after 2 years in orbit," *American Meteorological Society*, Atlanta GA, February 2014.

[3] C. Wang, D. Gu, A. Foo, G. De Amici, F. Weng, N. Sun, B. Li, and R. V. Leslie, "Remapped ATMS Radiance and its Validation for NPP Mission," *American Meteorological Society*, Atlanta GA, February 2014.

Poster # 6, STAR JPSS Annual Science Team Meeting, August 25, 2015, College Park, MD

Corresponding Author: Changyi.Tan@noaa.gov

Ongoing Monitoring and Validation of NOAA-Unique CrIS/ATMS Processing System (NUCAPS) Using NPROVS and its Expansion

Bomin Sun[1], Tony Reale[2], M. Pettey[1], F. Tilley[1], N. R. Nalli[1], Chris Barnet[3], Quanhua (Mark) Liu[2]

[1]I. M. Systems Group, Inc., Rockville, MD, USA, [2] NOAA/NESDIS/STAR, College Park, MD, USA, [3] STC, Columbia, MD, USA

Introduction

The NOAA-Unique CrIS-ATMS Processing System (NUCAPS) was developed by the NOAA/NESDIS Center for Satellite Application and Research (STAR) and has been running operationally at the NOAA/NESDIS Office of Satellite and Product Operation (OSPO) since 2013. In this report, we present the ongoing activity of monitoring and validation of the NUCAPS IR+MW and MW-only temperature and water vapor retrievals using the NOAA Products Validation System (NPROVS) and its expansion (NPROVS+), which are supported by the NOAA Joint Polar Satellite System (JPSS) EDR cal/val program.

The NUCAPS retrieval characteristics performance is analyzed using multiple reference datasets and compared with legal retrieval products. This validation is conducted in a variety of meteorological conditions and intensive cal/val campaigns and in terms of long-term variability and short-term time-averaging statistics.

NPROVS

NOAA Products Validation System (NPROVS)

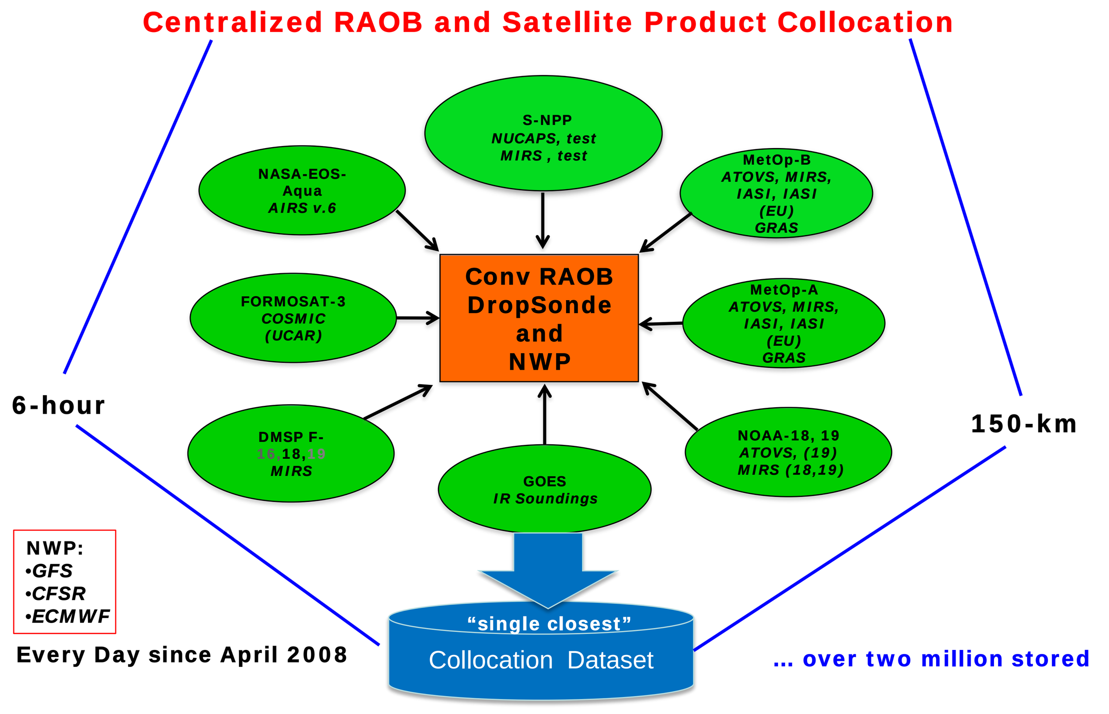

https://www.star.nesdis.noaa.gov/smcd/opdb/nprovs

NPROVS provides daily compilation of collocated conventional radiosonde observations (RAOBs) and derived satellite soundings from multiple satellites and product systems. The collocation strategy is consistent for all satellite products, including 6 hr/150 km time/space window, and "single, closest" satellite profile to a given sonde from each satellite product.

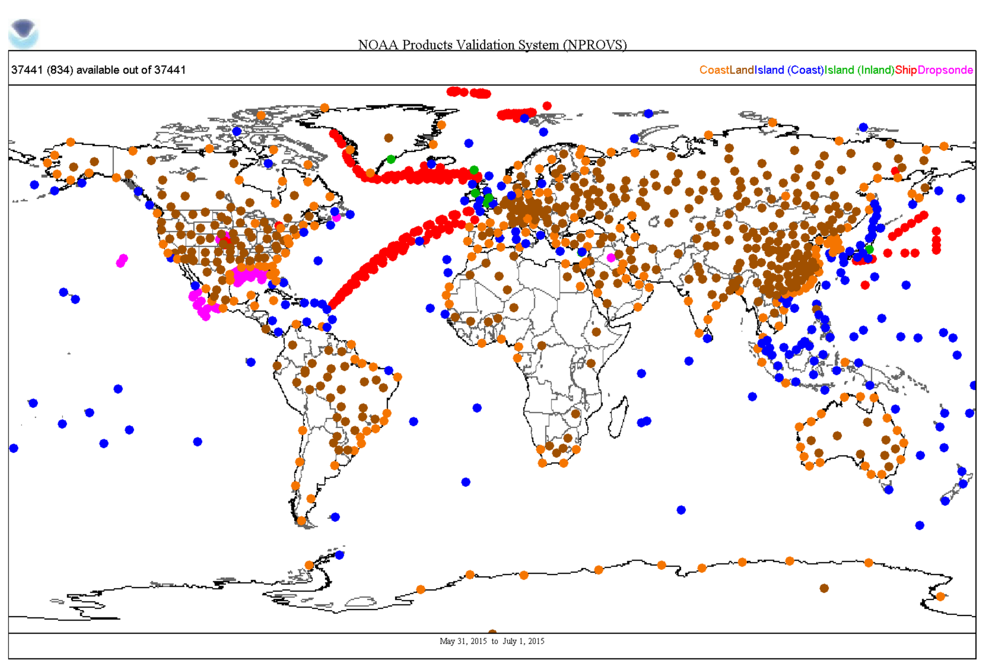

Map of sites of global operational radiosonde observations that are used as the anchor to collocate satellite data in NPROVS. Data of June 2015 are shown as an example. Different colors represent different terrain types of RAOBs.

NPROVS +

NPROVS+ leverages from NPROVS by providing daily compilation of collocated Global Reference Upper Air (GRUAN) and Dedicated RAOBs with satellite sounding and sensor data from multiple satellite product/sensor suites. The collocation strategy identifies the "single, closest" satellite profile to a given RAOB but also stores all products and sensor data within 500km of the RAOB, denoted as "granules", for supporting retrieval algorithm development.

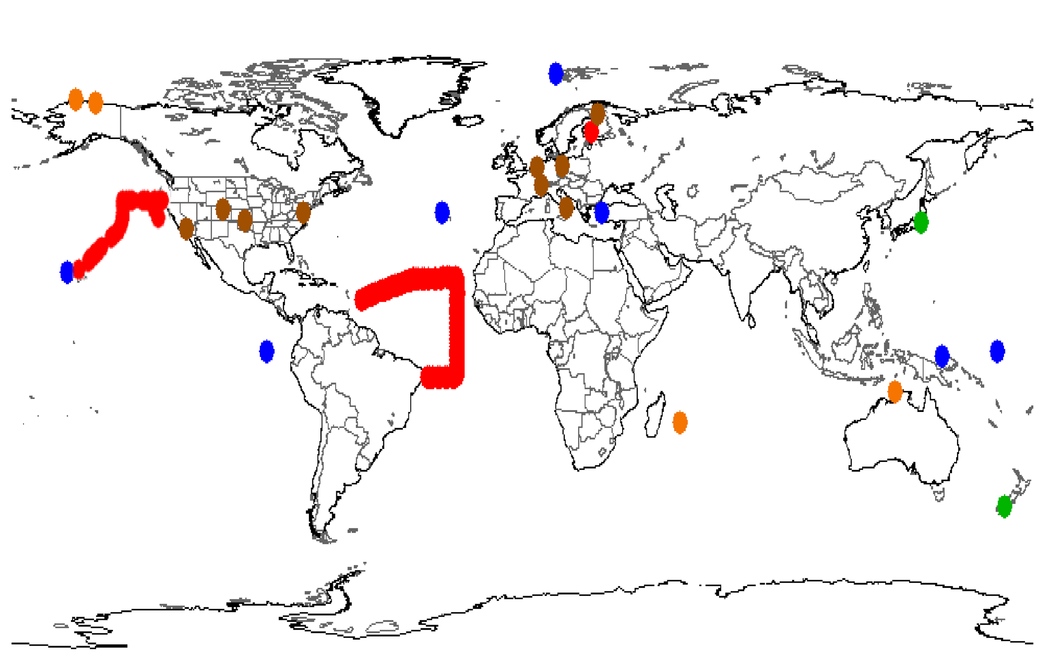

GRUAN processed RAOB (Vaisala RS92) are directly accessed from the DWD Lead Center (LC) and retain all qc checks and processing details appended by the LC. JPSS funded dedicated RAOB (also Vaisala RS92) synchronized to satellite overpass are accessed from ARM site holding files. This program also supports dedicated RAOBs launched in NOAA AEROSE and CALWATER/ACAPEX campaigns.

Long-term Monitoring

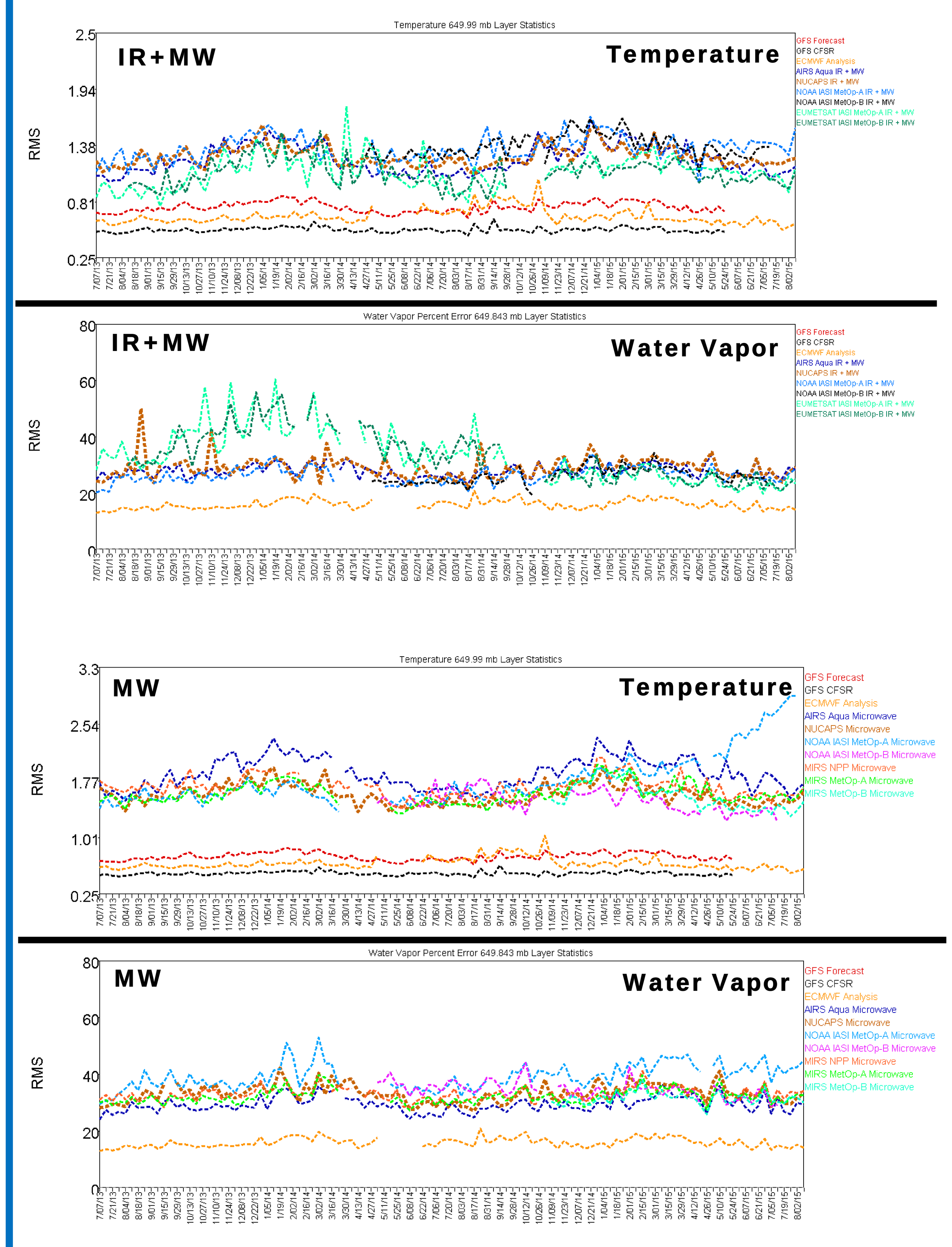

Root-Mean-Square (RMS) differences between satellite retrieval and RAOB data based on weekly global **maritime** data of July 2013 through July 2015. The statistics are at ~1-km layer for temperature (K) and ~2-km layer for water vapor mixing ratio percentage (%). Thicker curves denote NUCAPS data.

Short-term Monitoring/Analysis

a. MW temperature retrieval comparison: NUCAPS *vs.* S-NPP MiRS

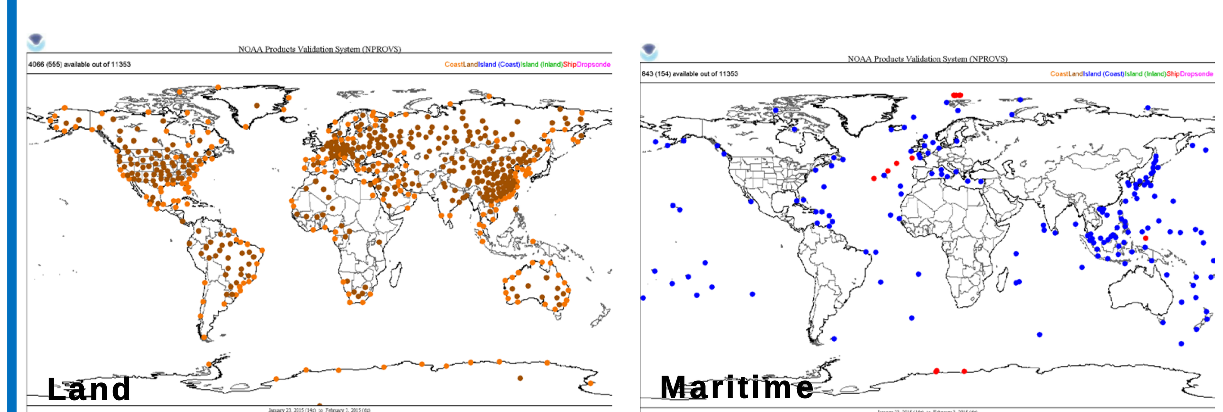

RAOB collocations common to both NUCAPS and S-NPP MiRS retrievals during 01/23 – 02/03 2015. Collocations with 6-hr and 150-km window are used to compute the statistics.

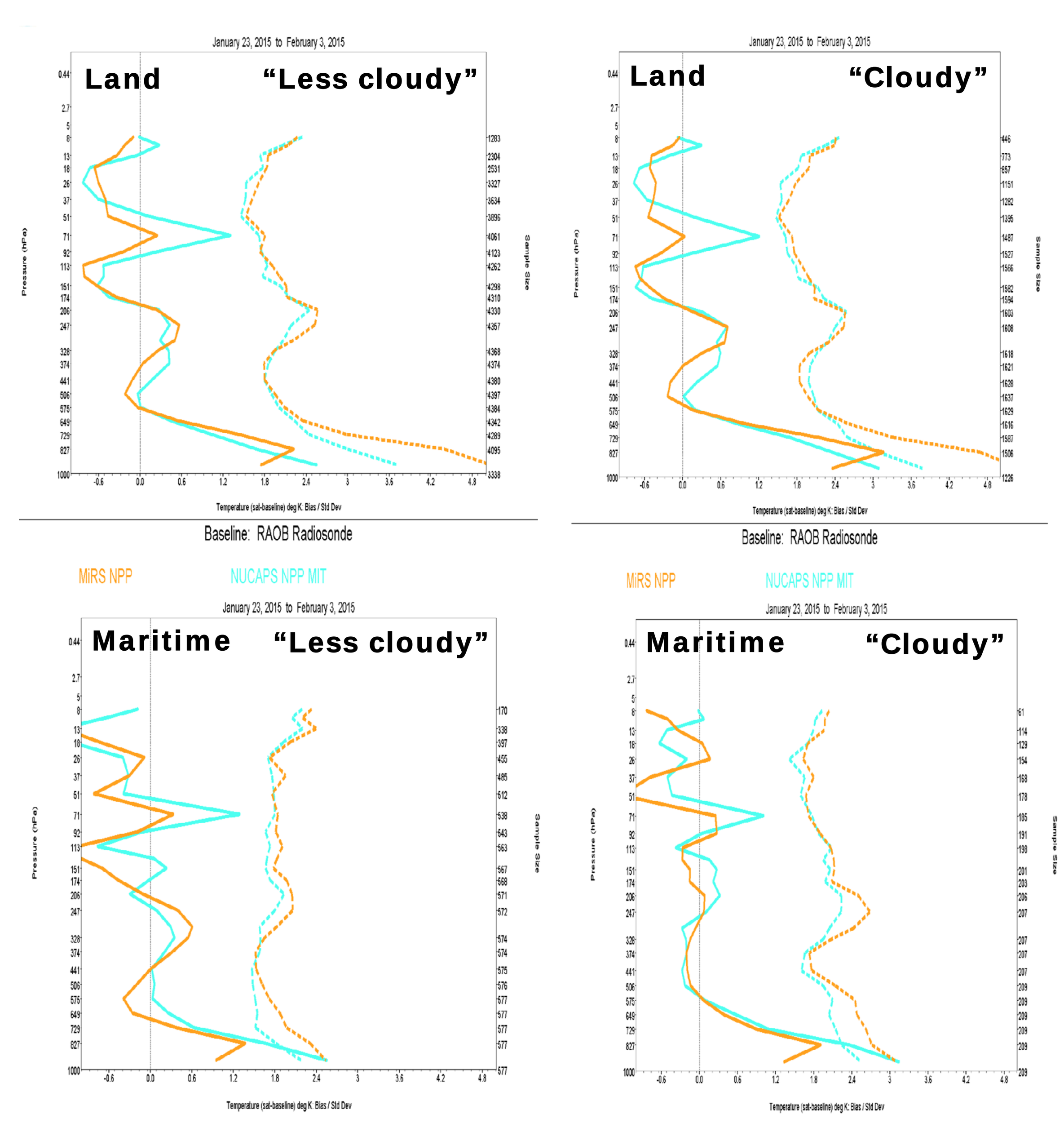

Coarse-layer MW temperature RMS differences from RAOB statistics. "Less cloudy" cases are the ones that pass NUCAPS IR+MW qc, and "Cloudy" cases are the ones that pass NUCAPS MW retrieval qc.

Continued

b. NUCAPS IR+MW in Intensive field cal/val campaigns

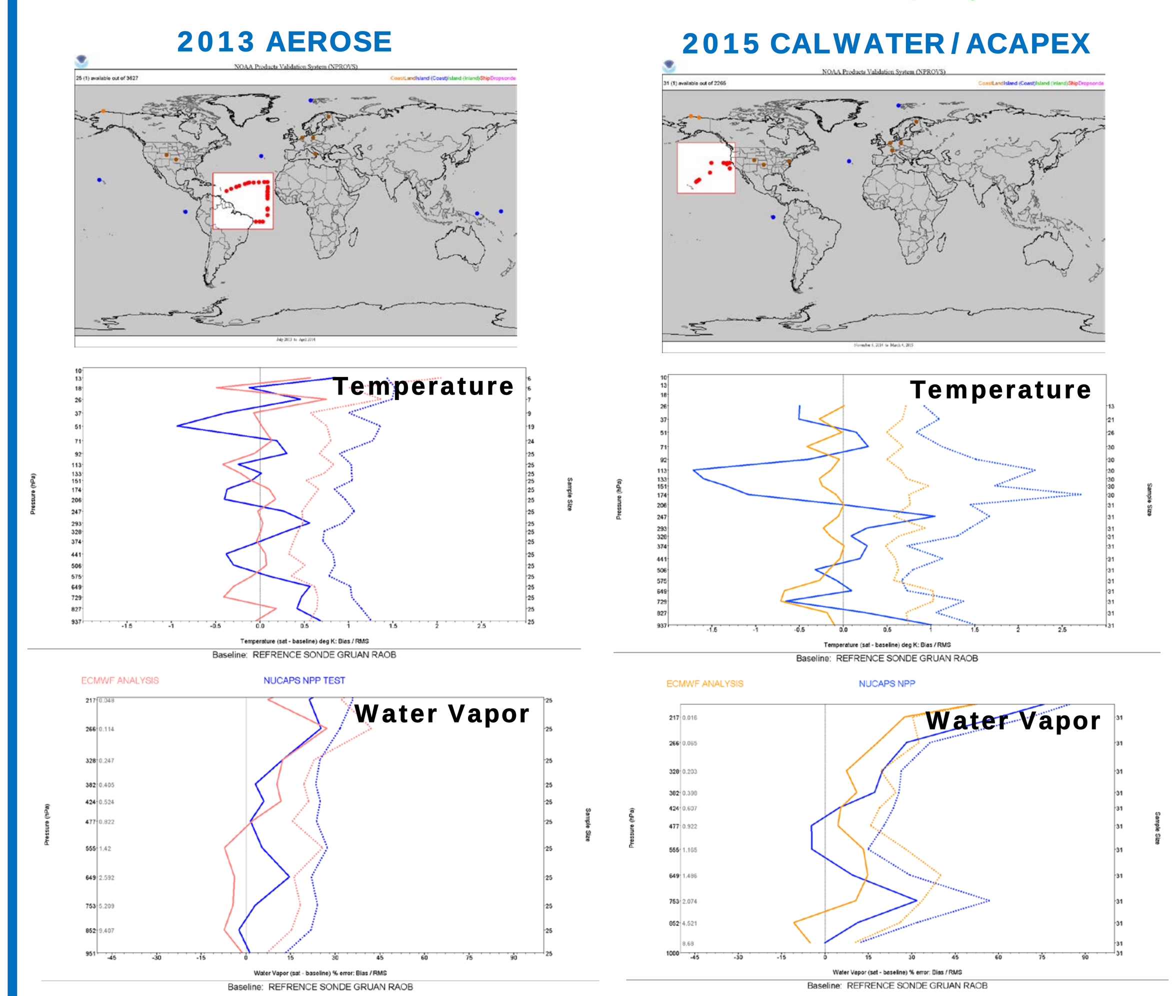

NUCAPS MW retrieval mean bias (solid) and RMS difference (dotted) from RAOBs. Collocations with 3-hr and 100-km of 2013 AEROSE (November 2014 through December 2013) and 2015 CALWATER/ACAPEX (January 2015 through February 10 2015) data are used. The statistics are in coarse layers.

c. AWIPS II Alaska Cold Core Event

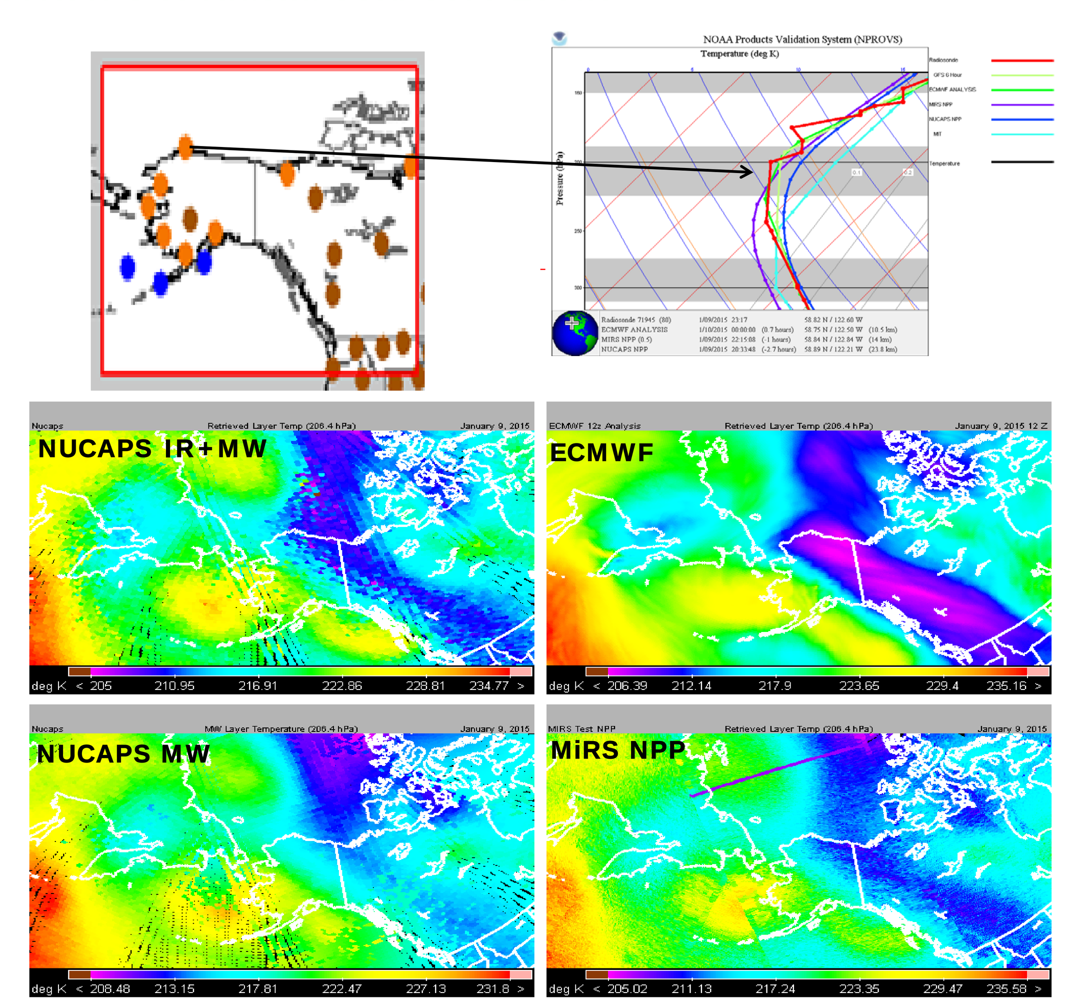

Alaska Cold Core case (with temperature below 201 K at ~10 km altitude) in January 9 2015. ECMWF and satellite retrieval temperatures are at around 206 hpa.

d. NUCAPS oper vs. test version

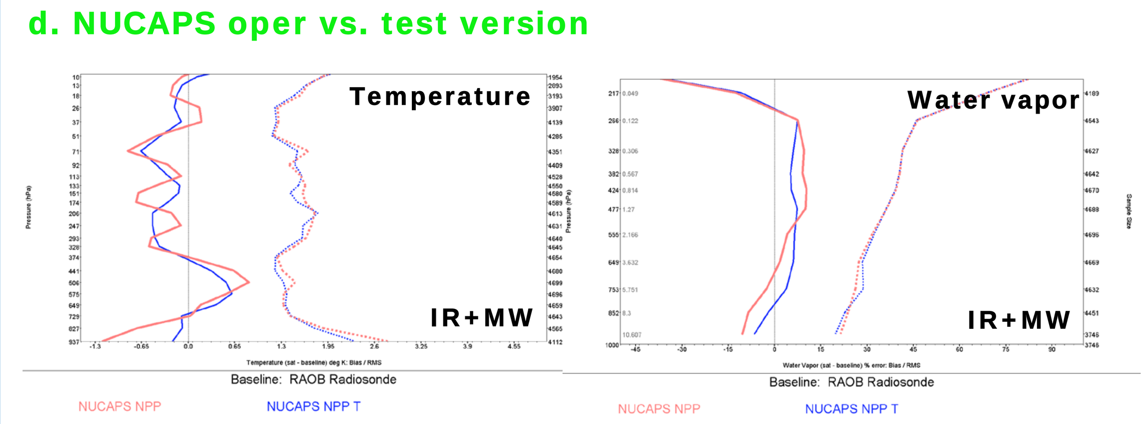

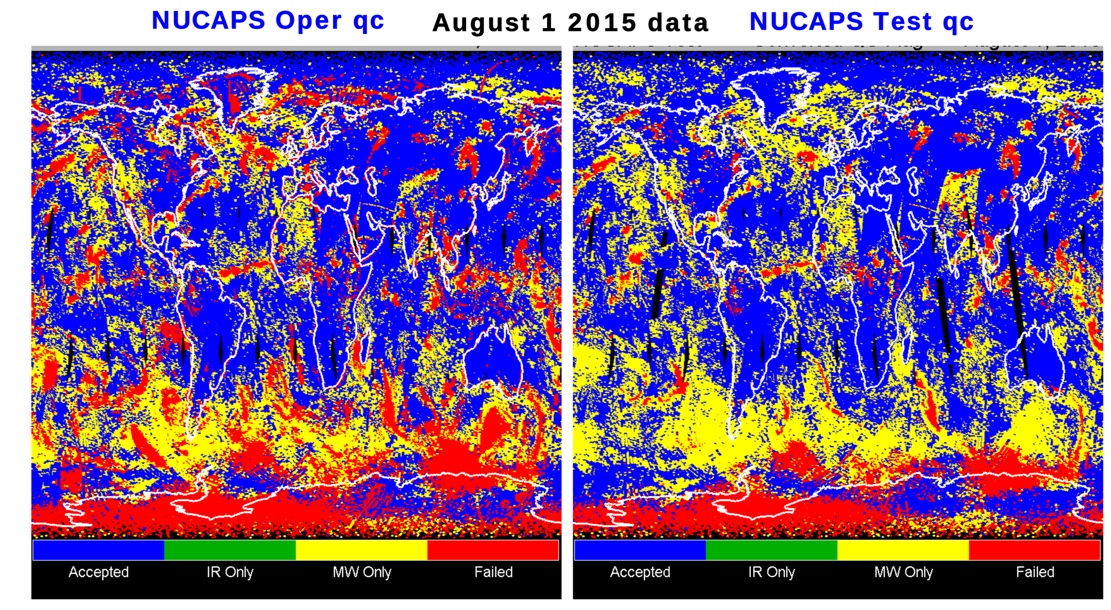

NUCAPS production test version is running at STAR. Among the improvements in the test version over the oper include using four days of ECMWF analysis data to generate regression coefficients for creating the IR first-guess and fixing some bugs in the retrieval processing code. The vertical statistics (bias and RMS) are computed using global data of July15-26 2015. The qc maps are for data of August 1 2015.

Summary

This presentation demonstrates the unique capability of NPROVS and its expansion (NPROVS+) in routine monitoring and analysis of NUCAPS and other satellite products characteristics performance and in retrieval algorithm development activities.

STAR Center for Satellite Applications and Research

Poster #, 2015 STAR JPSS Annual Science Team Meeting, 24-28 August 2015, NCWCP, College Park, MD (Corresponding author: Bomin.Sun@noaa.gov)

Graphical Programs For The Validation Of Satellite Sounding Products With The NOAA Products Validation System (NPROVS)

Michael Pettey[1], Charles Brown[1], Anthony Reale[2], Bomin Sun[1]

(1) I.M. Systems Group, Inc., Rockville, Maryland (2) NOAA/NESDIS/STAR, College Park, Maryland

NPROVS

The NOAA Products Validation System (NPROVS) was designed within the NOAA/NESDIS Office of Satellite Applications and Research (STAR) to compare, evaluate and monitor the performance of multiple satellite systems.

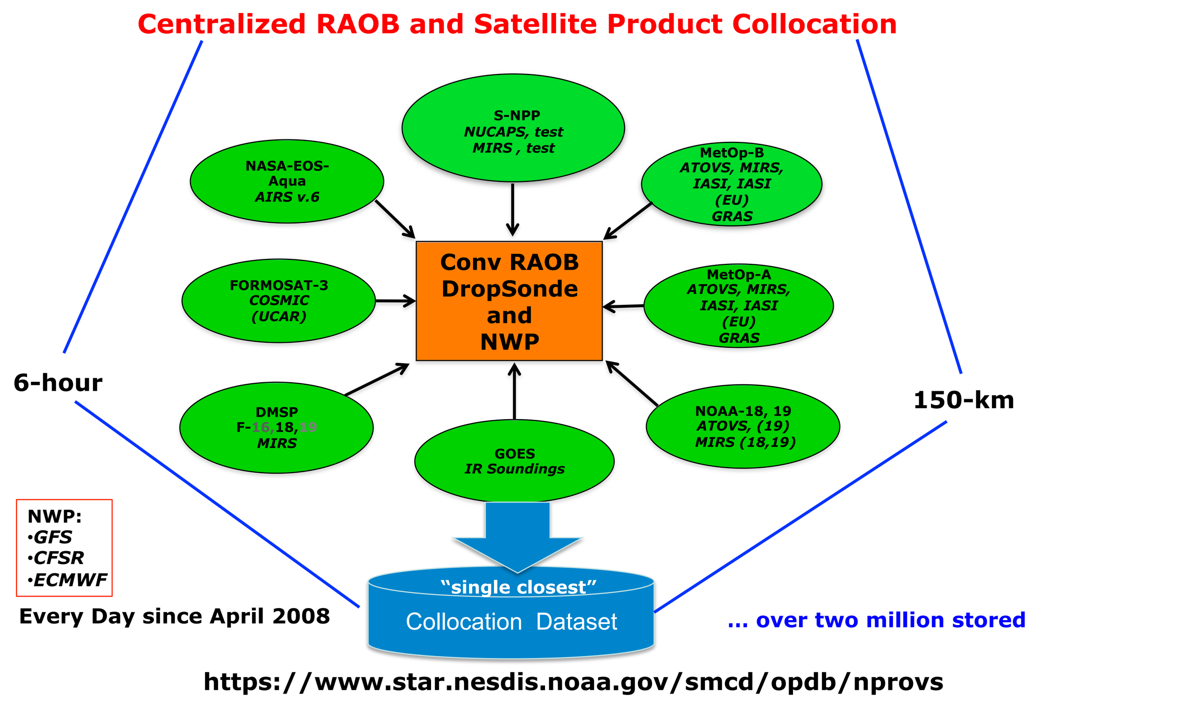

Selected sounding footprints from a variety of satellites and other processing systems are collocated with ground truth data, typically radiosonde data, by locating a footprint that is closest to the ground truth in space and time. Once collocated, the system data can be compared to the ground truth and to other systems.

The collocated data can be accessed by anyone interested in characteristic performance of the satellite derived products. Daily, weekly and monthly collocation files are made available in binary and netCDF formats.

As part of NPROVS, a set of graphical programs was developed to allow users to view and compare the NPROVS data. The **NPROVS Archive Statistics (NARCS)** provides a long-term view of the performance of each system. **ProfileDisplay (PDISP)** shows individual collocation data and computes vertical accuracy statistics of temperature and moisture profiles. The **Orbital Display System (ODS)** shows images of associated orbital data.

Accessing And Running The Programs

All of the graphical programs are written in Java and can be run on a variety of operating systems including Macintosh OS X, Linux and Windows. For most people, accessing and running the programs is as simple as copying the program to a local computer and double-clicking the icon. More information about running the programs is available in the Quick Start Guide for each program.

Links to the programs and quick start guides for each one are available on the STAR NPROVS web site. The pages for each program also contain links (via anonymous FTP) to the data files used by the graphical programs.

The main NPROVS page:
http://www.star.nesdis.noaa.gov/smcd/opdb/nprovs/index.php

Orbital Display System (ODS):
http://www.star.nesdis.noaa.gov/smcd/opdb/nprovs/ods.php

ProfileDisplay (PDISP):
http://www.star.nesdis.noaa.gov/smcd/opdb/nprovs/pdisp.php

NPROVS Archive Statistics (NARCS):
http://www.star.nesdis.noaa.gov/smcd/opdb/nprovs/narcs.php

Questions about NPROVS and specific requests for data access can be directed to Tony.Reale@noaa.gov

ProfileDisplay (PDISP)

Displays temperature and moisture profiles for the ground truth (RAOB) and every collocated processing system. All available raw data produced by each system and the associated ground truth can be viewed both graphically and as raw text.

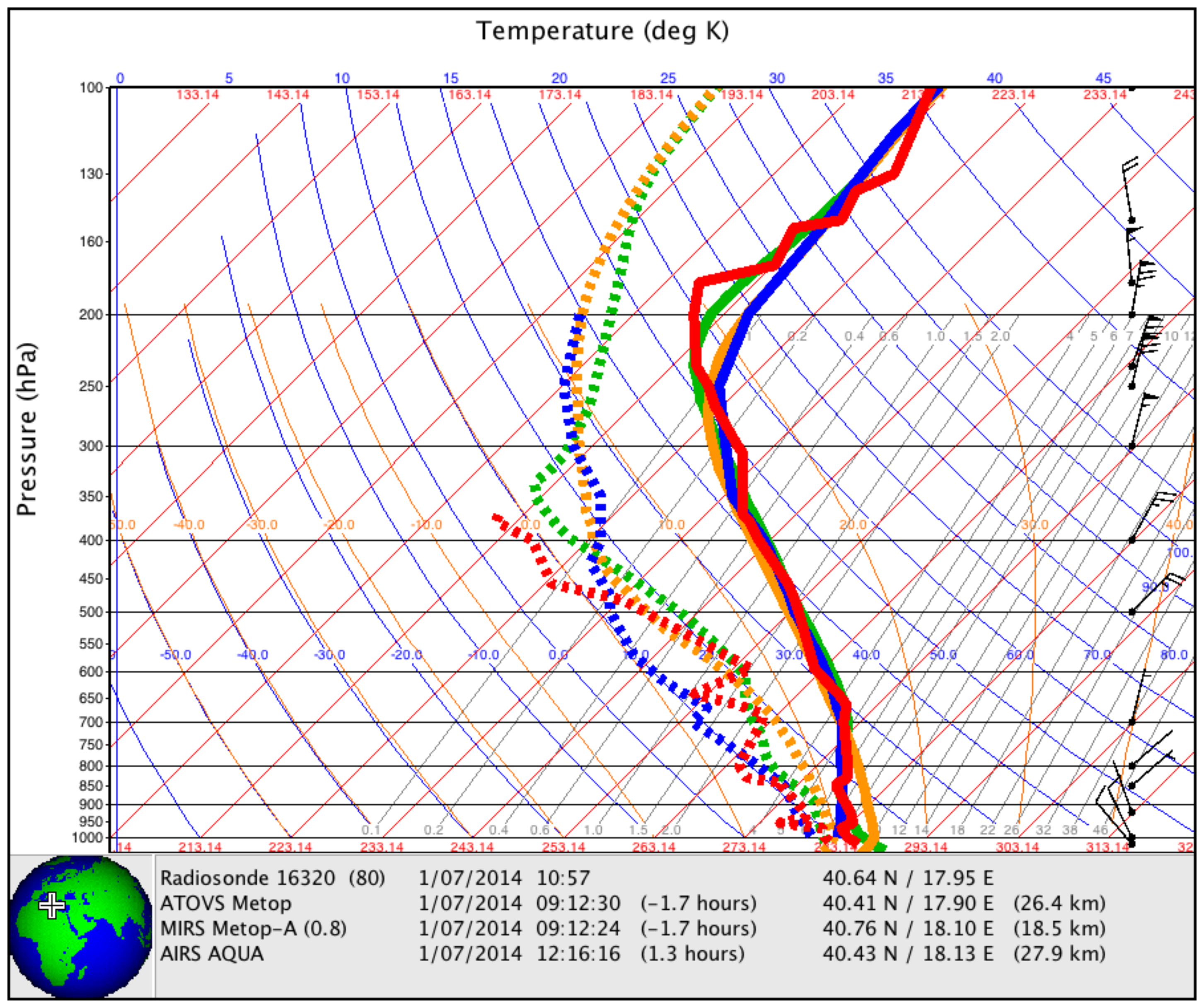

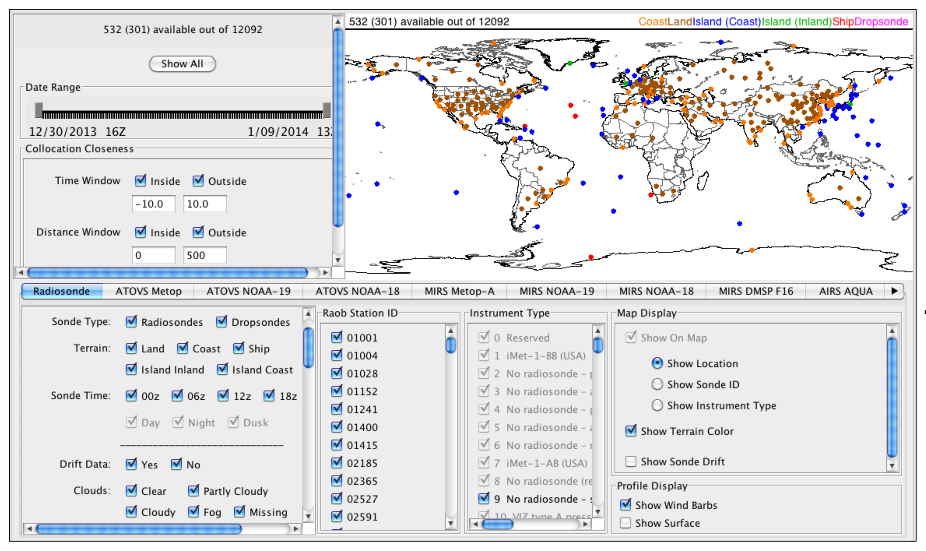

Data filtering capabilities allow for comparison and statistic generation for a user-defined subset of data

The map can be used to view the distribution of collocations as well as other features such as radiosonde balloon drift

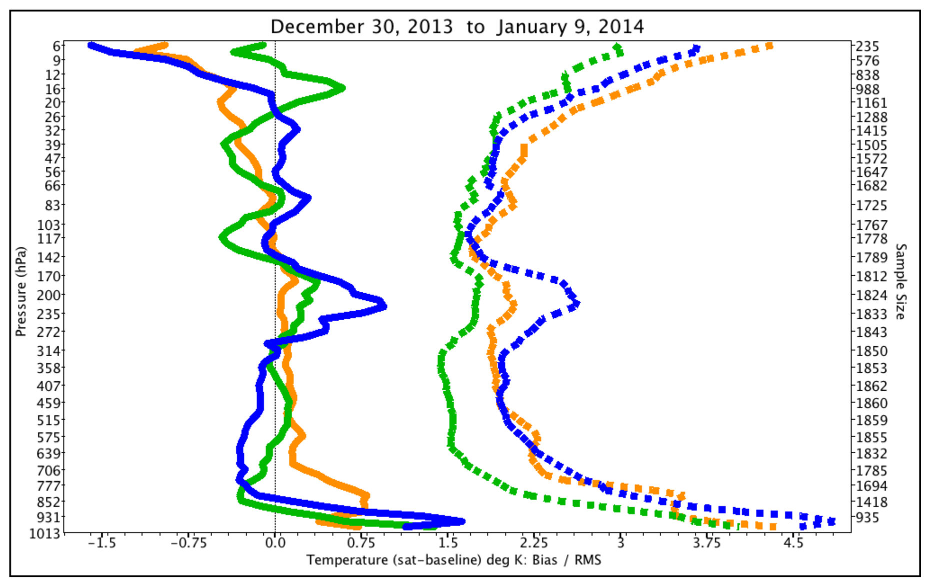

Satellite minus baseline vertical accuracy stats for temperature and water vapor can be generated for user-selected subsets of available collocations.

Bias, RMS and standard deviation statistics can be generated.

Scatter plots are available for user-selected satellite, ground profile data and collocations

These plots are available for temperature and moisture at every pressure level

Any collocation on the plot can be selected to quickly view the graph of the profiles from the collocation

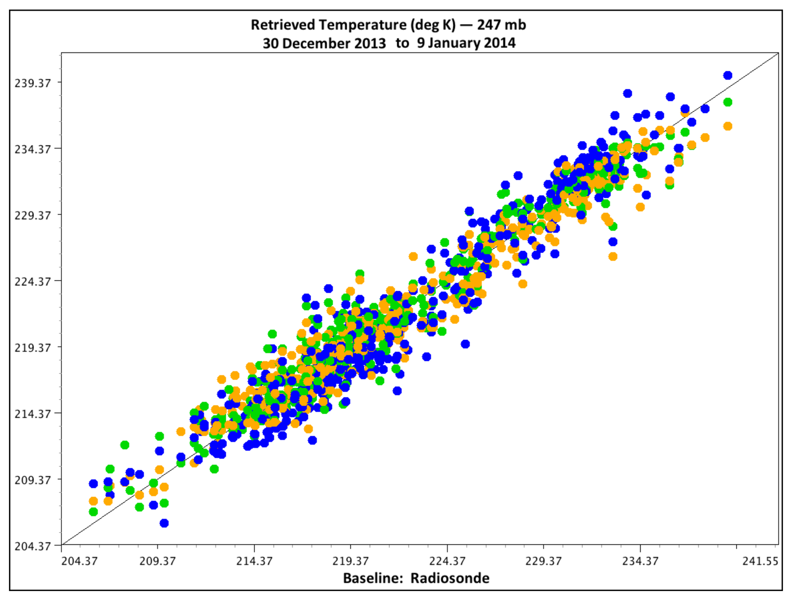

Orbital Display System (ODS)

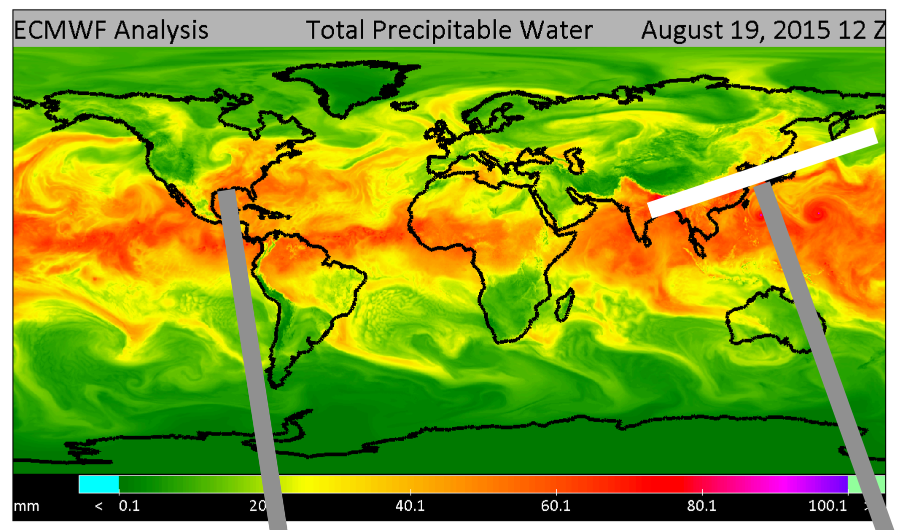

Graphical display of data from every product system used by NPROVS.

Views of the data can be customized using projection, zooming, smoothing and other controls.

Any location on the image can be clicked to display a graph that shows profiles and raw data from the selected location. A line can be drawn across an image to display a vertical cross sections of the atmosphere.

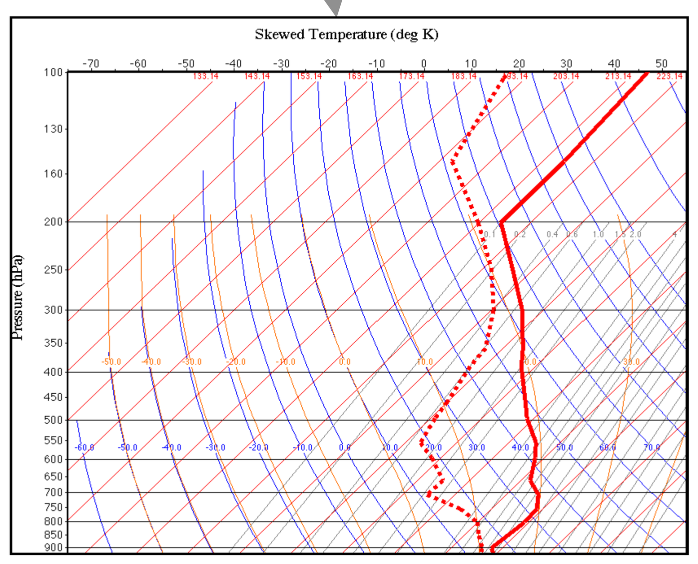

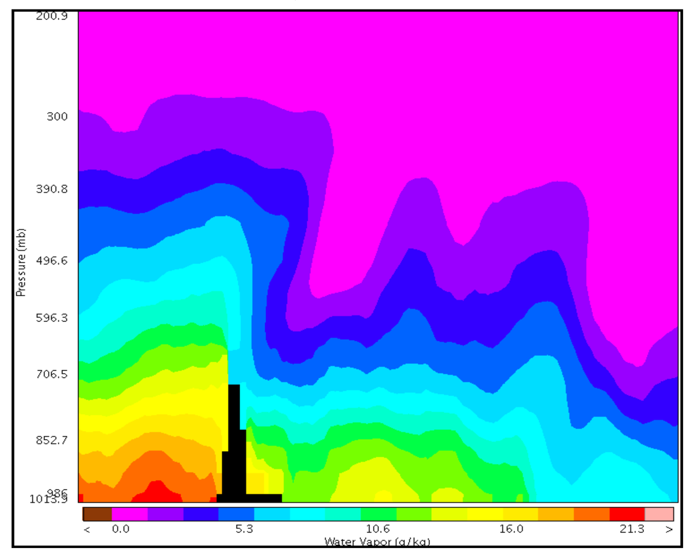

Two parameters from the same system or from different systems can be compared by using built-in math functions to subtract one image from another. White shows areas of agreement while red/blue show areas of disagreement.

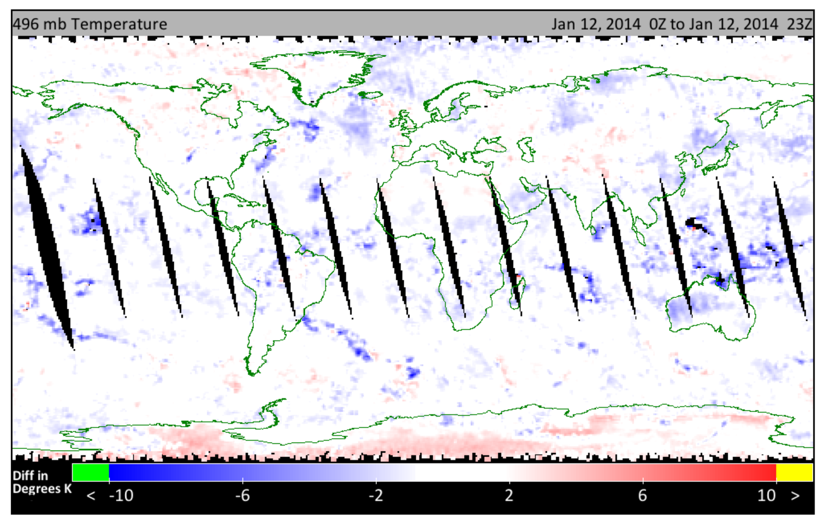

NPROVS Archive Statistics (NARCS)

Provides long-term trends of satellite minus baseline differences. Includes daily, weekly and monthly statistics of bias, standard deviation and rms.

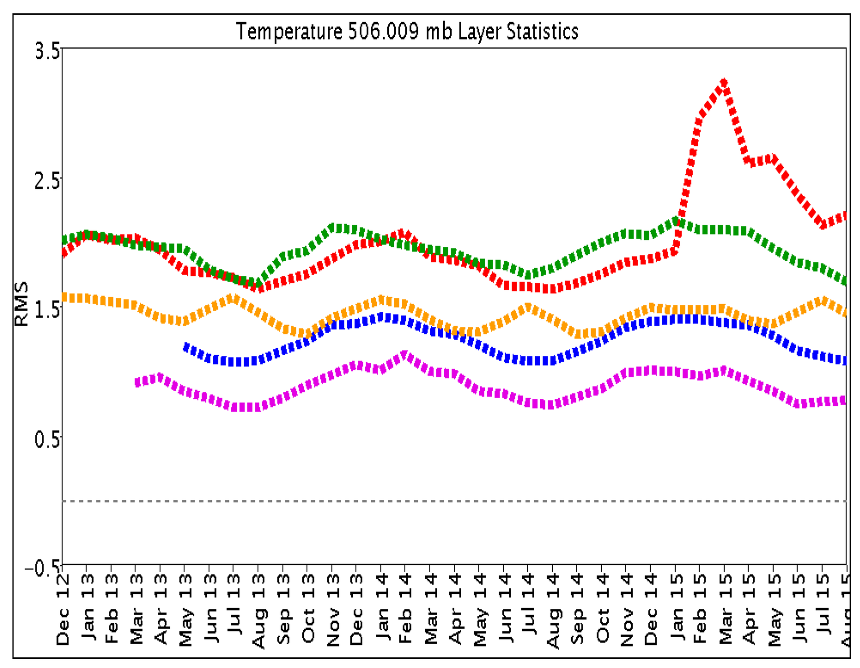

Temperature and water vapor statistics are available at pre-defined pressure levels and layers.

Statistics based on user-selected options (qc flag, terrain type, and retrieval type) can be displayed.

Long-term trends for a selected system at pre-defined pressure levels or layers can be displayed.

Red and blue blocks show warm and cold biases between the system and baseline system at each pressure and time period (day, week or month).

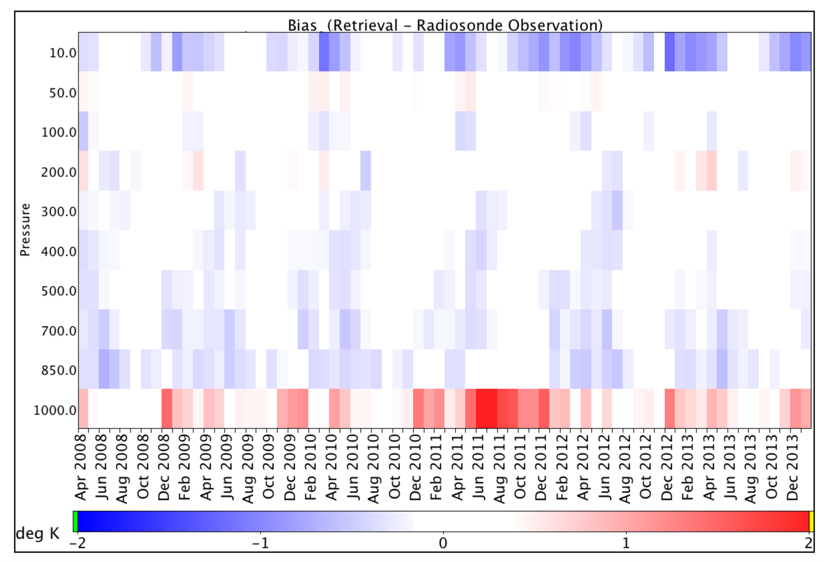

STAR Center for Satellite Applications and Research

Corresponding Author: Michael.Pettey@noaa.gov

I.M. Systems Group, Inc.

Evaluating SNPP CrIS Spectral Noise from 2012 to 2015 with Allan Deviation

Xin Jin[1], Yong Han[2], Ninghai Sun[1], Fuzhong Weng[2], Denis Tremblay[3], Yong Chen[4], Likun Wang[4]

[1] ERT, Inc., [2] NOAA/NESDIS/STAR, [3]Science Data Processing, Inc.,[4]UMCP Contact: Xin.jin@noaa.gov

Abstract

The Cross-track Infrared Sounder (CrIS) onboard the S-NPP (Suomi National Polar-orbiting Partnership) satellite has been running for about three and a half years. The spectral noise and response are analyzed in this presentation. The Allan deviation , which is effective in removing drifting trend in a time series, is used to calculate the spectral noise for each orbit. CrIS has three bands (LW/MW/SW). Each band has 9 field-of-views (FOVs) scanning in two directions. Four wavenumbers of each band are selected to show the temporal evolution: 650/720/830/1050 cm^{-1} for LW, 1240/1375/1580/1710 cm^{-1} for MW, 2150/2210/2355/2515 cm^{-1} for SW. It is found that the real part noise of the hot reference has almost no change since the beginning of the mission, indicating a sustainable stable sensor status. The imaginary part noise of the cold reference is very sensitive to the stability of the platform.

NEDN: ICT Real

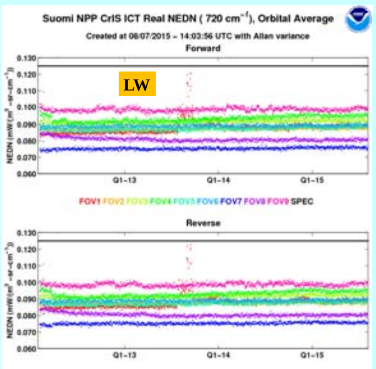

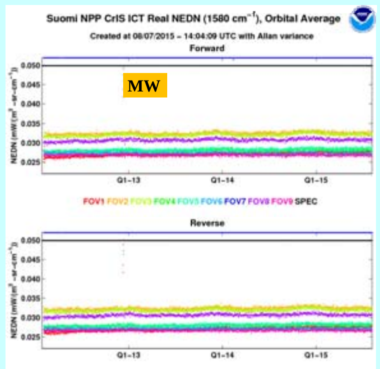

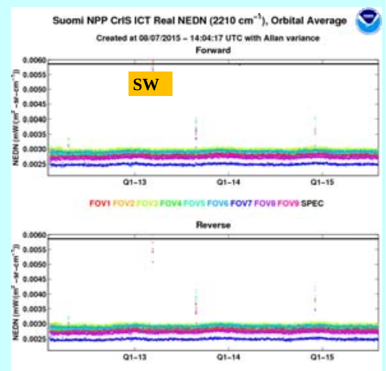

NEDN: DS Imaginary

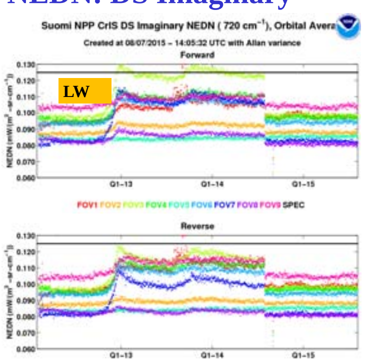

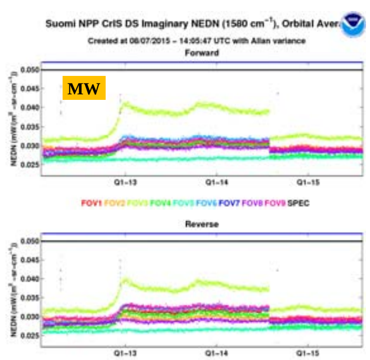

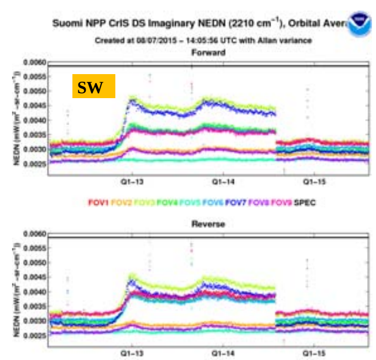

Gain

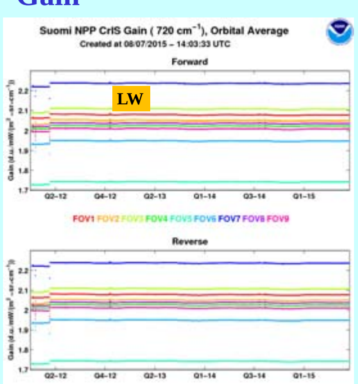

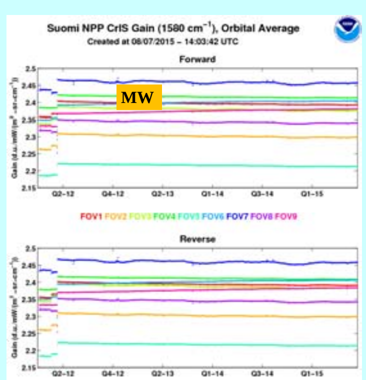

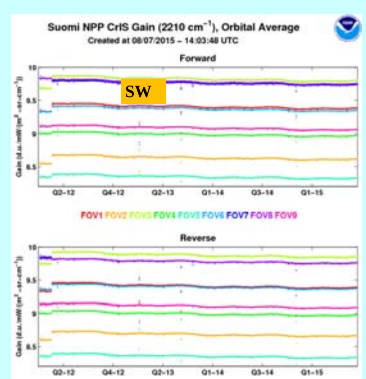

Method:

Step 1: Derive Gain of each orbit:

$$Gain = \frac{\langle S_{ICT} \rangle - \langle S_{DS} \rangle}{\langle P_{ICT} \rangle}$$

where S is the spectral count per scan; DS and ICT represent the cold and hot reference, respectively; P is the blackbody radiance; <> is the orbital average operator.

Step 2: Derive the radiance of reference target per scan:

$$R_{ICT} = \frac{S_{ICT} - \langle S_{DS} \rangle}{Gain}$$

$$R_{DS} = \frac{S_{DS} - \langle S_{DS} \rangle}{Gain}$$

where R_{ICT} and R_{DS} and are complex value.

Step 3: Derive the NEDN with Allan deviation:

$$\sigma_y^2(\tau) = \frac{1}{2}\langle(\bar{y}_{n+1} - \bar{y}_n)^2\rangle = \frac{1}{2\tau^2}\langle(x_{n+2} - 2x_{n+1} + x_n)^2\rangle$$

Conclusions:

The CrIS spectral noise is analyzed with Allan variance method. Most of the drifting effect is removed and it is found that CrIS sensors have very stable noise features in term of the hot reference, except the LW FOV1 which suffered a sudden jump of noise between July and Sept. of 2013, before returning back to normal status. All of the sensors, except the MW FOV7 which is known very noisy before launch, have much lower noise relative to the specification. The imaginary part noise of the cold reference, however, is sensitive to the shaking of the satellite platform, especially for the corner FOVs. ATMS main motor shaking in the late 2012 and the satellite orbital inclination angle adjustment on July 31, 2014 are two major events triggering the significant change of DS imaginary part noise.

The spectral response is also evaluated. It is found that the LW sensors have almost no degradation since the mission. The MW sensors have noticeable but different changes among difference sensors. All of the SW sensors have suffered a 2~3% degradation.

AHI Navigation and Radiometric Performance Assessment using VIIRS and Landsat 8

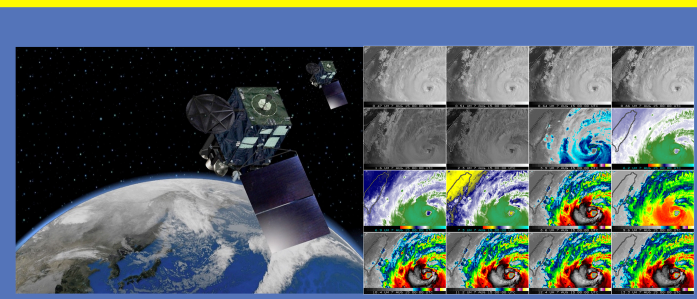

Mike Chu[1,2], Xiangqian Wu[2]

1. ERT, 2. NOAA/NESDIS/STAR – GOES-R Calibration Working Group

Introduction

The Advanced Himawari Imager (AHI) is the next-generation geostationary follow-on for the Japanese Meteorological Agency launched on October 7th, 2014. The instrument is a 16-band suite with 6 of the bands in the visible and near-infrared (VNIR) range. We use the matching moderate bands of the Visible Infrared Imaging Radiometer Suite (VIIRS) [1] to assess the multi-month radiometric response of the AHI VNIR bands from February to August, 2015 using deep convective clouds (DCC) near AHI sub-satellite point. To assess navigation accuracy we make Imagery comparisons of landmarks, both visual and quantitative, against VIIRS. We also present a preliminary high-accuracy comparison analysis against the 30m-resolution Landsat 8 imageries to quantify sub-100m AHI navigation deviations.

AHI			VIIRS		
Band Designation	Wavelength (μm)	Resolution (km)	Band Designation	Wavelength (μm)	Resolution (km)
1	0.47	1.0	M3	0.48	0.75
2	0.51	1.0	M3	0.48	0.75
3	0.64	0.5	M5	0.67	0.75
4	0.86	1.0	M7	0.87	0.75
5	1.60	2.0	M10	1.61	0.75
6	2.25	2.0	M11	2.25	0.75

The wavelengths and the resolutions of the AHI VNIR bands and the corresponding VIIRS moderate bands are well-matched

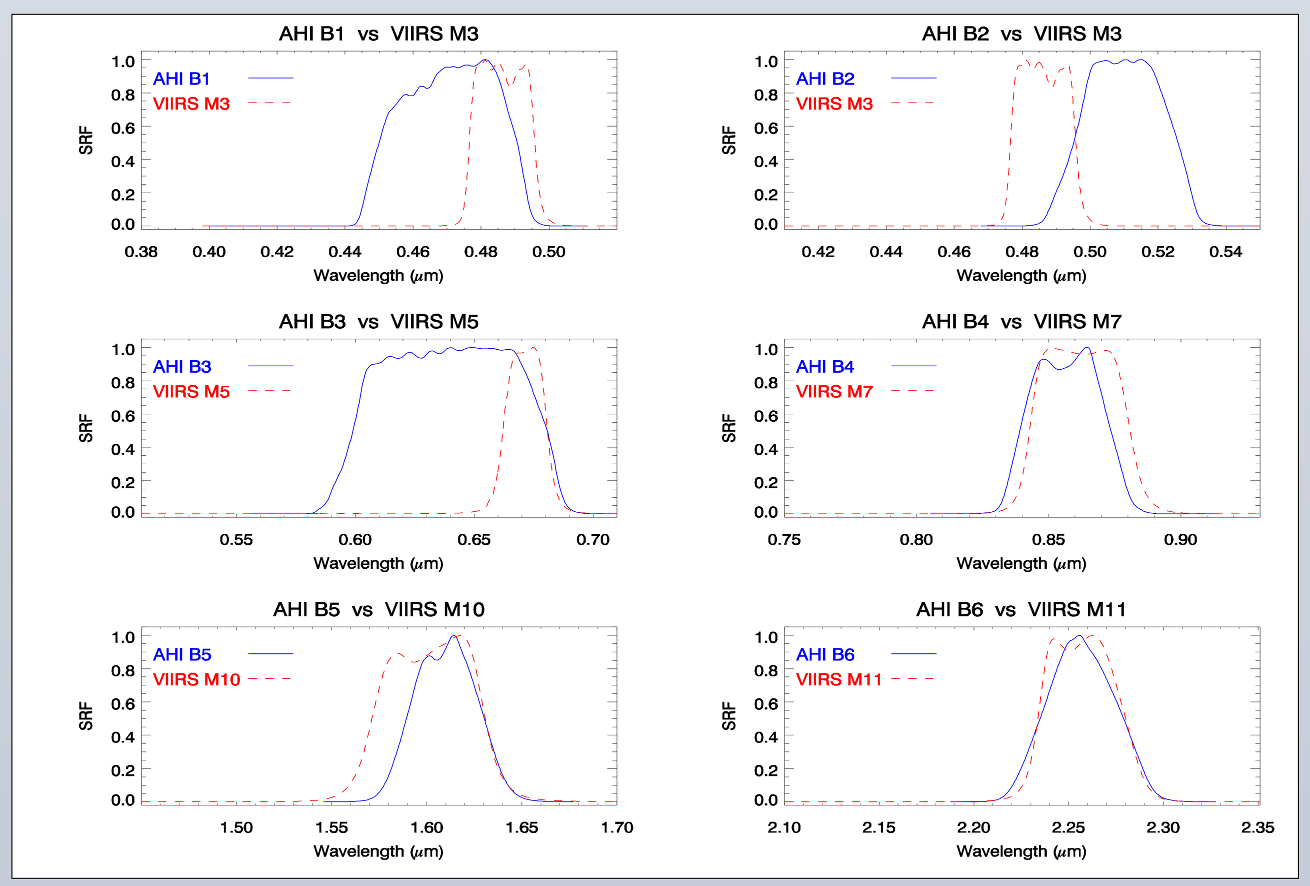

The spectral response functions of the AHI VNIR bands and the matching VIIRS bands.

Co-Registration, Frame-to-Frame Registration and Navigation Accuracy

The assessment of the AHI radiometric response against VIIRS is conducted at the single-pixel level, thus establishing both inter- and intra-bands pixel matching is necessary. Landmarks are used in examinations below.

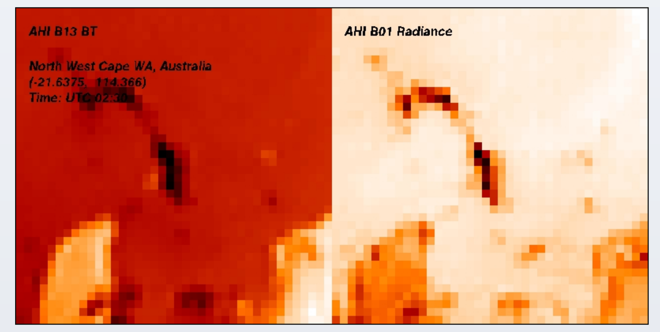

AHI Intra-band co-registration

- B13 (10.35μm) and VNIR bands match at sub-pixel (< .5 pixel)
- DCC pixels found by B13 and the corresponding VNIR bands radiance will correctly match

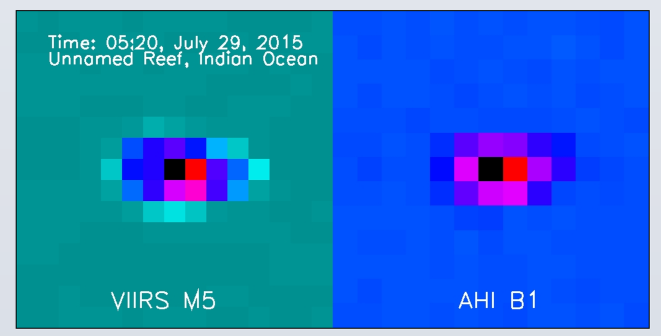

AHI navigation against VIIRS

- VIIRS navigation is accurate
- AHI B3 shows similar accuracy at UTC-0520

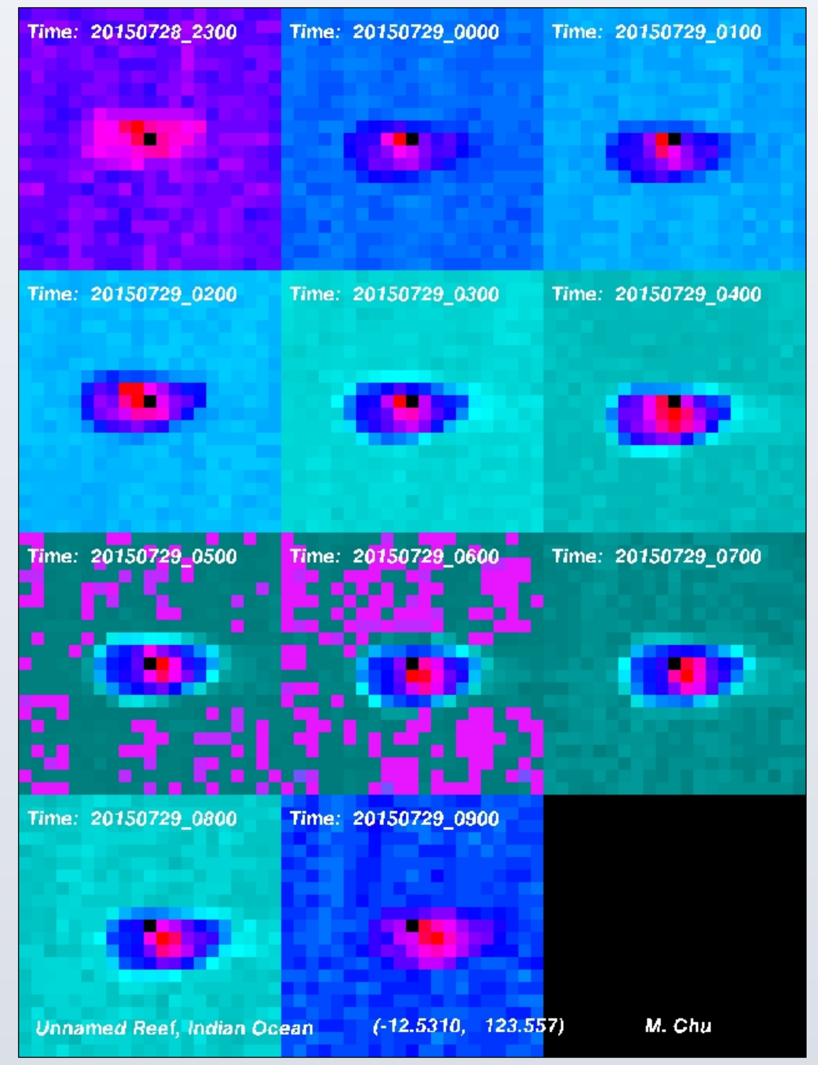

AHI frame-to-frame registration

- Up to 2 pixels (**1km**) deviation in B3
- Accuracy has improved since February, 2015 [2]

** Pixel shifts in each AHI radiance imagery used in the radiometric analysis have been examined and corrected*

High-Resolution Navigation Analysis of AHI using Landsat 8

A new effort has begun on the development of a high-accuracy quantitative analysis of AHI navigation accuracy using high-resolution Landsat 8 imageries (30m) to quantify low fractional-pixel deviations (<100m). The methodology is based on the NASA Geolocation Team's "landmark chips" approach. Recent preliminary result using Landsat 8 B4 against AHI B3 (red bands) demonstrates clear daily trends with deviations up to 1km.

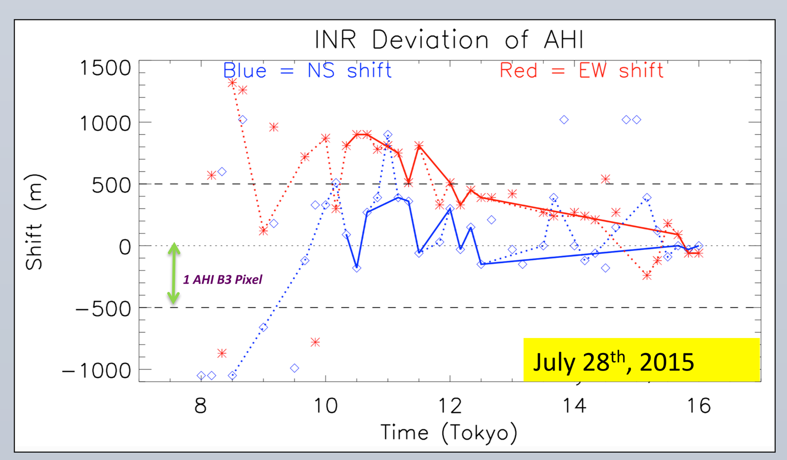

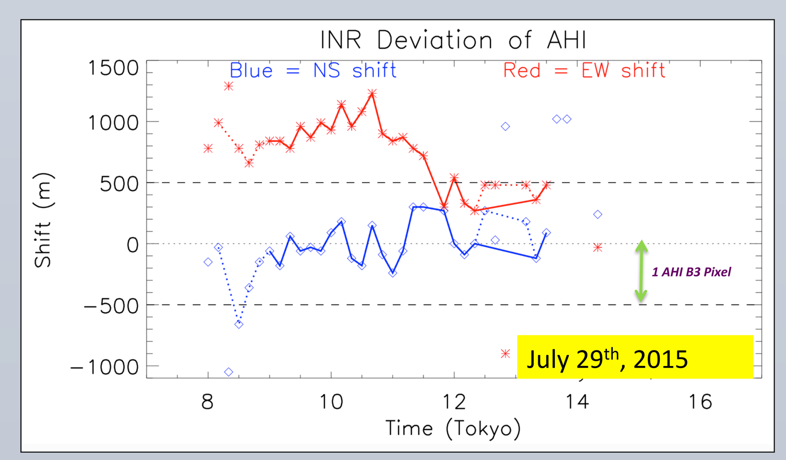

AHI-VIIRS Radiance Comparison Trend

DCC pixels are identified by AHI B13 (10.35μm). The corresponding radiance of the AHI and VIIRS VNIR bands for the identified DCC pixels is compared at the individual pixels level. Each monthly update, up to mid-August, combines 7 days worth of data. The spectral band adjustment factor (SBAF) for the first 4 matching band pairs are directly obtained from the web-calculator based on SCHIAMACHY visible hyper-spectral data [3] and the SBAF for the bottom 2 matching band pairs is an estimation to within 1% accuracy.

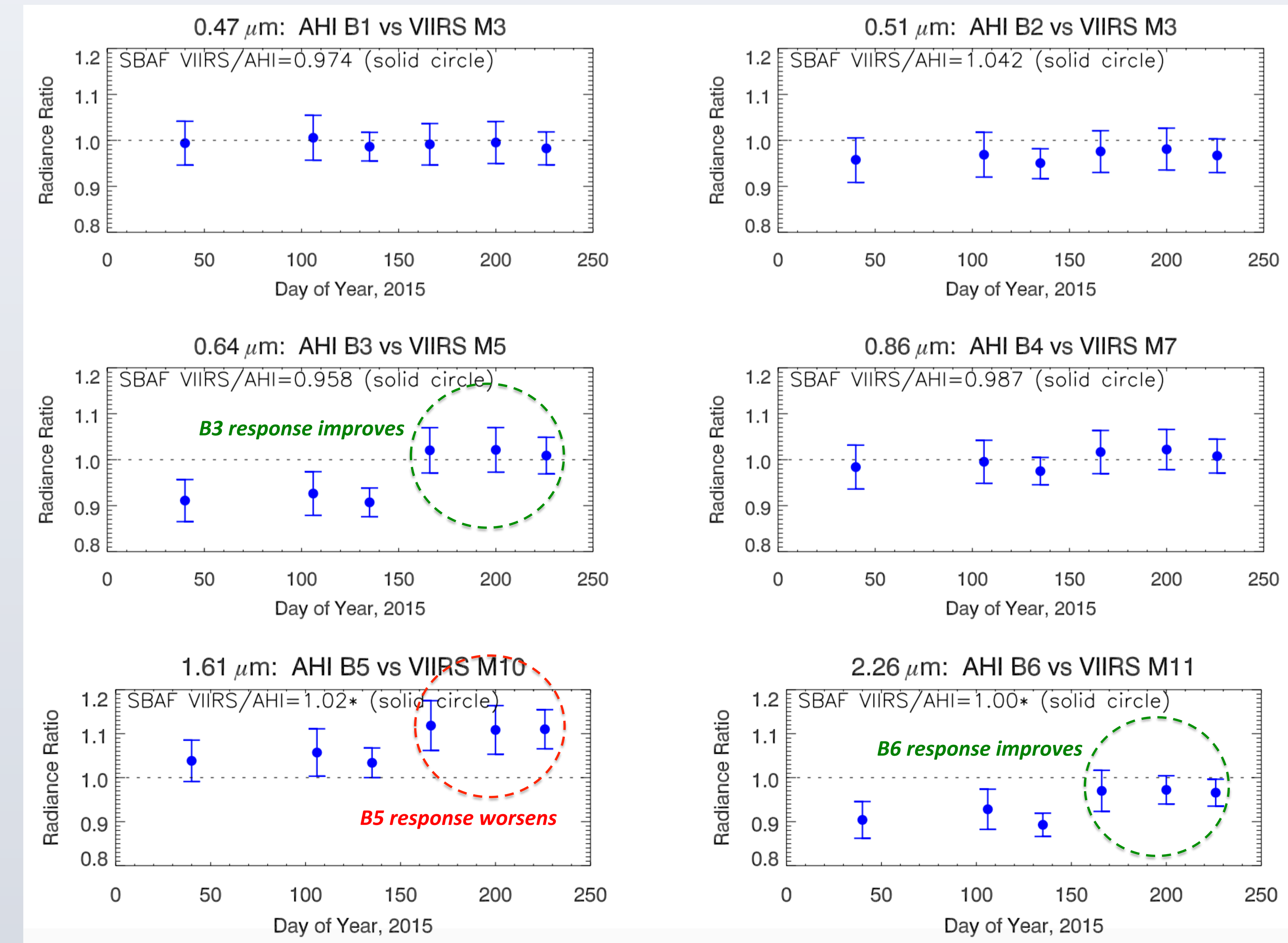

- JMA has made calibration adjustments between May and June
- B1 (0.47μm) the blue channel remains very accurate and stable
- B3 (0.64μm) and B6 (2.26μm), showing 10% dark bias earlier as was reported in April, 2015 [2], have been improved to within **3%** accuracy
- B5 (1.61μm) bias worsens up to **11%** higher (relative to VIIRS)

Summary

- **AHI radiometric response versus VIIRS up to *11%* difference at 1.61μm**
- **Radiometric response monitor using DCC readied as operational tool**
- **AHI navigation deviations up to *1 km* using VIIRS and Landsat 8**
- **Methodologies applicable to GOES-R Advanced Baseline Imager**

REFERENCES

[1] Uprety, S. and Cao, C. "*Suomi NPP VIIRS reflective solar band on-orbit radiometric stability and accuracy assessment using desert and Antarctica Dome C*", Remote Sensing of Environment. http://dx.doi.org/10.1016/j.rse.2015.05.021

[2] Chu, M., Wu, X., Yu, F., "*Early Inter-sensor comparison result of Himawari-8 Advanced Baseline Imager with the Visible Infrared Imaging Radiometer Suite*", Poster 3-44, 2015 NOAA Satellite Conference, Greenbelt, Maryland, April 27th – May 1st, 2015.

[3] Scarino, B., Doelling, D. R., P. Minnis, A. Gopalan, T. Chee, R. Bhatt, C. Lukashin, and C. O. Haney, "*A Web-based Tool for Calculating Spectral Band Difference Adjustment Factors Derived from SCIAMACHY Hyper-spectral Data*," Submitted to IEEE Trans. Geosci. Remote Sens., 2014.

www.PosterPresentations.com

Measurement of Band-to-Band Registration of the NPP VIIRS Instrument from On-Orbit Data

James C. Tilton[1], Bin Tan[2] and Guoqing (Gary) Lin[2]
email contact: James.C.Tilton@nasa.gov

[1] Code 606, NASA GSFC,
[2] Science, Systems and Application, Inc., Code 619, NASA GSFC

Introduction

The NASA/NOAA Visible Infrared Imaging Radiometer Suite (VIIRS) instrument onboard the Suomi National Polar-orbiting Partnership (SNPP) satellite was launched on 28 October 2011. VIIRS has 5 imagery resolution bands (bands I1 to I5) with 32 detectors each, 16 moderate resolution bands (bands M1 to M16) and a panchromatic day-night band (DNB) with 16 detectors each. In this study we estimate the along-scan and along-track band-to-band registration (BBR) of each band versus the other bands from on-orbit data. We utilized Normalized Mutual Information (NMI) between shifted image band pairs to determine the amount of shift required for the best match between the image band pairs. Subpixel accuracy was obtained by utilizing bicubic interpolation.

Normalized Mutual Information

Referring to [1-3], we can compute the Normalized Mutual Information (NMI) between two images as follows:

$$NMI\left(X_f;X_s\right) = \frac{\left[H\left(X_f\right)+H\left(X_s\right)\right]}{H\left(X_f,X_s\right)} - 1$$

where X_f is the fixed image and X_s is the shifted image. $H(X_f)$ ($H(X_s)$) is the entropy of image X_f (X_s) and $H(X_f,X_s)$ is the joint entropy of the images X_f and X_s. The entropy of an image X is computed as follows:

$$H(X) = -\sum\nolimits_{p>0} p \log p$$

where p is the probability density function (pdf) of image X.

The pdf of image X may be estimated from the histogram of an appropriately scaled and quantized image. According to [2], 8-bit quantization is usually sufficient. To avoid potential problems with outlier values, we apply a 3σ filter such that μ-3σ (the mean minus 3 times the standard deviation) corresponds to the value 1 and μ+3σ corresponds to the value 255. The values are rounded to the nearest integer value (value "0" is reserved as a "no data" mask).

Bicubic Interpolation

Our implementation of bicubic interpolation is based on K. Joy's [4] summary description of the Catmull-Rom Splines [5]. A cubic curve can be represented parametrically by the polynomial function:

$$P(t) = a_0 + a_1 t + a_2 t^2 + a_3 t^3$$

that has the first derivative (slope):

$$P'(t) = a_1 + 2a_2 t + 3a_3 t^2.$$

An interpolated curve for t in the range of 0 to 1 can be specified by setting the values of $P(0)$, $P(1)$, $P'(0)$ and $P'(1)$ and solving the resulting system of equations:

$$P(0) = a_0$$
$$P(1) = a_0 + a_1 + a_2 + a_3$$
$$P'(0) = a_1$$
$$P'(1) = a_1 + 2a_2 + 3a_3$$

To fit an interpolative curve passing through n+1 control points (P_0, P_1, …, P_n) we define the curve for the segment P_i to P_{i+1} by setting $P(0) = P_i$, $P(1) = P_{i+1}$, $P'(0) = (P_{i+1} - P_{i-1})/2$ and $P'(1) = (P_{i+2} - P_i)/2$. Several algebraic steps lead to the following matrix equation for the interpolative curve $P(t)$ for each line segment P_i to P_{i+1}:

$$P(t) = [1\ t\ t^2\ t^3] M \begin{bmatrix} P_{i-1} \\ P_i \\ P_{i+1} \\ P_{i+2} \end{bmatrix} \text{ where } M = \frac{1}{2}\begin{bmatrix} 0 & 2 & 0 & 0 \\ -1 & 0 & 1 & 0 \\ 2 & -5 & 4 & -1 \\ -1 & 3 & -3 & 1 \end{bmatrix}$$

The above cubic interpolation for a single dimensional curve is extended to a two dimensional image by first performing the cubic interpolation along the column dimension and then applying it along the row dimension.

Analysis Scheme

1. Selected four relatively cloud free NPP VIIRS data sets from differing geographic areas:

NPP VIIRS data set	Date	Location
A2012065.1835.P1_03110	March 5, 2012	Eastern United States
A2014176.1720.P1_03110	June 25, 2014	Eastern Canada
A2014176.1900.P1_03110	June 25, 2014	Central Canada
A2014192.0855.P1_03110	July 11, 2014	Northwestern Russia

2. For each data set and band combination, found the 100 "best" chips:

a. Scanned through each data set to find relatively cloud-free "chips" that were not entirely over water. For the I-bands the chips were 64 cols. by 32 rows, and for the M-bands the chips were 32 cols. by 16 rows.

b. For each chip selected in step 2, calculated the zero-shift NMI with the data bicubic interpolated to 4 times finer resolution. Saved a list of the location of chips with the 100 highest NMI values.

c. For the 100 "best" chips found in step 3, calculated the NMI with at various row and column shift locations with the data bicubic interpolated to 40 times finer resolution.

3. Looking across all four data sets, for each band combination and aggregation zone, selected the chips with the highest NMI value more than 0.15.

4. If fewer than 20 chips were found in step 3 for a band combination (and also aggregation zone in the along scan direction), the BBR analysis was terminated due to inadequate data. Otherwise the analysis continued.

5. For each band combination (and also aggregation zone for the along scan direction) computed the average BBR shift of the 20 chips with the highest NMI value. Also computed the standard deviation of these shifts. We also noted the minimum NMI value as a relative quality factor.

References

[1] A. A. Cole-Rhodes and P. K. Varshey, "Image registration using mutual information," in *Image Registration for Remote Sensing*, J. L. LeMoigne, N. S. Netanyahu and R. D. Eastman, Eds., pp. 131-149, 2011.

[2] J. P. Kern and M. S. Pattichis, "Robust multispectral image registration using mutual information models," *IEEE Trans. Geosci. Remote Sens.*, 45(5), pp. 1494-1505, 2007.

[3] C. Studholme, D. L. G. Hill and D. Hawkes, "An overlap invariant entropy measure of 3D medical image alignment," *Pattern Recognition*, 32(1), pp. 71-86, 1999.

[4] K. I. Joy, "Catmull-Rom Splines," *On-Line Geometric Modeling Notes*, (http://graphics.cs.ucdavis.edu/~joy/ecs278/ notes/Catmull-Rom-Spline.pdf, last accessed Aug. 5, 2015).

[5] E. Catmull and R. Rom, "A class of local interpolating splines," in R. E. Barnhill and R. F. Riesenfled (eds.), *Computer Aided Geometric Design*, Academic Press, New York, 1974.

Abridged Results

Largest BBR Offsets

Along Scan in 3x1 Aggregation Zone:

Fixed band	Shifted band	Minimum peak NMI	Mean*	Std. Dev.
M2	M13	0.28	0.0338	0.019
M3	I5	0.16	-0.0388	0.093
M12	I1	0.18	-0.0338	0.078
M6	I1	0.18	0.0713	0.124
M8	I1	0.19	0.0375	0.074
M8	I3	0.27	0.0375	0.056
M11	I1	0.20	0.0413	0.067
M11	I4	0.25	0.0525	0.067

Along Scan in 2x1 Aggregation Zone:

Fixed band	Shifted band	Minimum peak NMI	Mean*	Std. Dev.
M1	M6	0.19	-0.1113	0.115
M2	M6	0.20	-0.0975	0.116
M3	M6	0.22	-0.0575	0.122
M6	M13	0.25	0.0563	0.018
M8	M13	0.28	0.0500	0.020
M11	M13	0.32	0.0475	0.026
M5	I4	0.18	0.0538	0.078
M5	I5	0.17	0.0625	0.100

Along Scan in 1x1 Aggregation Zone:

Fixed band	Shifted band	Minimum peak NMI	Mean*	Std. Dev.
M3	M13	0.21	0.0825	0.053
M6	M12	0.18	0.0963	0.055
M8	M10	0.50	0.0613	0.017
M11	M12	0.30	0.0700	0.026
M12	I1	0.17	-0.0688	0.047
M12	I3	0.17	-0.0638	0.047
M12	I5	0.21	-0.0700	0.046
M13	I3	0.15	-0.1050	0.063
M13	I4	0.23	-0.0900	0.032
M13	I5	0.23	-0.0838	0.076
M2	I1	0.17	0.0625	0.077

*Negative means shift to west, positive means shift to east.

Along Track BBR Across Aggregation Zones:

Fixed band	Shifted band	Minimum peak NMI	Mean+	Std. Dev.
M14	I2	0.18	-0.0550	0.078
M15	I2	0.20	-0.0563	0.061
M15	I3	0.20	-0.0500	0.041
M16	I2	0.18	-0.0588	0.061
M6	I5	0.18	0.0725	0.101
M7	I5	0.18	0.0688	0.118
M13	I5	0.33	0.0613	0.052
M14	I2	0.18	-0.0550	0.078
I1	I5	0.28	0.0588	0.015
I2	I5	0.25	0.0588	0.025
I3	I5	0.32	0.0525	0.016

+Negative means shift to north, positive means shift to south.

Pre-launch BBR (vs. I1)

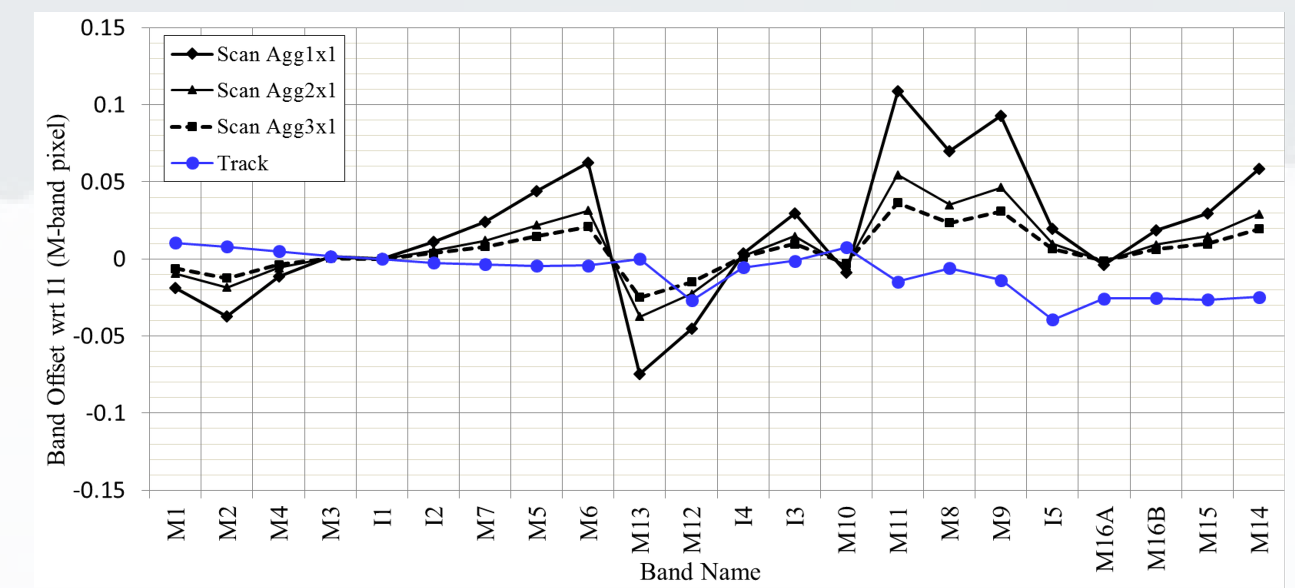

Discussion

The BBR values for band combinations not shown are lower than the shown cases. However, the BBR values for some band combinations could not be reliably measured. We considered finding at least 20 chips with peak NMI of at least 0.15 to be the minimum requirement for reliable measurement. Reliable measurements were found for most band combinations, with the main exception being band M9 versus any other band, where minimum peak NMI values greater than 0.15 were rarely found. Some other band combina-tions also had low minimum peak NMI values – mainly in the 1x1 aggregation zone. Full results are available in supplementary material.

A plot of pre-launch measurements of BBR versus band I1 is shown below. Many consistencies can be seen between these measurements and the on-orbit values. For example, band I5 is offset about 0.05 pixel from the other I-bands along track. Also band M6 is offset about 0.05 pixel from band M13 along scan in the 2x1 aggregation zone.

Some inconsistencies are also seen. A 0.045 pixel offset is seen between band I2 and I4 along scan in the 1x1 aggregation zone. But this may just be an inaccurate measurement since the minimum peak NMI is only 0.18.

NOTE: Measured BBR values between I-bands are fractions of I-band pixels. Other-wise the BBR values are fractions of M-band pixels.

Conclusions

Our approach for on-orbit measurement of the BBR of pairs of VIIRS bands has produced results that are largely consistent with the pre-launch measurements with maximum BBR offsets on the order of 0.1 pixel (10%).

Suomi NPP VIIRS Detector Dependent Relative Spectral Response Variation Effects using Line-by-Line Radiative Transfer Model Calculations

Zhuo Wang[a] and Changyong Cao[b]

[a] University of Maryland, College Park, Maryland, [b] NOAA/NESDIS/STAR, College Park, Maryland

Abstract

The Visible Infrared Imaging Radiometer Suite (VIIRS) is a modern focal plane array based satellite radiometer, which has many detectors with slightly different relative spectral response (RSR). Effect of RSR differences on imaginary artifacts, as well as geophysical retrieval uncertainties has not been well studied. Previous studies used the MODTRAN model for detector-level radiance simulations. However, it is limited by the spectral resolution of the model relative to the narrow spectral bandwidth of the detectors. This study evaluates detector level RSR using Line-by-Line Radiative Transfer Model (LBLRTM) at higher spectral resolution 0.01 cm^{-1} for VIIRS bands M15 and M16 under different atmospheric conditions. From the model simulation and case studies of VIIRS SDR brightness temperature data, we found that the striping in imagery is most likely related to the difference between band averaged and detector level RSR, which has some atmospheric dependency. Cumulative histogram method is utilized to quantify the striping. These findings will help S-NPP and J1 to better understand the impact of the difference in detector-to-detector RSR on VIIRS geophysical retrieval and reduce the uncertainties.

Background

Previous studies have been performed to identify the possible causes for SST striping issue [*Padula and Cao, 2015*]. They used MODTRAN model to simulate the spectral radiance at the spectral resolution of 1cm^{-1} for five standard atmospheric profiles. Their results indicate that the SST product is likely affected by small differences in detector-level SRF, and the detector-to-detector differences have small atmospheric dependence.

A study from SST EDR team [*Dash and Ignatov, 2008*] evaluated the biases in the top-of-atmosphere (TOA) brightness temperature (BT) modeled with MODTRAN model. They concluded that MODTRAN brightness model does not reproduce spectral, angular, and water vapor dependencies with accuracies acceptable for SST analyses. Therefore, in this study, we use LBLRTM with higher resolution to investigate the SST striping issue.

VIIRS Daytime SST Algorithm & Imagery Analysis

The daytime VIIRS SST is computed from a non-linear split window algorithm using the brightness temperatures from bands M15 and M16 :

$$SST = a_0 + a_1 \times T_{11} + a_2 \times (T_{11} - T_{12}) \times T_{ref} + a_3 \times (T_{11} - T_{12}) \times (\sec\theta_{sat} - 1) \qquad (1)$$

Where T_{11} and T_{12} are the brightness temperatures at M15 (11µm) and M16 (12µm), respectively. T_{ref} is the first guess SST from either numerical weather prediction or analysis fields. a_0, a_1, a_2, and a3 are the coefficients derived from the regression process.

VIIRS SST EDR group found an anomalous striping pattern in daytime SST product, and they developed an algorithm to improve the operational SST imagery. However, we still need to analyze the striping at the SDR or L1b level to reduce the propagation of any system artifacts to SST product. Figure 1 shows striping at SDR brightness temperature.

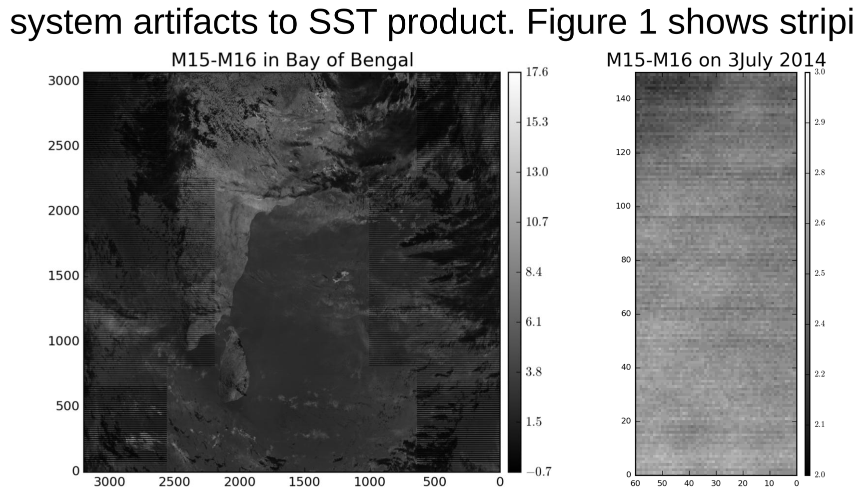

Figure 1. Suomi NPP VIIRS SDR brightness temperature product in M15–M16 over the bay of Bengal on July 3, 2014 (Left); Subset of SDR BT for a uniform ocean surface under clear sky condition.

Line-by-Line Radiative Transfer Model

LBLRTM [*Clough et al. 1981*] is an accurate and efficient line-by-line radiative transfer model which provides spectral radiance calculations with accuracies consistent with the measurements [*Clough et al. 2004*]. LBLRTM 12 is used in this study to simulate the TOA spectral radiance under six standard LBLRTM atmospheric profiles.

The output spectral radiance is then convolved with VIIRS relative spectral response (RSR) to get the channel effective radiance:

$$L_{eff} = \frac{\int_{\nu_1}^{\nu_2} L\, R_\nu\, d\nu}{\int_{\nu_1}^{\nu_2} R_\nu\, d\nu} \qquad (2)$$

where L is the at sensor radiance and R_ν is the RSR of a given band. The simulated effective radiance for each band (L_{eff}) was converted to BT (T_{eff}) using the numerical method by minimizing the difference between BB radiance and channel effective radiance.

In this study, we will check the difference in effective brightness temperature (ΔT_{eff}) [K] between using the detector-level RSR and the band averaged RSR.

$$\Delta T_{eff} = T_{eff\,(\det RSR)} - T_{eff\,(avgRSR)} \qquad (3)$$

Where $T_{eff\,(det\,RSR)}$ is the effective brightness temperature computed using the detector-level RSR and $T_{eff\,(avg\,RSR)}$ is the effective temperature computed using the band averaged RSR.

Model Results

Figure 2 shows the effective brightness temperature differences between the detector-level and band averaged RSR in VIIRS M15 (Top left), M16 (Top right), and M15 – M16 (Bottom) from the LBLRTM radiance output for six atmospheres. Results indicate that there is a small but obvious atmospheric dependency. The odd/even detector pattern is also observed. In M15, the smallest BT difference is at

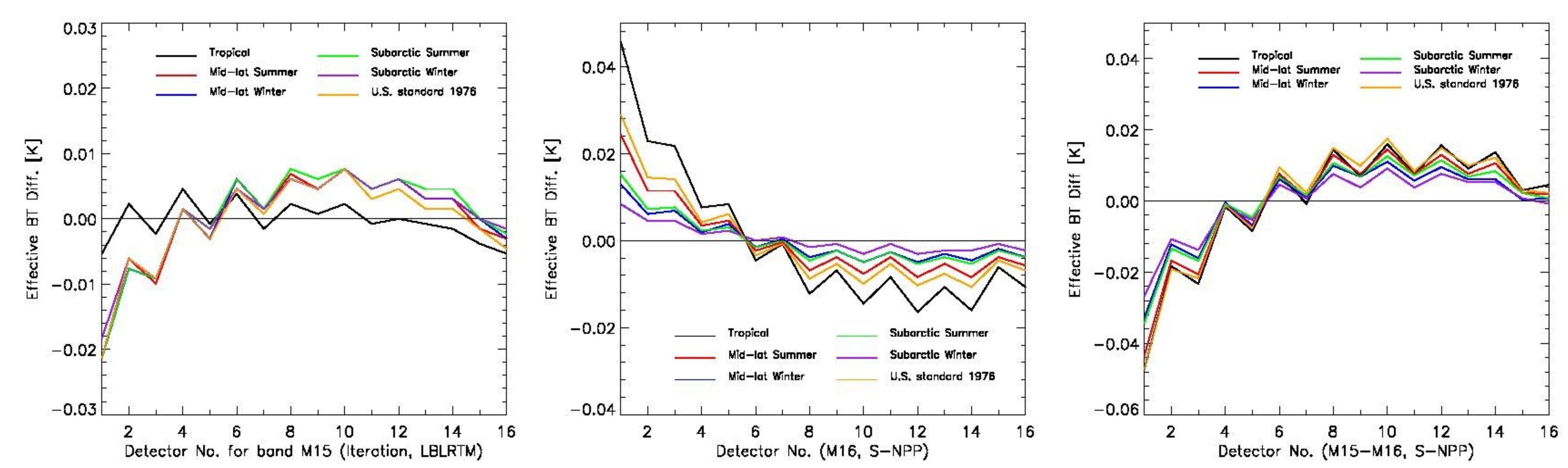

Figure 2. Effective BT difference between detector-level RSR and band averaged Relative Spectral Response using LBLRTM in VIIRS band M15 (Top left), M16 (Top right), and M15 – M16 (Bottom).

The magnitude in effective BT difference among detectors is 0.01K for tropical atmosphere, and 0.025K for subarctic atmosphere (top left panel in Figure 2). To see the impact of spectral range, we extend M15 from [800, 1100] cm^{-1} to the entire spectral range [800, 1333.33] cm^{-1} and M16 from [769, 950] to [769, 1250] cm^{-1} to include the out-of-band response. The results and BT difference patterns are similar as Figure 2 (figure not shown). In M16 (top right panel of Figure 2), there is more obvious atmospheric impact on BT difference than M15, and the tropical atmosphere pattern has the largest variation. Band M16 is more sensitive to water vapor variation due to more water vapor absorption in M16. Detector 6 has the smallest BT difference. Detectors 1 to 6 are more closer to band averaged and then deviate from band average for detectors 8 to 16. For detectors 4 to 16, although Sub-arctic Summer has higher temperature and more water vapor, it has almost same variation as Mid-latitude winter. Therefore, besides water vapor and temperature, other instrument factors may also affect the striping. The term (BT_{15}–BT_{16}) is important because it is used in the VIIRS SST retrieval algorithm. The bottom panel shows that M15–M16 has larger magnitude of variation than single band, for example, they are 0.072K and 0.063K for tropical atmosphere in (M15–M16) and M16, respectively.

Satellite Data Analysis

In order to investigate the relationship between water vapor and striping in VIIRS temperature images, The SDR brightness temperature observation data in band M15 and M16 are analyzed in sample cases from 2012 to 2014. Ten cases over the "uniform" clear sky ocean surface near tropical and polar region are used in this study. In each image, the small uniform region under clear sky conditions was selected based on VIIRS Cloud Mask Intermediate Product (IICMO).

We used the striping index (called SI thereafter) defined in a previous study (Li, 2015) to quantify the striping pattern. The cumulative histogram defined by Li is used to quantify the striping in the image:

$$H_{i,d}(k) = \frac{1}{N_{i,d}} \sum_{l=0}^{k} \left(\sum l \in (l,i,d) \right) \qquad (4)$$

Figure 3. The cumulative histogram for Bay of Bengal over tropical region on June 9, 2013 in M15–M16 (Left), as well as M15 and M16 (Right).

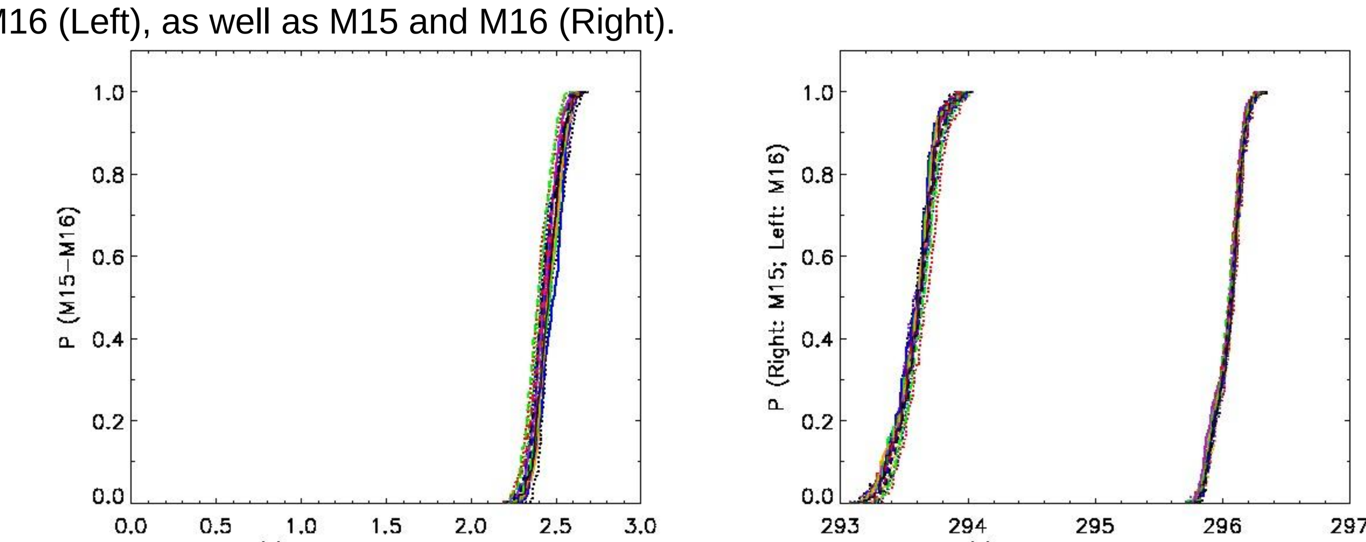

In Figure 3, Y-axis is the percentage of the pixels with value less than the value in X-axis. X-axis represents BT difference in M15–M16 and BT in M15 & M16, respectively. Each line represents one detector. We found that the horizontal distance between histograms is almost a constant. BT_{15}–BT_{16} also represents the water vapor. The left panel also shows that striping does not depend on water vapor within the small water vapor range. The relative magnitude, i.e., the ratio of horizontal distance to the X-axis range is defined as R=g(50%)/$Range_{Xaxis}$. The ratios in M15–M16, M15 and M16 are 0.187, 0.067 and 0.107, respectively. M15–M16 has larger ratio than single band. These horizontal distances are a little bit larger than LBLRTM magnitudes in BT difference for M15–M16, M15, and M16. Over polar regions, the ratios are 0.149, 0.044, and 0.015 for M15-M16, M15, and M16, respectively, which are smaller than those over tropical regions.

The effective BT difference from LBLRTM and VIIRS observation are compared in Figure 4. In M15–M16 and M16, both LBLRTM and VIIRS observation show larger BT difference in tropical than in polar region. In most cases, VIIRS observation has larger magnitude in BT difference among different detectors than LBLRTM except for polar case in M15–M16. In general, the magnitude of variation among 16 detectors over tropical region is much more affected by water vapor than that over polar region, i.e., which is larger for high BT difference (high water vapor absorption). Therefore, the water vapor has impact on the striping pattern, but it is not the dominant factor.

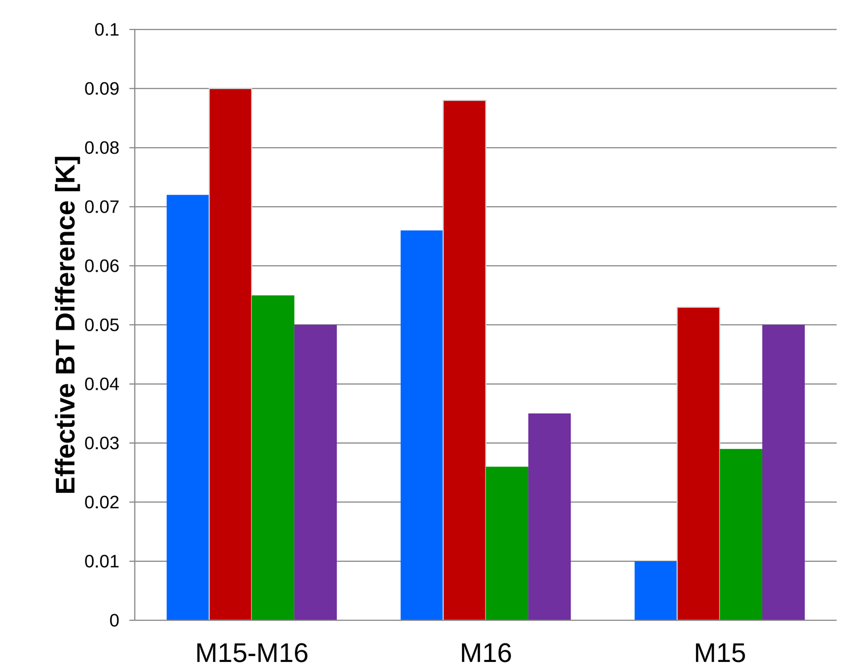

Figure 4. The comparison of effective BT difference between LBLRTM and the VIIRS observation for tropical and polar cases.

Summary

• LBLRTM results show that the striping pattern in VIIRS SST imagery is most likely related to the difference between band averaged RSR and detector level RSR. The effective BT difference has some atmospheric dependency. The results are consistent with MODTRAN results.

• Ten case studies using VIIRS SDR BT observation over tropical and polar regions also show that the detector level difference in tropical region is more obvious than that in polar region. The BT bias is larger for warm and moist atmosphere, but smaller for cold and dry atmosphere. Band M16 is more sensitive to the atmospheric conditions.

• In general, VIIRS SDR BT observation has larger variability when comparing with the model output. It is not easy to effectively validate. The difference due to atmospheric conditions or water vapor is small and not a dominant factor for striping.

• Further study will focus on detector stability and fixed pattern noise.

Acknowledgement: Thanks Yan Bai for providing sample data.

References

Clough, S.A., Kneizys, F.X., Rothman, L.S., Gallery, W.O. (1981), Atmospheric spectral transmittance and radiance: FASCOD1B. *Proc Soc Photo Opt Instrum Eng*, Vol. 277, 152–166.

Clough, S.A., M.W. Shephard, E.J. Mlawer, J.S. Delamere, M.J. Iacono, K. Cady-Pereira, S. Boukabara, P.D. Brown (2005), Atmospheric radiative transfer modeling: a summary of the AER codes, J. Quantitative Spectroscopy & Radiative Transfer, Vol. 91, 233 –244.

Dash, P., and A. Ignatov (2008), Validation of clear-sky radiances over oceans simulated with MODTRAN4.2 and global NCEP GDAS fields against nighttime NOAA15-18 and MetOp-A AVHRR data, *Remote Sens. Environ.*, *112*, 3012-3029, doi:10.1016/j.rse.2008.02.013.

Francis Padula and Changyong Cao (2015), Detector-Level Spectral Characterization of the Suomi NPP VIIRS Long-Wave Infrared Bands M15 & M16. Applied Optics.

Li, Zhenping, 2015: Real Time De-Striping Algorithm for Geostationary Operational Environmental Satellite (GOES) P Sounder Images.

Assessment of scan-angle dependent radiometric bias of Suomi-NPP VIIRS day/night band from night light point source observations

Yan Bai[a], Changyong Cao[b], Xi Shao[a],
[a] University of Maryland, College Park, MD, [b] NOAA/NESDIS/STAR, College Park, MD

Abstract

The low gain stage of VIIRS Day/Night Band (DNB) on Suomi-NPP is calibrated using onboard solar diffuser. The calibration is then transferred to the high gain stage of DNB based on the gain ratio determined from data collected along solar terminator region. The calibration transfer causes increase of uncertainties and affects the accuracy of the low light radiances observed by DNB at night. Since there are 32 aggregation zones from nadir to the edge of the scan and each zone has its own calibration, the calibration versus scan angle of DNB needs to be independently assessed. This study presents preliminary analysis of the scan-angle dependence of the light intensity from bridge lights, oil platforms, power plants, and flares observed by VIIRS DNB since 2014. Effects of atmospheric path length associated with scan angle are analyzed. Other effects such as light changes at the time of observation are also discussed. The methodology developed will be especially useful for JPSS J1 VIIRS due to the nonlinearity effects at high scan angles, and the modification of geolocation software code for different aggregation modes. It is known that J1 VIIRS DNB has large nonlinearity across aggregation zones, and requires new aggregation modes, as well as more comprehensive validation.

Introduction

The Visible Infrared Imaging Radiometer Suite (VIIRS) is one of the key instruments on the Suomi National Polar-orbiting Partnership (Suomi NPP) satellite designed primarily to observe clouds and earth surface variables. Among the twenty-two bands of VIIRS onboard the NPP satellite, the Day/Night Band (DNB) represents an unprecedented night observation capability. It is superior to its predecessor, the Operational Line Scanner (OLS) on the Defense Meteorological Satellite Program (DMSP), in both spatial and radiometric performance because it has a finer spatial resolution of constant 742 m across the three thousand kilometer scan. The Day/Night band (DNB) is also the first to utilize onboard calibration [1].

The VIIRS DNB uses advanced onboard aggregation techniques to achieve constant spatial resolution across scan with 32 aggregation zones. Since each zone has its own calibration, it is not easy to validate the calibrated radiances across the zones. It is also found that in J1 VIIRS prelaunch testing, a large nonlinearity exists in the higher aggregation zones, which would lead to a significant bias across zones along scan. This study attempts to evaluate the response versus scan by using point sources [2] such as bridge lights, oil platforms, and flares to potentially quantify the effect. The challenges in this work are also discussed.

Methodology

To evaluate the DNB radiometric response versus scan angle, we select ground based night light sources. Ideal sources should be stable over time and spatially isotropic (or radiating equally in all directions). However, not many targets are truly stable due to fluctuations of power supplies, and atmospheric changes. Analysis of night lights from DNB led us to focus on bridge lights, oil platforms and gas flares. We are mostly interested in the lights over water because this greatly reduces lunar reflection from the surrounding areas, which would complicate the analysis.

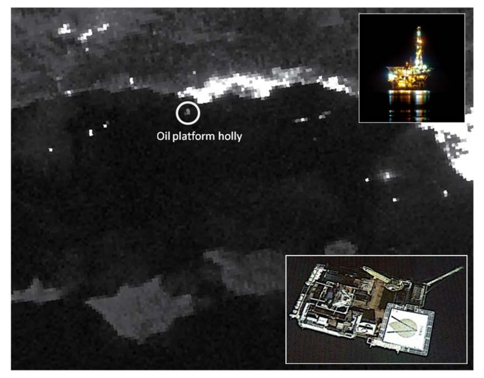

Figure 1. DNB image of the oil platform Holly

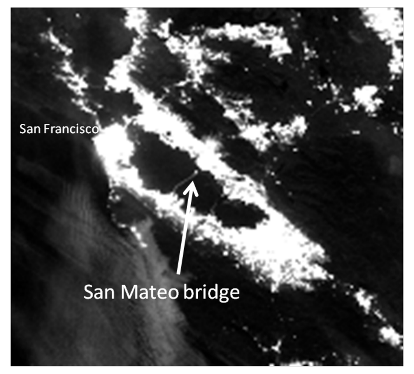

Figure 2. DNB image of the San Mateo bridge

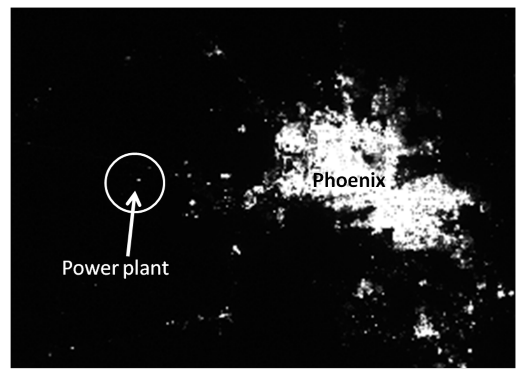

Figure 3. DNB image of the the power plant near Phoenix, Arizona

Figure 1 shows an example of night lights from the oil platform Holly located near Los Angeles. It is about 50 meters long and 29 meters wide over the water. The lights appear to be always on at night and are relatively stable as a point source for DNB radiance and geolocation analysis. Although oil platforms have lights on overnight, their stability long term is not well known. For example, some lights on the platform may be turned on and off at a given schedule. This increases the uncertainties for radiance validation.

The San Mateo bridge in San Francisco (Figure 2) is another point source over the water. In comparing with the oil platform holly, the bridge has more points and they are assumed to be more stable over time since the lights are turned on over night as a requirement for transportation safety. Some of the bridge lights have been replaced with LEDs which are extremely stable.

Figure 3 shows the power plant located on the west about 40 miles away from Phoenix AZ, which is a good candidate for a ground based night light source. Although there is little light around the power plant, and also Arizona has more clear sky at night, the ground lunar reflection may affect the stability of DNB radiance and geolocation.

Finally, gas flares are assumed to be on all the time, but the stability is unclear. Furthermore, it is not clear how gas flare intensity is related to oil production volume, and whether there is a daily schedule. In this study, we also tested using gas flares in the mid-east region. Despite the challenges, we believe that by using multiple sites and multiple types of light source, the uncertainties in those factors can be reduced.

Other uncertainties include the atmospheric effects, which may have a different attenuation at different view angles. In addition, the sensor spatial response (aka MTF or point spread function) is different at different aggregation zones.

In this study, we use the following procedure to analyze the DNB response at different scan angles:

1. The DNB observations at nadir are collected at 16 day orbital repeating cycles to evaluate the stability of the night light source. [3]
2. The DNB observations at different scan angles for all days are collected and plotted against the scan angle to study the response vs. scan angle.
3. The results are analyzed in relation to various factors to estimate the effect of the scan angle or frame
4. The potential use of this method for J1 DNB aggregation (Figure 4) evaluation is assessed.

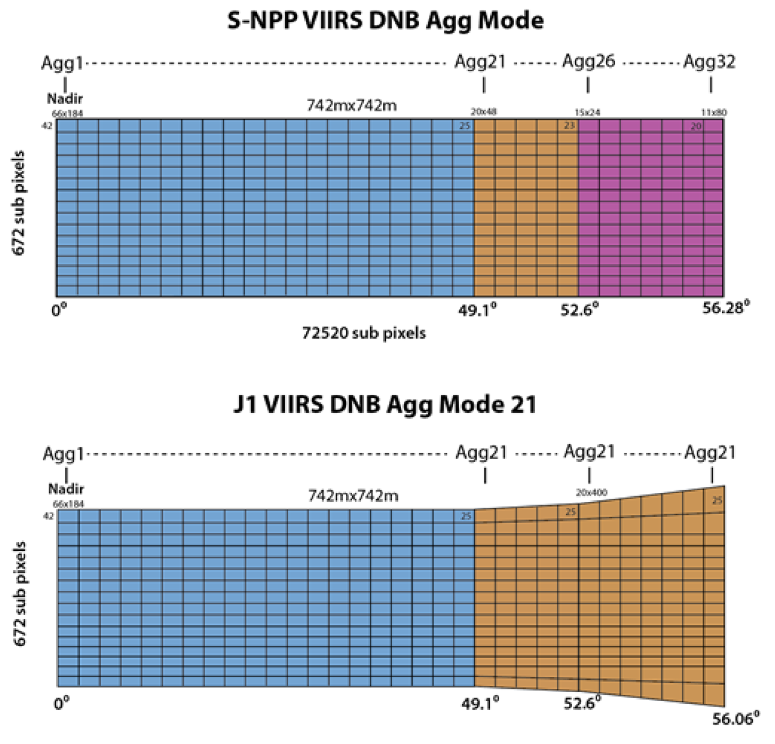

Figure 4. VIIRS DNB aggregation scheme for NPP and J1 (Notional drawing, not to scale, subject to change)

Data Sets and Analysis Results

The data set we used for the analysis is VIIRS DNB SDR data with geolocation/terrain correction for Suomi NPP.

- The data sets used are from time period 2014 and 2015 (Table1).
- The max radiance vs. frame number for San Mateo bridge, platform Holly, power plant in AZ and Bahrain passport control are shown in Figure 5.

Table 1. Data sets used in the study

Location	Time series
San Mateo bridge (San Francisco)	12/04/2014 – 04/02/2015
Oil platform holly (Los Angeles)	12/15/2014 – 04/06/2015
Power plant (AZ)	12/11/2014 - 04/12/2015
Bahrain passport control	12/02/2014 - 04/13/2015

Figure 5 shows that there appears to be a scan angle dependent radiance bias across scan. At nadir, the radiance is lower than those at the beginning and end of the scan. The magnitude of the radiance variation over different scan angle for the east end of the bridge is about 1e-8 to 4e-8 w/cm^2-sr, which is a change of about 4x time (or from 3e-9 to 1.5e-8 w/cm^2-sr for the middle site). Note that this pattern is consistent for the two sites used, one on the east end of the bridge and the other is in the middle of the bridge.

There are several possible causes for the scan angle dependent bias. First of all, it is possible that there is a radiometric bias across the aggregation zones. This was not extensively studied for Suomi NPP VIIRS DNB, although more attention was paid during the J1 VIIRS DNB prelaunch testing. If this is the case, then the plot here would be very useful for comparing with J1 VIIRS DNB once it is launched, since it is known that J1 VIIRS DNB has a much larger effect in scan dependent bias.

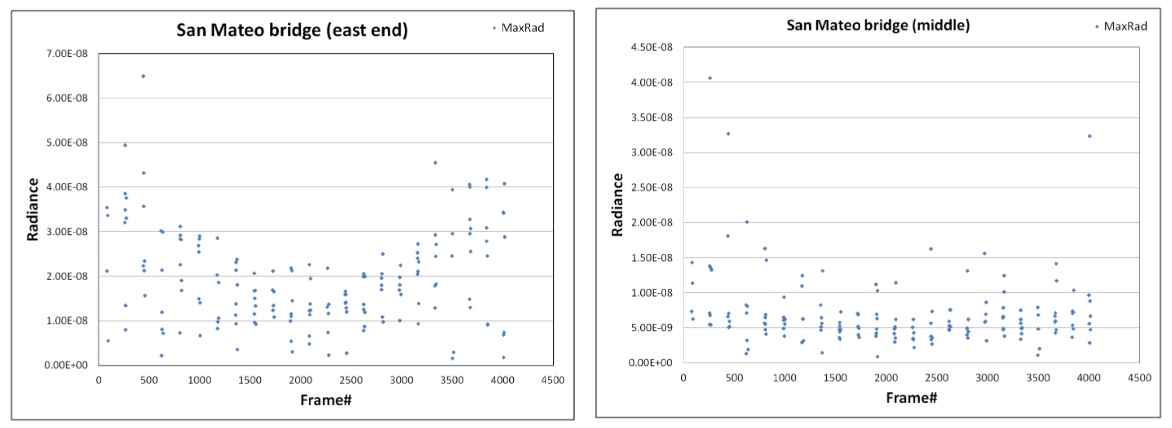

Figure 5. Radiance vs. scan angle for San Mateo bridge (left: east end; right: middle of bridge)

Other causes include atmospheric path length and scattering, response versus scan (RVS) angle, the point spread function changes from nadir to end of scan, time of the observation due to traffic lights, calibration bias across aggregation zones. Finally, air glow [4] may have an impact but the magnitude is on the order of 1.0e-9 which cannot explain the pattern in Figure 5.

Figure 6 shows the response vs. scan for the oil platform holly located on the west coast near Los Angeles. A similar scan angle dependent bias is also found here. At nadir, the radiance of 5e-9 w/cm^2-sr is much lower than those at the end of the scan (Compared to the lights on the San Mateo bridge, it seems that the radiance from the oil platform Holly is not as stable).

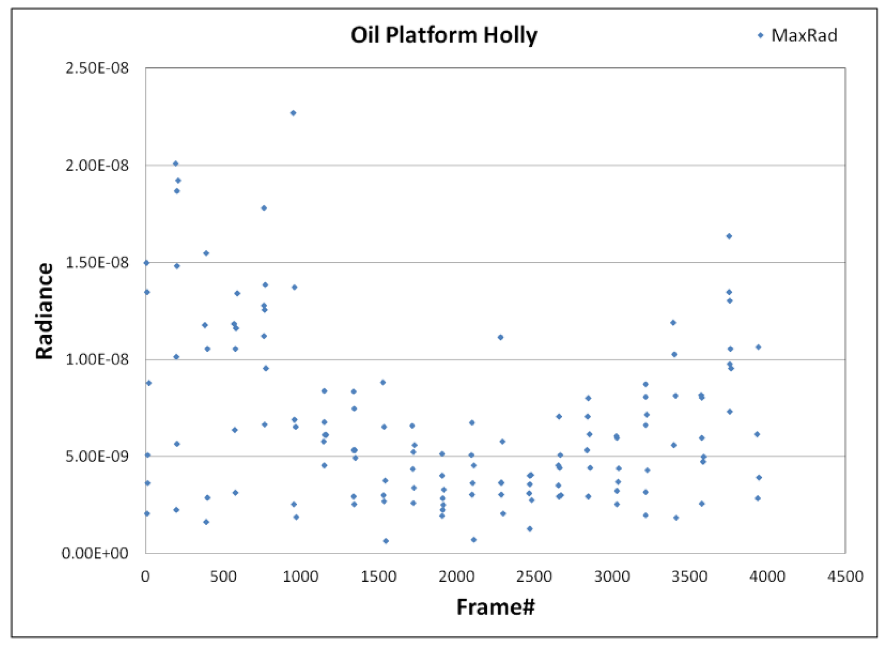

Figure 6. Radiance vs. scan angle for Oil Platform Holly

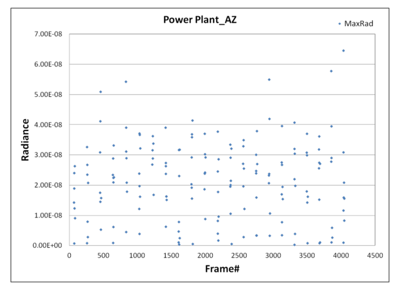

Figure 7. Radiance vs. scan angle for the power plant in Arizona

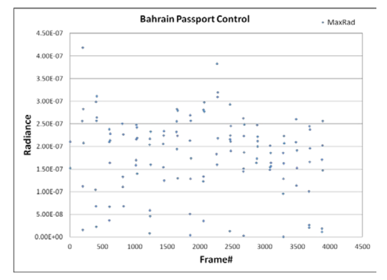

Figure 8. Radiance vs. scan angle for the passport control of Bahrain

The power plant in Arizona and the passport control of Bahrain are the ground base point sources. In comparison with Figure 5 and Figure 6, the pattern for Figure 7 and Figure 8 are not very clear. It might be due to the effect of the ground lunar reflection which may have disrupted the pattern. Also it can be due to ground reflection of street light.

Conclusion

Preliminary analysis of the scan-angle dependence of the light intensity from bridge lights, oil platform, power plants, and flares observed by VIIRS DNB since 2014 are presented in this study. Results show that there appears to be a scan angle dependent radiometric bias, with a low radiance at nadir while gradually increases towards edge of the scan. This pattern is found in both the San Mateo bridge and the oil platform holly samples, although it is less clear for the Arizona power plant and Bahrain cases. It is possible that this effect is due to the VIIRS DNB aggregation zones on Suomi NPP VIIRS, which would also help study the effect of J1 VIIRS DNB nonlinearity at high scan angles, which requires the use of new aggregation modes. However, the results are preliminary and more analysis is needed to get a better understanding of this effect. Other effects such as atmospheric path length and light on/off schedule as well as traffic volume may also contribute to this pattern. We found that the point sources over water have the clear advantage than the ground base point sources for the radiance and geolocation validation analysis since there is little reflection from the water and this reduces the uncertainties compare with the ground point source.

References

[1] Cao, C., J. Xiong, S. Blonski, Q. Liu, S. Uprety, X. Shao, Y. Bai and F. Weng, Suomi NPP VIIRS sensor data record verification, validation, and long-term performance monitoring, JGR, Volume 118, Issue 20, October 2013, Pages 11,664–11,678, DOI: 10.1002/2013JD020418.

[2] Cao, C. and Y. Bai, Quantitative Analysis of VIIRS DNB Nightlight Point Source for Light Power Estimation and Stability Monitoring, Remote Sens. 2014, 6(12), 11915-11935; doi:10.3390/rs61211915

[3] Bai, Y., C. Cao, X. Shao, Monitoring Suomi-NPP VIIRS Day/Night band stability using bridge lights, Eumetsat conference 2015.

[4] Lee, S., K. Chiang, X. Xiong, C. Sun, and S. Anderson, The S-NPP VIIRS Day-Night Band On-Orbit Calibration/Characterization and Current State of SDR Products, Remote Sens. 2014, 6(12), 12427-12446; doi:10.3390/rs61212427

Acknowledgment :
This study is partially funded by the Joint Polar Satellite System (JPSS) program.

Field Campaign Support Capabilities for VIIRS at University of Maryland

Department of Astronomy

Xi Shao[1], Yan Bai[1], Changyong Cao[2],

[1] Department of Astronomy, Cooperative Institute for Climate & Satellite-Maryland, University of Maryland, College Park, MD, USA

[2]NESDIS/STAR, National Oceanic and Atmospheric Administration, College Park, MD, USA

Outline

We present an overview of the field campaign support capabilities in various areas at University of Maryland

- Overflight field campaign support
- Lunar observation at UMD Astronomical Observatory
- Ground measurements of aerosol optical thickness (AOT) and PM 2.5
- Integration of modular spectrometer and Unmanned Aviation Vehicle (UAV) rotary drone system to support field measurements
- Hardware integration to enable automatic data acquisition.

Over-Flight Field Campaign Support at UMD

•An example of participating field measurements in support of the NASA HYSPIRI mission to collect ground spectral reflectance and aerosol data near Los Angles with ASD spectrometer and sun photometer provided by NOAA/NESDIS/STAR.

• The team performed measurements for about 20 types of ground covers at ~ 30 locations near Los Angles.

• These ground spectral reflectance and aerosol data are analyzed to calibrate over-flight remote sensing measurements.

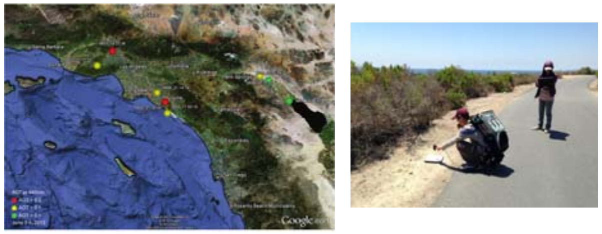

Figure 1: Left: Aerosol Optical Thickness (AOT) measurements from the field campaign (June 3-6, 2013); Right: Performing field measurement.

Figure 2: Typical Ground Covers Measured

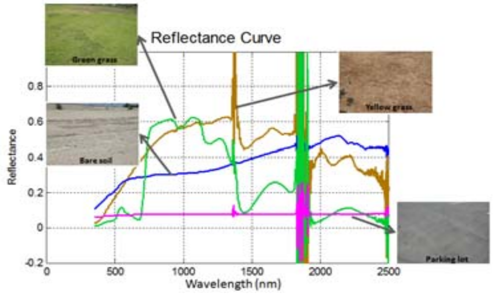

Figure 3: Measured reflectance for several types of ground cover

Lunar Observation at UMD Astronomical Observatory

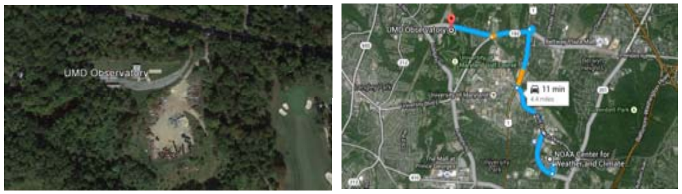

Figure 4: UMD Astronomical Observatory (3202 Metzerott Road, College Park, MD 20740)

- The University of Maryland Astronomical Observatory serves as an important component of the teaching and research program in the Department of Astronomy. It also brings the excitement of astronomy to the University community and the general public through public program.
- The Observatory has four permanently mounted telescopes on site, and a collection of 12 portable telescopes used both on and off site.
  - 8" NASA Refractor; 7" Astro-Physics Refractor
  - Celestron 14" Schmidt-Cassegrain Reflector; 20" Eichner Bent Cassegrain Reflector

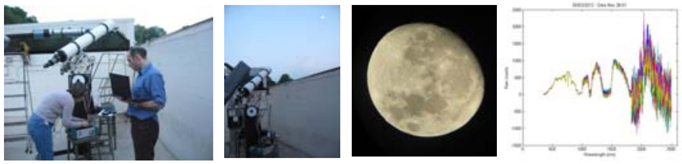

Figure 5: Lunar observation with NOAA/NESDIS/STAR scientists at UMD Astronomical Observatory.

Figure 6: State of the Art polarimeter with automation in collaboration with L-1 Standards and Technology LLC., which enables polarization measurements of the moon, atmosphere and surfaces. (To be tested at UMD Observatory)

Ground Measurements of PM 2.5 and Hardware Integration

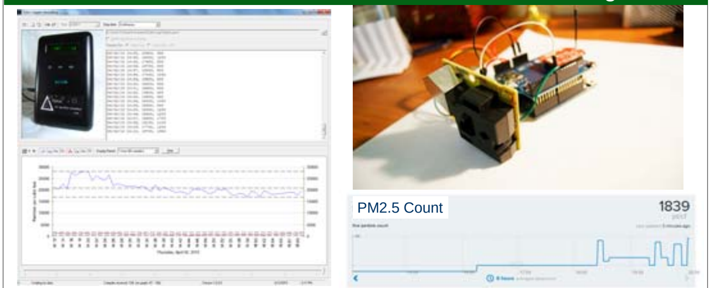

Figure 7: Left: PM2.5 and PM10 data acquired with Dylos; Right: An integrated prototype Wi-Fi-enabled PM2.5 data collection system (Arduino-based, Shinyei PPD-42 Dust Sensor, Roving Networks RN-XV Wi-Fi module) Data can be collected wirelessly through Wi-Fi router and made available online.

Integration of Modular Spectrometer with UAV (Rotary System) to enable Aerial Radiometric Data Acquisition

Ocean Optics Modular Spectrometer

- Versatile, general-purpose UV-Vis-NIR spectrometers for absorption, transmission, reflectance, emission, color and other applications.
- Compact size, robust optoelectronics and easy modularity
- The most popular spectrometers in the world, supporting thousands of applications, from research and life sciences to education and materials identification.
- Spectral Range: 350 nm to 1000 nm; Spectral Resolution: 0.38 nm.

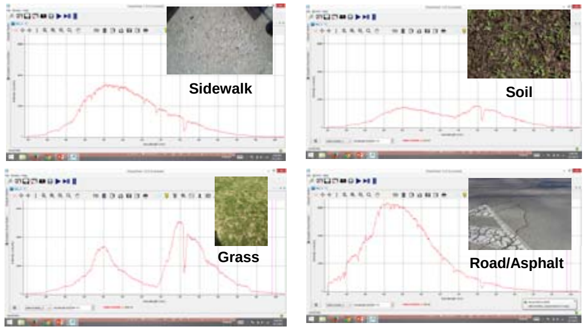

Figure 8: Spectral measurements of various land surfaces at UMD using Ocean Optics spectrometer

Figure 9: UAV drone measurements in action by UMD students

Summary

- UMD has a long-history and tradition with capabilities and experiences in supporting field campaign with ground measurements, drone system and variety of sensors.
- UMD has been supporting VIIRS Cal/Val work in many areas.
- Unique advantage of leveraging resources at UMD such as Astronomical Observatory, engineering students
- Provide opportunities for education and outreach to university students.

Acknowledgement

We thank Frank Padula and Aaron Pearlman for close collaboration with GOES-R Calibration Working Group. Thanks are extended to JPSS program scientists for field campaign opportunities. We look forward to supporting VIIRS field campaign.

S-NPP VIIRS Significant Events in 2014 Monitored by NOAA ICVS Web-page

Taeyoung (Jason) Choi[1], Ninghai Sun[1], Wanchun Chen[1], Changyong Cao[2], Fuzhong Weng[2]

[1]Earth Resource Technology (ERT), [2]STAR/NESDIS/NOAA

Abstract

- As a part of post-launch Cal/Val, NOAR STAR developed and has maintained the Integrated Calibration and Validation System (ICVS) for Long-Term Monitoring (LTM) of the sensor performance. The Visible Infrared Imaging Radiometer Suite (VIIRS) is the one of the key instruments onboard the Suomi National Polar orbiting Partnership (S-NPP) satellite, which was successfully operational since its launch on October 28, 2011.
- This poster is focused on significant VIIRS significant anomalous events in year 2014 that were identified and analyzed through the ICVS LTM webpage. Firstly, the Single Board Computer (SBC) lock-up events randomly occurred four times in last year. It was caused by the cosmic high energy particle hits and the improved design was applied to the next J1 VIIRS. During the SBC lock-up events, there were unrecoverable data losses. The second event affected reflectance (or radiance) in the Reflective Solar Band calibration. The sudden SD degradation LUT (H-factor) changes were occurred on June 28th and July 11th of 2014, which had ripple effect on F-factors. The H/F-factor changes affected VIIRS radiometry up to 1.5 percent approximately especially in band M1. Thirdly, the calibration coefficients (C0) were updated on May 9th to be zero mostly affecting I3 approximately 1 percent drop in F-factor. Lastly, other operational anomalies such as 'Night Time Day Mode' and 'Sync Loss' events are explained in detail.
- The VIIRS ICVS LTM webpage has provided in-depth instrument monitoring information with very simple web-interface from imagery analysis to radiometric calibration. The calendar based browsing capability also provided excellent accessibility to locate the timing of the anomalous events. The VIIRS ICVS LTM webpage will be improved to meet the growing needs for the high quality satellite data providing essential information on the satellite performance.

Introduction

- STAR Integrated Cal/Val System (ICVS) Long-Term Monitoring (LTM) system
  - ✓Turn instrument measurements into accurate environmental parameters.
  - ✓Ensure high-quality satellite imagery for forecasts
    - ➢e.g., hurricane tracking and monitoring.
  - ✓Deliver accurate products for weather forecasts and environmental monitoring.
  - ✓Ensure the integrity of the climate data records from broader satellite instruments.
- VIIRS ICVS LTM webpage provides (as shown in Figure 1)
  - ✓Imagery Analysis (Global true color image, VIIRS single band image, VIIRS overall SDR quality)
  - ✓Calibration factor trending plots (RSB/TEB F factors, H factor)
  - ✓Solar Diffuser Stability Monitor (SDSM) related trending results
  - ✓Solar Diffuser (SD) related plots per band, Blackbody (BB) related plots per band, Space View (SV) related plots per band.
  - ✓Instrument health, Volt and current trending plots, Instrument/Focal Plane/Circuit Card Assembly/Scan Cavity temperatures.

Figure 1. ICVS LTM Webpage with VIIRS sensor at http://www.star.nesdis.noaa.gov/icvs/status_NPP_VIIRS.php

Significant Events in Year 2014

- **Single Board Computer (SBC) Lock-Up Events**
  - ✓Data loss occurred during the SBC Lock-Ups in Figure 1 on October 9th.
  - ✓Caused by high energy particle hits and improvements are implemented to the next J1 [1].
  - ✓The staring locations and orbits were varying for all the events as shown in Table 1.
  - ✓ SV counts were reset to higher values because of the new DC restore values in Figure 2.
  - ✓SD counts were also moving along with the SV, the bias corrected SD responses remained in stable levels in Figure 2.
  - ✓The SBC lock-up didn't affect the Reflective Solar Band (RSB) calibration
  - ✓No huge impact on TEB calibration, since the blackbody (BB) temperature was immediately went back to the normal temperature of 292.66K as shown in Figure 3.

Table 1. Detailed information on S-NPP VIIRS SBC lock-up events in 2014.

SBC lock-up event #	Date	Time	Duration	Starting Location	orbit
6	2/4/2014	17:38 – 21:35	3 hours 37 minutes	South America	Day
7	8/8/2014	14:20 – 18:50	4 hours 30 minutes	East Australia	Night
8	9/26/2014	18:25 – 18:35	10 minutes	Arctic near America	Day
9	10/9/2014	17:22 – 19:31	2 hours 9 minutes	South America	Day

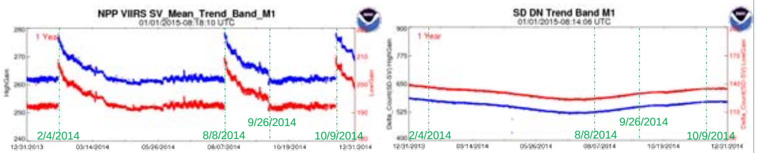

Figure 2. VIIRS SV and bias corrected SD trending results along with the SBC lock-up events in 2014.

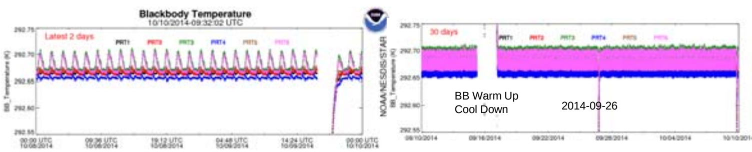

Figure 3. VIIRS BB temperature trending near the 8th and 9th SBC lock-up events..

- **Reflective Solar Band (RSB) F and H factor Trend Changes**
  - ✓Due to flattening anomaly in SD degradation in 2014, there were two times of sudden updates in SD degradation, i.e. the H-factors on May 23rd and July 11th, 2014.
  - ✓ The flattening anomaly started approximately from Feb 4th to May 19th as shown as red dotted lines in Figure 4.
  - ✓To compensate the flattening effects, two sudden H-factor updates were applied in operational H factor in blue dotted lines.
  - ✓Figure 5 show significant F-factor discontinues directly affected radiometric calibration especially in M1~M4 bands.

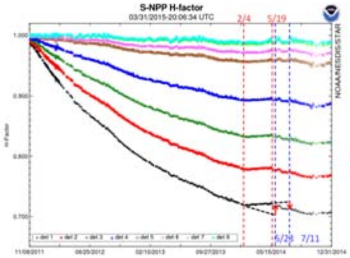

Figure 4. SD degradation flattening start dates (in red) and update dates (in blue).

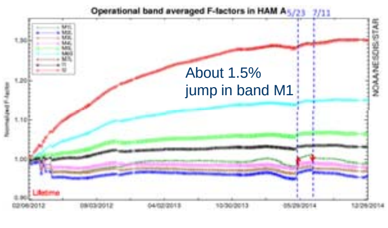

Figure 5. operational F-factors affected by H-factor updates on May 23rd and July 11th in 2014

- **Delta C_0=0 Coefficient Update**
  - ✓The C coefficients represent thermal responses of the detectors and electronics.
  - ✓The C0 values were set to zero for all RSB bands and the C2 values were derived by the prelaunch test results starting from May 9th.
  - ✓Changes were < 0.5% in most of the RSB bands, but I3 had approximately 1% change in Figure 6.

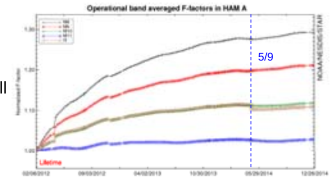

Figure 6. VIIRS delta C0=0 coefficient update on May 9th, 2014.

- **Night Time Day Mode Anomaly**
  - ✓Day mode collections (Op_day) were reversed to night mode operation (Op_night) approximately between 15:00 and 21:00 on June 12th.
  - ✓Operational team quickly recovered the anomaly. RSB SDR data are missing except bands M7, M8 and M10.
  - ✓Figure 7 shows quality flag images and the quality flags were reversed responses during the anomaly periods.

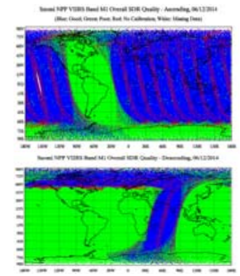

Figure 7. Night time day mode anomaly capture by the global quality flag images.

- **VIIRS RTA and HAM Synchronization Loss (Sync Loss)**
  - ✓The root cause of this event is accumulation of charges in the Scan Control Electronics assembly (SCE) [2].
  - ✓The improved design was applied to J1.
  - ✓There were 5 Sync Loss events during 2014 as listed in Table 2.
  - ✓Figure 12 shows global image of quality flag in band M2 on 4/2/2014.

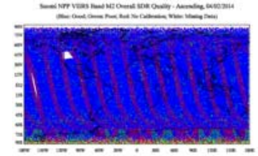

Figure 7. The global quality flag captured the Sync Loss event on 4/02/2014.The white patch indicates the data loss during the Sync Loss event from 20:14:21 to 20:15:52 UTC.

Table 2. Detailed information on the Sync Loss in 2014.

Sync Loss #	Date	Starting Time	Ending Time	Duration
36	3/8/2014	16:29:26	16:31:06	1 min 40 sec
37	3/12/2014	03:15:53	03:17:32	1 min 39 sec
38	4/2/2014	20:14:21	20:15:52	1 min 31 sec
39	5/20/2014	07:53:39	07:55:19	1 min 40 sec
40	11/8/2014	15:09:51	15:11:30	1 min 39 sec

Summary

- The NOAA ICVS LTM webpage for VIIRS sensor is continually providing critical global images, quality flags and calibration related trending plots.
  - ✓Indicating sensor status and data coverage.
- The S-NPP VIIRS related significant events in year 2014 are summarized here such as, Single Board Computer (SBC) Lock-Up Events, RSB F and H factor trend changes, delta C_0=0 coefficient update, night time day mode anomaly, RTA and HAM synchronization loss events.
- The VIIRS ICVS LTM team is ready to apply current system to next J1 trending.

References

[1] Changyong Cao, "JPSS STAR Science Team Annual Meeting: VIIRS SDR Team Report," 2014 STAR JPSS Annual Meeting, May 12-16, 2014, College Park, MD.

[2] Robert Wolfe, et al., "Suomi NPP VIIRS prelaunch and on-orbit geometric calibration and characterization," JOURNAL OF GEOPHYSICAL RESEARCH: ATMOSPHERES, VOL. 118, 11,508–11,521

Radiometric Performance Assessment of Suomi NPP VIIRS SWIR Band (2.25 µm)

Sirish Uprety[a] and Changyong Cao[b]

[a]CIRA, Colorado State University, College Park, MD, [b]NOAA/NESDIS/STAR, College Park, MD

Abstract

Suomi NPP VIIRS SWIR band M11 (2.25 µm) has larger radiometric uncertainty compared to the rest of the reflective solar bands. This is due to a number of reasons including prelaunch calibration uncertainties. One of the most commonly used technique to verify the radiometric stability and accuracy of VIIRS is by intercomparing it with other well calibrated radiometers such as MODIS. However one of the limitations of using MODIS is that VIIRS band M11 RSR doesn't overlap with MODIS bands at all. Thus the accuracy of intercomparison relies completely on how well the spectral differences are analyzed over the given target. This study uses desert sites to analyze M11 radiometric performance. In order to better match the RSR between instruments, we have chosen Landsat 8 OLI SWIR band 2 (2.20 µm) to perform intercomparison. This is mainly because OLI SWIR band 2 fully covers the VIIRS band M11 even though OLI has much wider RSR compared to VIIRS. The impact due to spectral differences is estimated and accounted for using EO-1 Hyperion observations and MODTRAN.

Introduction

- The radiometric stability and accuracy of VIIRS is critical to make its data useful for weather and climate applications.
- VIIRS on-orbit radiometric performance is regularly monitored and analyzed using well established calibration sites (such as Libya-4, Sudan-1, Dome C calibration sites) and through the inter-comparison with other satellite instruments such as AQUA MODIS and Landsat 8 OLI.
- This study uses a well characterized Libya-4 Saharan desert calibration site to monitor the radiometric performance of VIIRS SWIR band M11 (2.25 µm).
- It is more complicated and challenging to accurately calibrate VIIRS M11 band at lower radiance because the reflected radiance for M11 is very small on the order of 0.1 - 0.2 w/m^{2}sr^{-1} or less over ocean compared to nearly 7-8 w/m^{2}sr^{-1} over desert.
- We have focused on Libya-4 calibration site under the assumption that the detectors are linear and results obtained at higher radiance is also valid at lower radiance.
- It is assumed that both AQUA MODIS and Landsat-8 OLI are correct in absolute scale and the sensor intercomparison is performed with MODIS and OLI to assess how well the band M11 is calibrated.
- M11 doesn't overlap with any AQUA MODIS bands. Still the comparison study is performed with closest matching MODIS band assuming that the spectral differences could be characterized using hyperspectral measurements.

Methodology

Sensor	S-NPP VIIRS	Landsat-8 OLI	AQUA MODIS	EO-1 Hyperion
Spatial Resolution	750 m	30 m L1GST	1 km	30 m

Libya-4 Desert calibration site

- Libya-4 (28.55°, 23.39°) is a CEOS endorsed cal/val site.
- It is a Saharan desert calibration site used mostly for on-orbit cal/val of VNIR radiometers.

Figure 1. Calibration Site

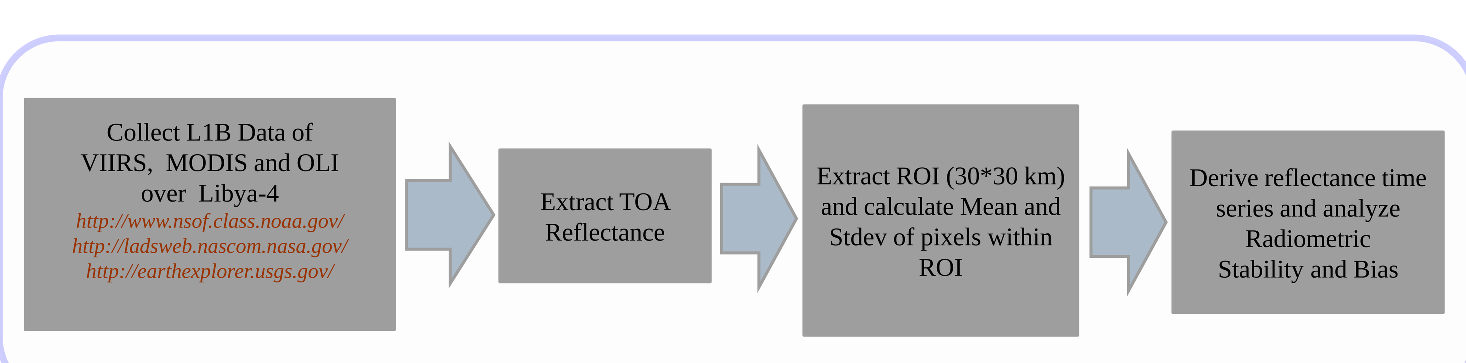

Figure 2. Estimate VIIRS bias over Libya-4

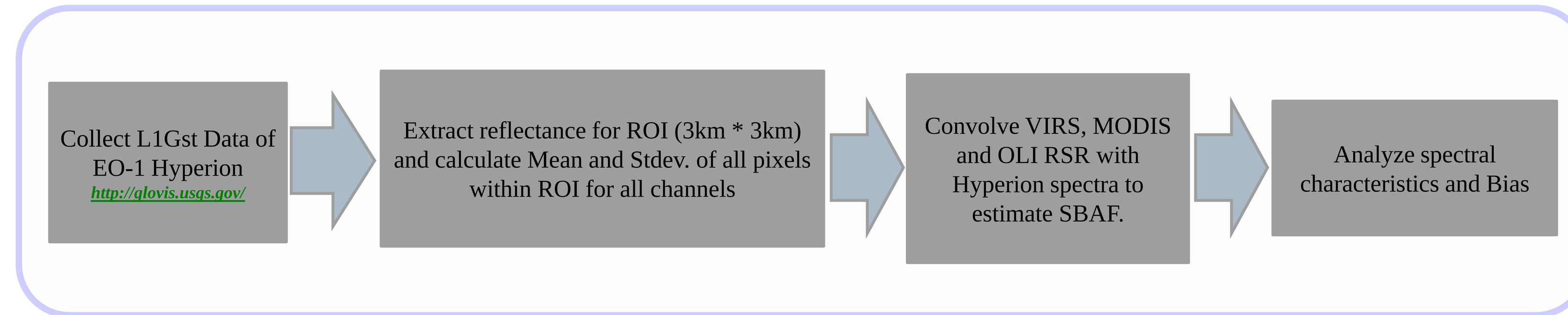

Figure 3. Estimate VIIRS spectral bias over Libya-4 using EO-1 Hyperion

Results

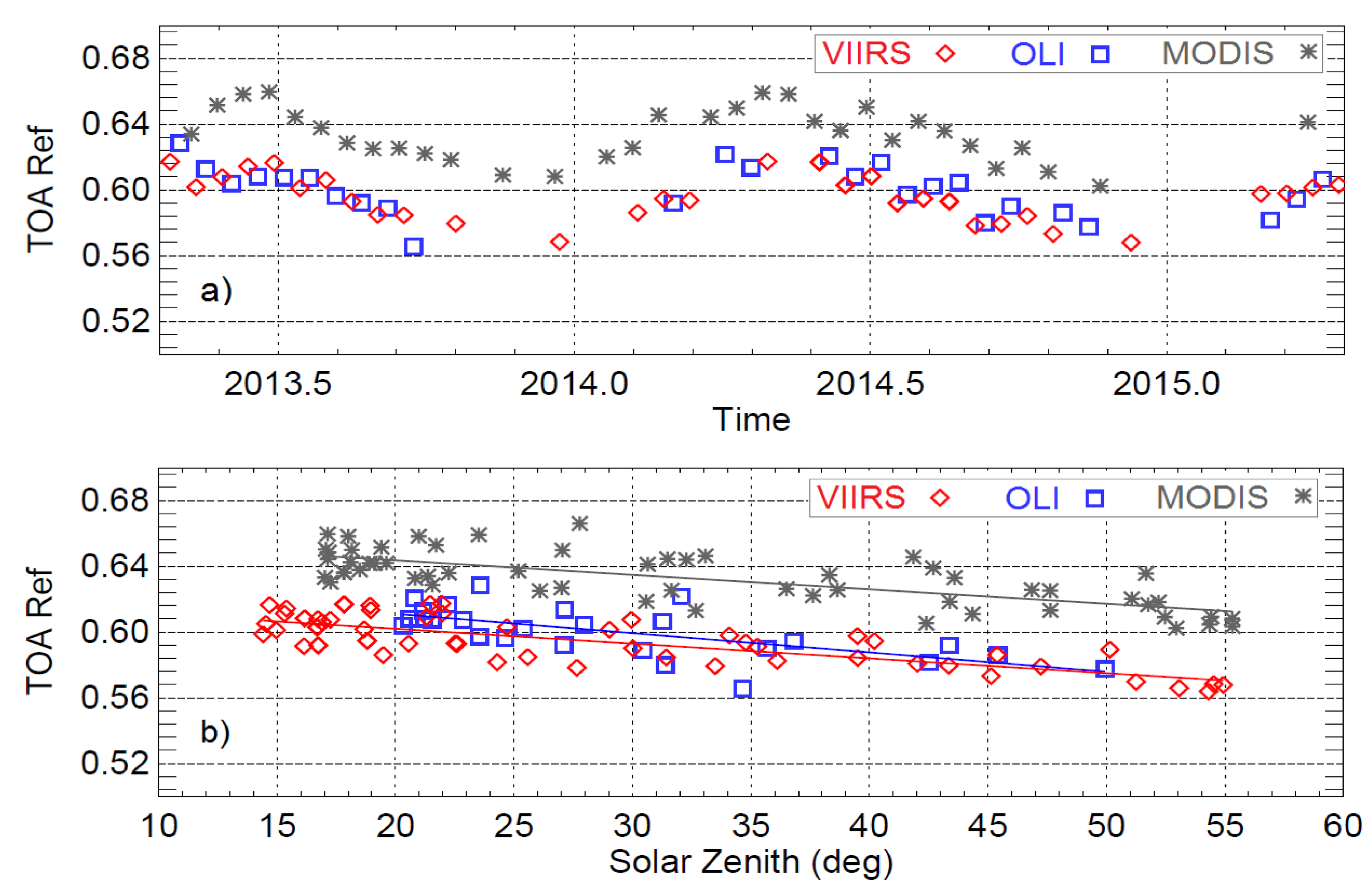

Figure 4. VIIRS, MODIS and OLI TOA reflectance over Libya-4 as a function of a) Time b) Solar Zenith Angle

- VIIRS M11 band and its matching MODIS and OLI bands suggest noisier time series.
- OLI and MODIS RSRs are near the water vapor absorption wavelength and are impacted by atmospheric water vapor absorption variability.
- Bias is analyzed as a function of solar zenith angle to reduce the impact due to bidirectional reflectance distribution function (BRDF).
- VIIRS observed bias (before accounting impact due to spectral differences) is 1.44% relative to OLI and 6.5% relative to MODIS with 1-sigma uncertainty on the order of 1.4%.
- Short term anomalies are not clearly noticeable due to higher variability in the time series. Change in data trend due to major calibration updates and anomalies further increases the uncertainty.

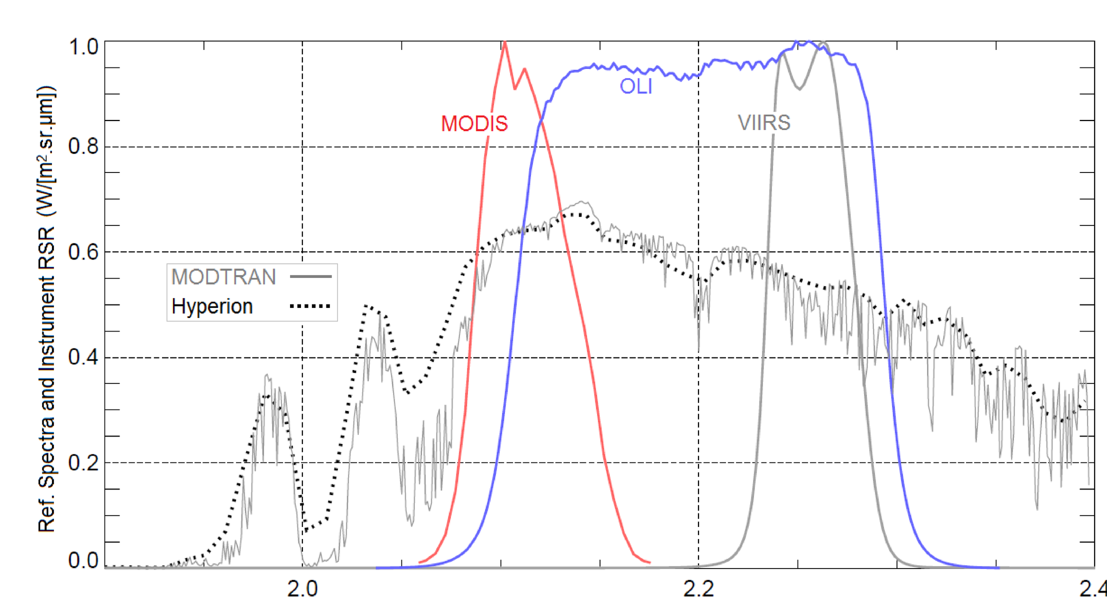

Figure 5. VIIRS, MODIS and OLI matching bands. MODIS and M11 RSR doesn't overlap at all. OLI completely covers M11 RSR but has much wider bandwidth.

- MODTRAN reflectance is scaled to match the maximum value with Hyperion near 2.2 µm.
- Reflectance spectra from Hyperion and MODTRAN match well with each other except over the region where atmospheric absorption is large.
- The reason is mainly because the atmospheric water vapor contents are different for Hyperion and MODTRAN.
- Spectral bias computed using Hyperion is 6.7% relative to MODIS and 6.9% relative to OLI.
- The uncertainty is much larger for MODIS (3.1%) compared to OLI (0.9%).

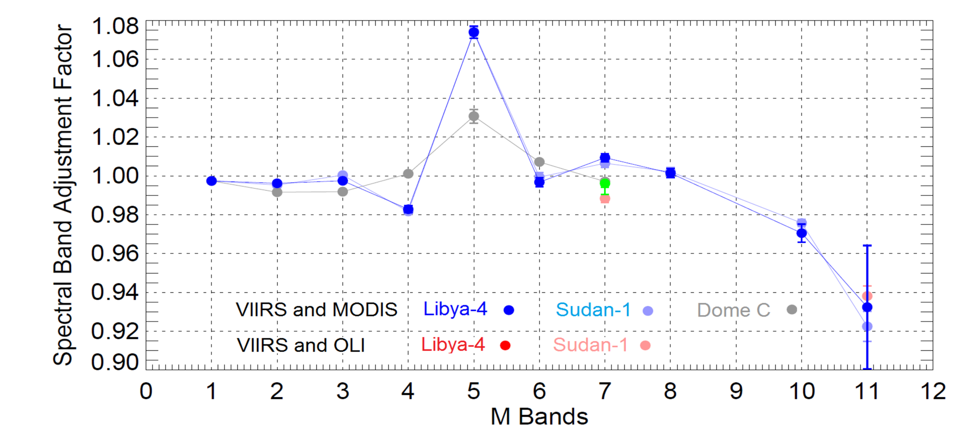

Figure 6. SBAF of VIIRS bands computed using MODIS and OLI (*Ref: Uprety et al. 2015*). Large number of Hyperion observations (150 over Libya-4) used to estimate the SBAF.

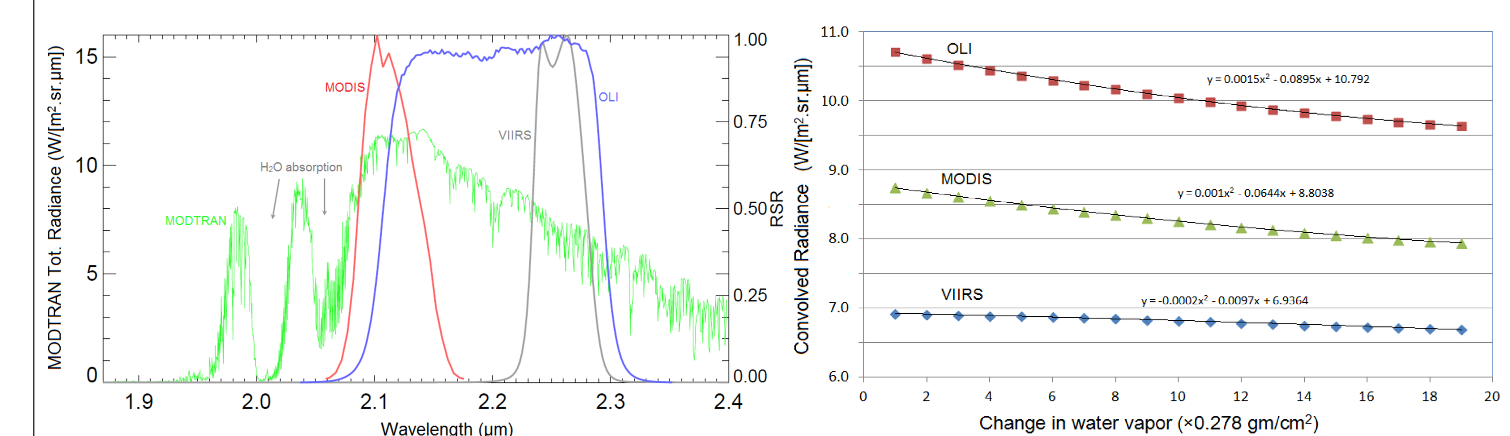

Figure 7. Left: Radiance spectra over desert using MODTRAN. MODIS and OLI are more susceptible to water vapor absorption Right: Radiance trend generated by changing water vapor from 0.278 to 5.28 gm/cm^2

- With change in water vapor input, the maximum change in radiance is 3.1% for VIIRS, 9% for OLI and 10% for MODIS indicating MODIS and OLI bands being largely impacted by atmospheric water vapor compared to VIIRS.

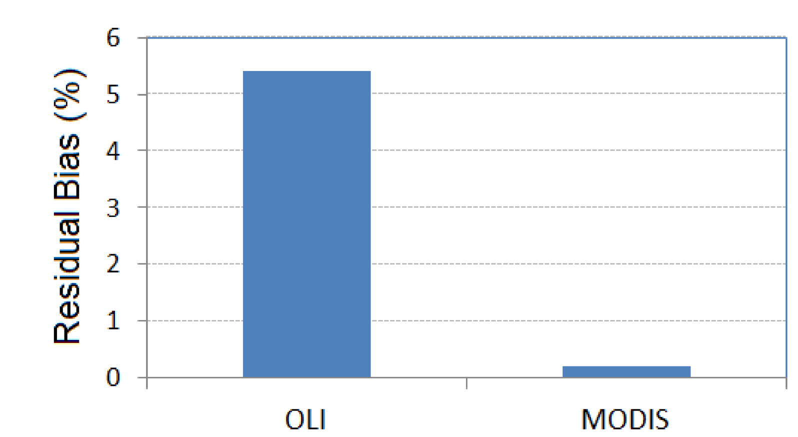

Figure 8. VIIRS M11 bias over Libya-4 desert estimated using TOA reflectance trending, Bias=(V-M)×100%/M (after accounting RSR differences between the matching VIIRS and MODIS bands).

- The residual bias of VIIRS is the difference between observed bias and spectral bias.
- Even though VIIRS and OLI measurements agree very well to less than 1.5%, the spectral differences suggest large true bias.
- The residual bias of VIIRS is nearly 6% relative to OLI and nearly 0.5% relative to MODIS.

Summary

- The radiometric stability of VIIRS moderate resolution reflective solar band M11 analyzed using Libya-4 desert site is better than 1% with uncertainty less than 1%.
- VIIRS M11 radiometric bias (analyzed after accounting for spectral differences) estimated through VIIRS band M11 inter-comparison using TOA reflectance time series over desert suggest nearly 5.4% relative to OLI and less than 0.5% relative to MODIS.
- The result from this study is valid for low radiance under the assumption that detector responses are linear over the dynamic range (Lmin: 0.12 to Lmax: 31.8 W m^{-2} sr^{-1}µm^{-1}) of M11.
- The root cause for large VIIRS bias relative to OLI needs to be investigated in the future.
- The discrepancy in bias relative to OLI and MODIS also needs to be further investigated in more detail.

References:

[1] Cao, C., F. Deluccia, X. Xiong, R. Wolfe, and F. Weng, "Early on-orbit performance of the Visible Infrared Imaging Radiometer Suite onboard the Suomi National Polar-Orbiting Partnership (S-NPP) satellite." IEEE Trans. Geosci. Remote Sens., doi:10.1109/TGRS.2013.2247768

[2] Cao, C., J. Xiong, S. Blonski, Q. Liu, S. Uprety, X. Shao, Y. Bai, and F. Weng, "Suomi NPP VIIRS sensor data record verification, validation, and long-term performance monitoring", Journal of Geophysical Research: Atmospheres 118 (20), 11,664-11,678 (2013).

[3] Uprety, S., & Cao, C. Suomi NPP VIIRS reflective solar band on-orbit radiometric stability and accuracy assessment using desert and Antarctica Dome C, Remote Sensing of Environment http://dx.doi.org/10.1016/j.rse.2015.05.021

[4] Uprety, S., C. Cao, X. Xiong, S. Blonski, A. Wu, and X. Shao, "Radiometric Inter-comparison between Suomi NPP VIIRS and Aqua MODIS Reflective Solar Bands using Simultaneous Nadir Overpass in the Low Latitudes," Journal of Atmospheric and Oceanic Technology (2013).

[5] Uprety, S., C. Cao, S. Blonski, & W. Wang, "Assessment of VIIRS radiometric performance using vicarious calibration sites," *SPIE Optical Engineering+ Applications* , pp. 92180I-92180I (2014)..

Acknowledgment :

This study is partially funded by the Joint Polar Satellite System (JPSS) program.

Monitoring the VIIRS Reflective Solar Band Calibration Stability Using Deep Convective Clouds

Wenhui Wang[a] and Changyong Cao[b]

[a] Earth Resource Technology, Inc., Laurel, MD, USA; [b]NOAA/NESDIS/STAR, College Park, MD USA

1. Introduction

The Visible and Infrared Imaging Radiometer Suite (VIIRS) onboard the Joint Polar Satellite System (JPSS) / Suomi National Polar-Orbiting Partnership (NPP) satellite has 22 spectral bands, with 14 Reflective Solar Bands (RSB), 7 Thermal Emissive Bands (TEB) and 1 Day Night Band (DNB). Onboard calibration of VIIRS is complex, especially for the RSBs and DNB, which are calibrated using a full-aperture solar diffuser (SD) and the degradation of SD is monitored by a solar diffuser stability monitor (SDSM). Significant SD degradations were observed in the visible and near-infrared spectrum. It is important to use independent validation time series to evaluate post-launch calibration stability of VIIRS RSBs and DNB.

Deep Convective Clouds (DCC) are extremely cold clouds that start from the planetary boundary layer and ascend to the tropical tropopause transition layer. The absorptions due to water vapor and other gases over DCCs are minimal. DCCs are bright targets and have nearly Lambertian reflectance . DCCs have been widely used as bright calibration targets for post-launch calibration and stability monitoring of radiometers in the visible and near-infrared spectrums for a variety of satellite instruments in the past decade. The purpose of this study is to investigate radiometric calibration stability of VIIRS RSB and DNB bands (M1-M5, M7-M11, I1-I3, and DNB) using the DCC technique.

2. VIIRS Dataset Used

Figure 1 Area of interest.

- **Area of Interest**: Latitude -25° – 25°; Longitude: -150 ° – -60°
  An area also observed by GOES-East & GEOS-West
- **Bands Used**:
  RSB bands: M1-M5, M7-M11, I1-I3, DNB
  TEB bands: M15 (10.729 µm) & I5 (11.469 µm)
- **Time Period**: March 2012 – June 2015

3. VIIRS DCC Identification Method

VIIRS DCC identification criteria (Wang and Cao 2014; 2015) :

1. **TB11 (M15 or I5) <= 205 K;**
2. **Standard deviation of TB11 of the subject pixel and its eight adjacent pixels <= 1K;**
3. **Standard deviation of VIS/NIR reflectance of the subject pixel and its eight adjacent pixels<= 3%;**
4. **Solar zenith angle (SZA) <= 40 degree;**
5. **View zenith angle (VZA) <= 35° (to avoid the bow-tie effect in VIIRS dataset);**
6. **DNB radiances were mapped to M15 lat/lons before DCC pixels were identified using M15 TB11.**

4. Monthly Probability Distribution Functions for VIIRS DCC

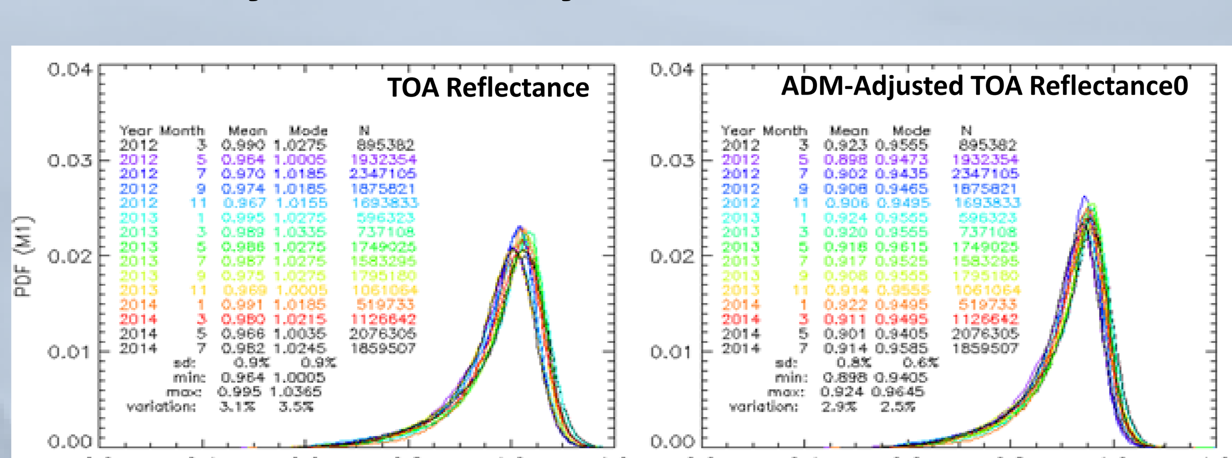

Figure 2 Monthly probability distribution functions (PDFs) of VIIRS DCC reflectance for before (left panel) and after (right panel) the correction of the anisotropic effects.

- **Anisotropic effect is corrected using Hu et al. (2004) Angular Distribution Model (ADM)**
- **Mean & mode of the monthly PDFs are two Important indices when using DCC for calibration**
- **Mode is used for individual bands calibration stability monitoring**
  -- **More stable than mean in the VIS/NIR spectrum**
- **Mean ratio is used for inter-channel relative calibration stability monitoring**
  -- **Mean ratio more stable than mode ratio**

5. DCC Time Series for Individual Bands Cal. Stability Monitoring

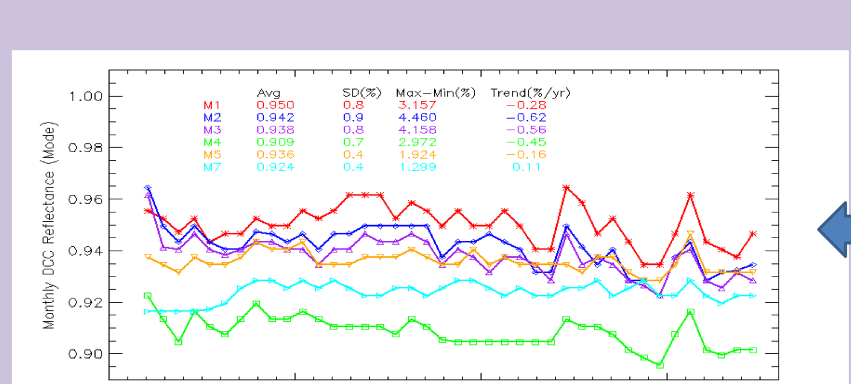

M1-M5,M7 (VIS/NIR 0.411 – 0.862 µm)

- **SD : <=0.9%**
- **Max - Min <=4.5%**
- **M5 & M7 are relatively more stable**
- **M6 saturated over DCCs, not considered**

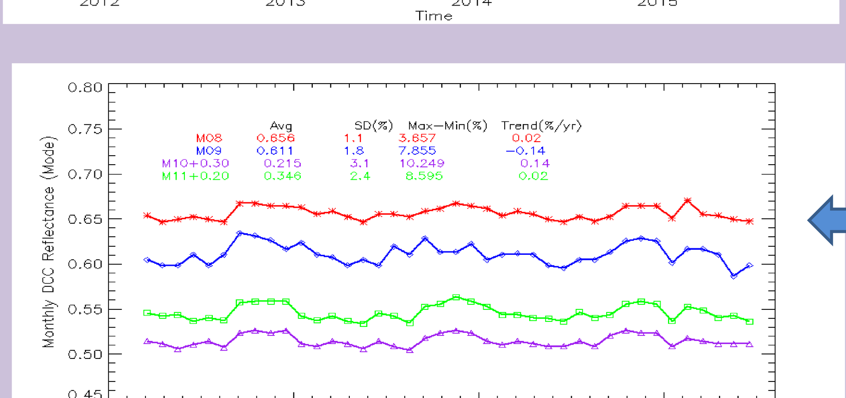

M8-M11 (SWIR 1.238 – 2.257 µm)

- **SD : 1.1 – 3.1 %**
- **Max – Min: 3.6 – 10.2 %**
- **M8 is relatively more stable**

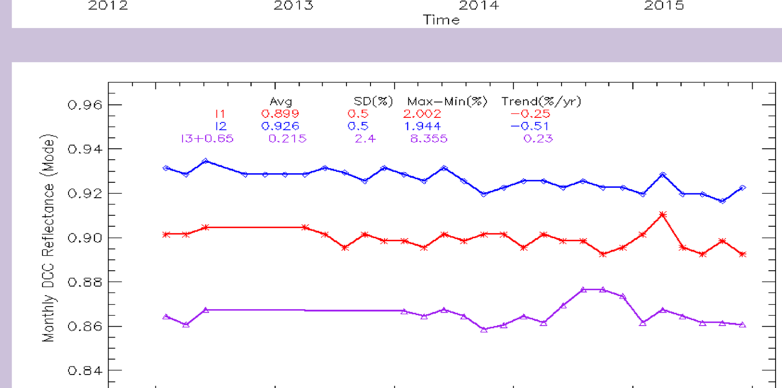

I1, I2 & I3 perform similar as M5, M7, M10, respectively

Figure 3 Monthly DCC mode time series for M1-M5 & M7, M8-M11, and I1-I3

5. DCC Time Series for Individual Bands Calibration Stability Monitoring (Continued)

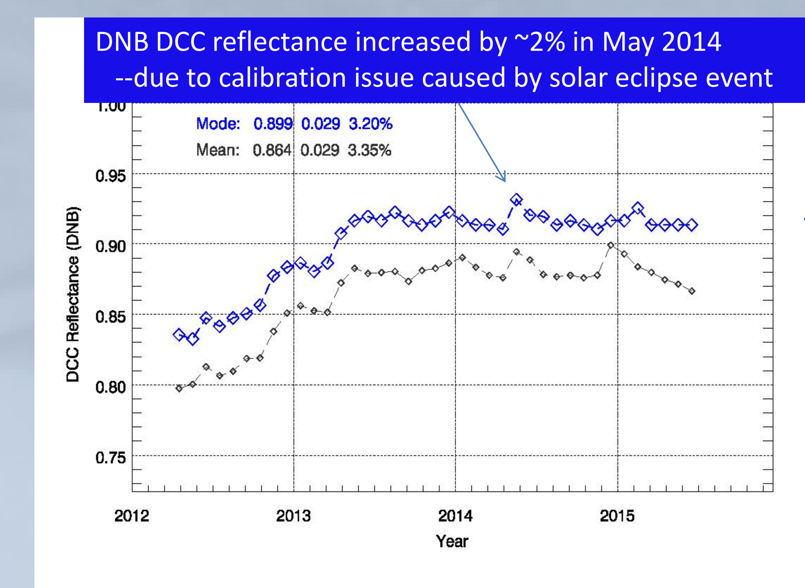

DNB (Daytime, Low Gain Stage)
- Generally stable since April 2013, after RSR update was implemented into operations.

Figure 4 Monthly DCC mode time series for DNB

6. Inter-Channel Relative Calibration Stability Monitoring Using DCC Mean Band Ratio Time Series

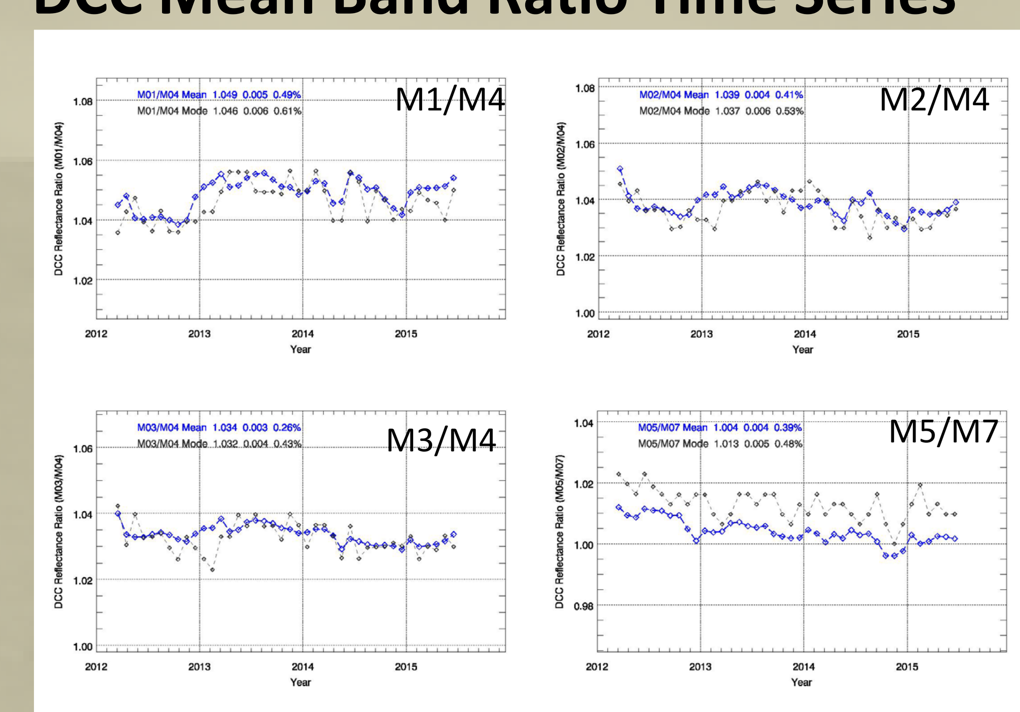

Figure 5 M1/M4, M2/M4, M3/M4, I5/I7 band ratio time series

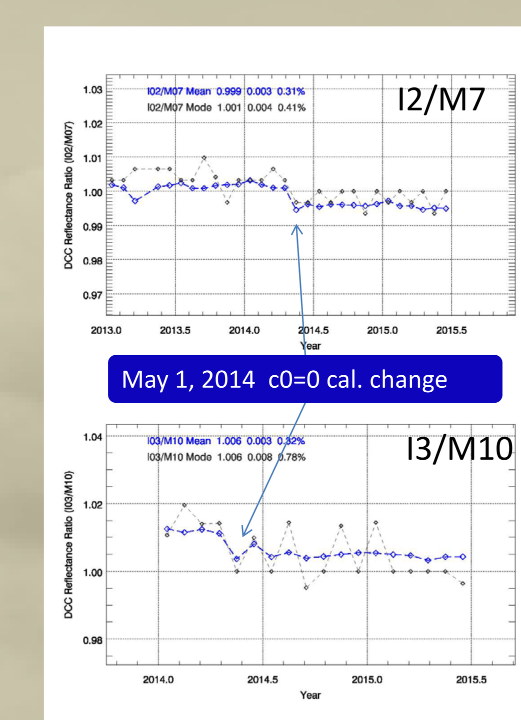

Figure 6 I2/M7, I3/M10 time series

- M1/M4 & M2/M4: 2012 & 2013 show different ratio patterns → coincident with OC group complains
- A downward trend is observed in the M5/M7 band ratio time times.

- I2 & M7 become less consistent after cal. change
- I3 & M10 become closer after cal. change

7. DCC Time Series vs. IDPS F-factor Time Series

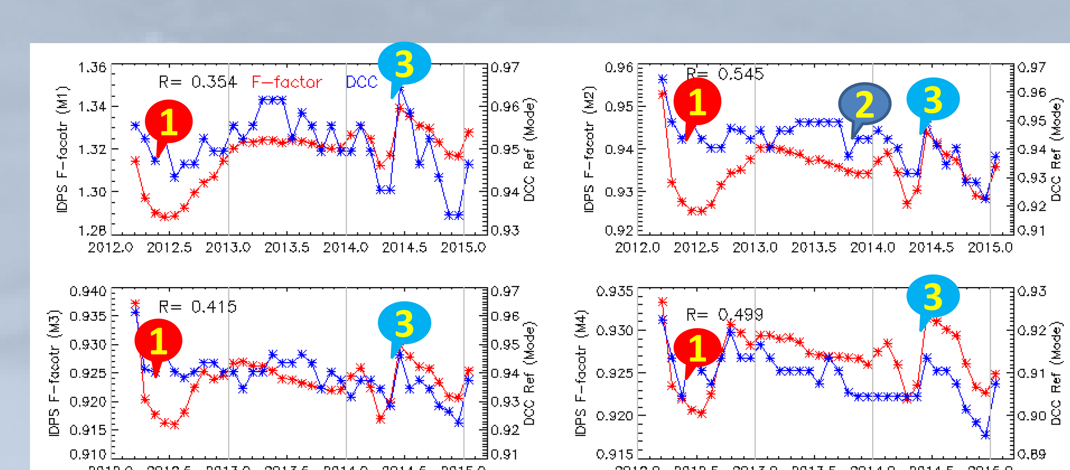

Figure 7 Comparing DCC mode and IDPS F-factor time series

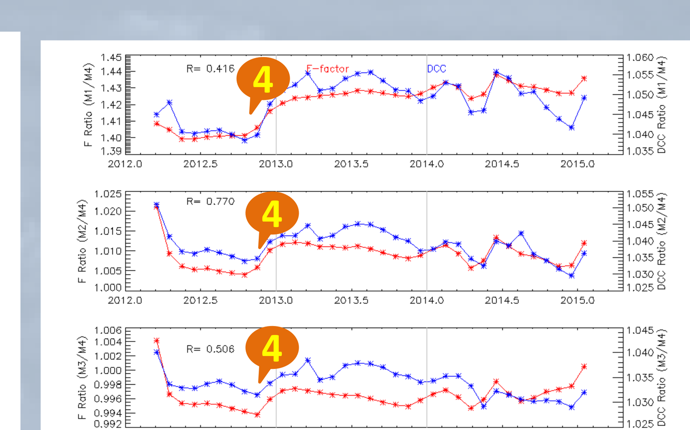

Figure 8 Comparing DCC mean band ratio and IDPS F-factor ratio time series

1. Apr 2012 IDPS code & LUTs changes
2. Oct 2013 SDSM misalignment
3. May 22, 2014 cal. Change
4. Nov 2012 SD processing param. change

DCC time series correlated with F-factor time series Correlations are stronger since Janunary 2014

8. Summary

- **STAR VIIRS SDR support team developed DCC time series for VIIRS calibration stability monitoring**
  - **https://cs.star.nesdis.noaa.gov/NCC/VSTS , update monthly**
  - **Completed M1-M5, M7-M11 & DNB (2012/03 – present)**
  - **Capable of capture calibration changes**
- **RSB calibration stability**
  - **M-Bands VIR/NIR Bands (M1-M5,M7)**
    --M1-M4 have large calibration changes
    --M5&M7 are relatively stable
    --M1/M4 & M2/M4 show different patterns in 2013 & 2014
  - **M-Bands SWIR Bands (M8-M11)**
    --M9-M10 large calibration changes
    --M8 is relatively stable
  - **I-Bands (I1-I3) perform similar as M5,M7,M10, respectively**
  - **DNB is relatively stable after April 2013**

References

Cao, C., and Coauthors, 2013b: Suomi NPP VIIRS sensor data record verification, validation, and long-term performance monitoring. *Journal of Geophysical Research: Atmospheres, 2013JD020418.*
Doelling, D. R., D. Morstad, B. R. Scarino, R. Bhatt, and A. Gopalan, 2013: The Characterization of Deep Convective Clouds as an Invariant Calibration Target and as a Visible Calibration Technique. *Geoscience and Remote Sensing, IEEE Transactions on*, 51, 1147-1159.
Hu, Y., B. A. Wielicki, Y. Ping, P. W. Stackhouse, Jr., B. Lin, and D. F. Young, 2004: Application of deep convective cloud albedo observation to satellite-based study of the terrestrial atmosphere: monitoring the stability of spaceborne measurements and assessing absorption anomaly. *Geoscience and Remote Sensing, IEEE Transactions on*, 42, 2594-2599.
Minnis, P., D. R. Doelling, L. Nguyen, W. F. Miller, and V. Chakrapani, 2008: Assessment of the Visible Channel Calibrations of the VIRS on TRMM and MODIS on Aqua and Terra. *Journal of Atmospheric and Oceanic Technology*, 25, 385-400.
Wang, W. and C. Cao (2015). "DCC Radiometric Sensitivity to Spatial Resolution, Cluster Size, and LWIR Calibration Bias Based on VIIRS Observations." Journal of Atmospheric and Oceanic Technology **32(1): 48-60.**

Intercomparison of SNPP/VIIRS Longwave Infrared Channels Using Hyperspectral Radiance from GOSAT FTS and MetOp-A IASI

Bin Zhang [1,2], Changyong Cao [3]

1 Earth Resourses Technology, Inc, College Park, MD 20740, USA
2 CICS/ESSIC, University of Maryland, College Park, MD, USA
3 NOAA/NESDIS/SMCD, College Park, MD, USA

Introduction:

- The Visible Infrared Imaging Radiometer Suite (VIIRS) onboard Suomi-NPP has four longwave infrared bands(I5, M14, M15 and M16).
- Calibration of VIIRS thermal band radiance has been performed onboard. Inter-comparison between VIIRS and Cross-track Infrared Sounder (CrIS) becomes difficult for M14-16 because CrIS has a spectra gap (8.26um to 9.14um) that does not cover M14, and the Spectral Response Function(SRF) of M15 and M16 are not fully covered.
- The Greenhouse Gases Observing SATellite (GOSAT) is equipped with a Fourier Transform Spectrometer (FTS). The band 4 of FTS measures hyper-spectral radiance (5um-15um). It is feasible to compare the FTS measurements with the VIIRS longwave infrared channels.
- Infrared Atmospheric Sounding Interferometer(IASI) onboard MetOp-A covers a complete hyper-spectra (3.63um-15.5um). It can also be used to compare with VIIRS M14-16 bands.
- In this study, inter-comparison between FTS and VIIRS, between IASI and VIIRS for the three longwave infrared bands are carried out.

IASI	Full Spectra 15.5-3.63um,0.5cm^{-1} Resolution, 0.25 cm^{-1} sampling interval
CrIS	3 Frequency Bands, 9.14-15.38 um (0.625 cm^{-1}), 5.71-8.26 um(1.25cm^{-1}), 3.92-4.64um (2.5cm^{-1})
FTS	Band4: 5.5-14.3um, Sampling interval: ~0.2 cm^{-1}; resolution: 0.27 cm^{-1}

Hyperspectral characteristics for IASI, CrIS and FTS. The CrIS longwave infrared band has a gap of 8.26-9.14um.

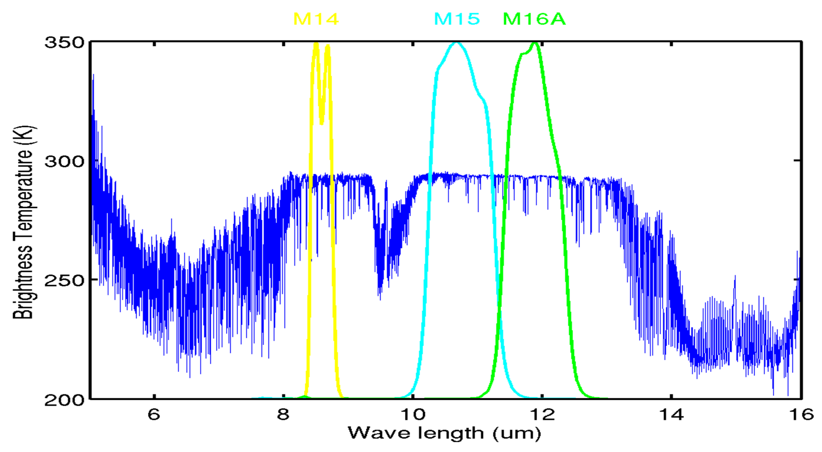

VIIRS M14-16 SRF overlapped with FTS observed hyperspectral brightness temperature.

Methods:

- Simultaneous Nadir Overpass (SNO) locations and time between FTS and VIIRS, and between IASI and VIIRS are determined using orbital model(SGP4) and Two-line-elements data. Collocated pixels are obtained by comparing actual geolocations near the given SNO location and time.
- We use the FTS/VIIRS datasets of 01/2014-06/2014, and IASI/VIIRS datasets of 01/2014-01/2015.
- Convolving VIIRS M band SRF and hyperspectral radiance from FTS and IASI at the collocated FOVs to obtain the simulated VIIRS radiance.

  $R=\frac{\int S(l)\cdot r(l)dl}{S(l)dl}$, where s is SRF, l is wavelength, r is hyperspectral radiance in wavelength.
- Averaging all the VIIRS observations (resolution of 750m) in the FTS (or IASI) FOVs. For FTS, we look at all FOVs falling within VIIRS 5° scan angle. For IASI, we look at the 15th and 16th FOVs.
- Inter-comparison is made between the simulated and observed values. The radiance ratio and brightness temperature difference are calculated.

SNO locations and collocation of FOV between FTS/VIIRS and between IASI/VIIRS

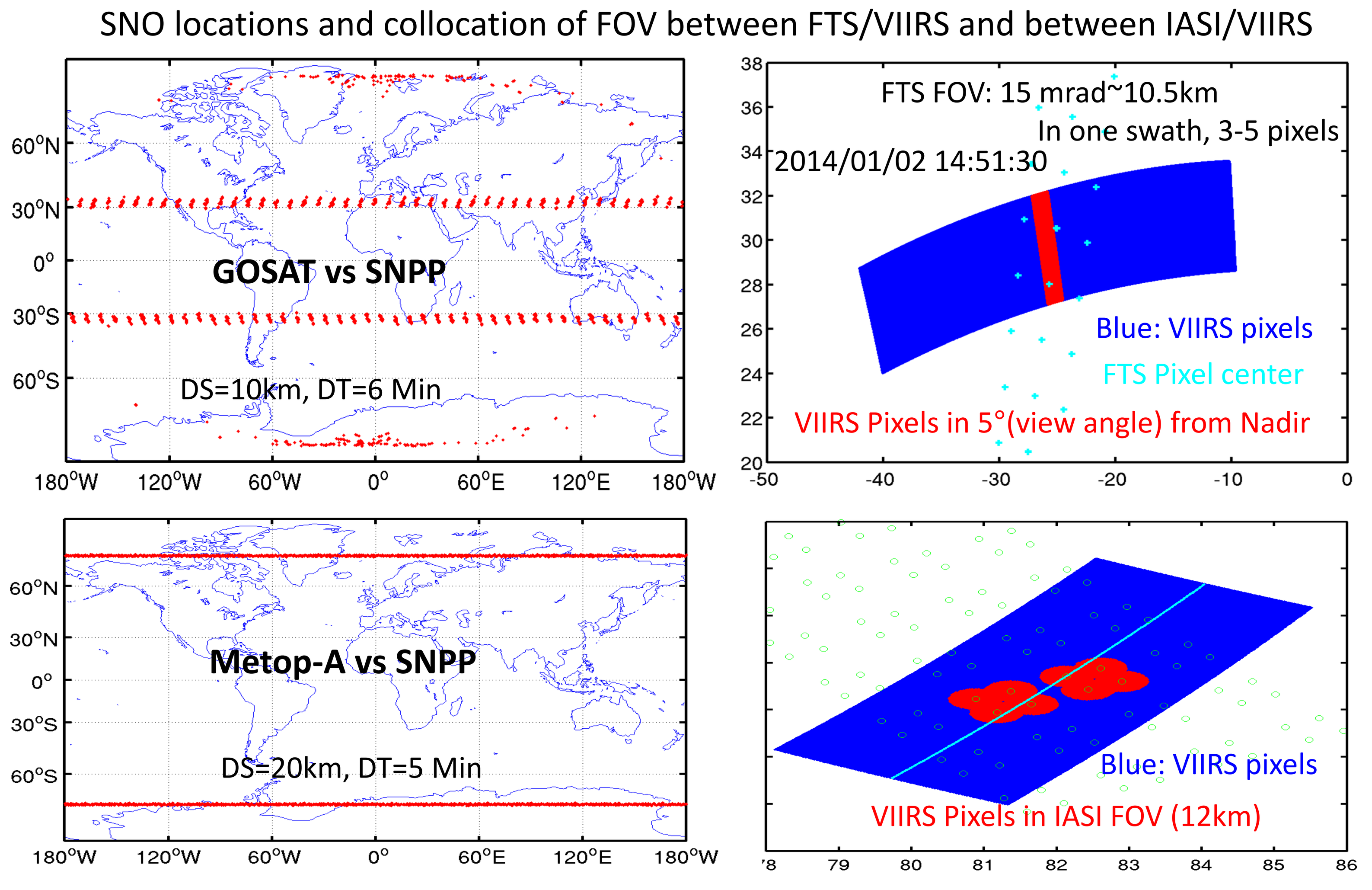

Results:

FTS/VIIRS: The simulated VIIRS radiance is close to observed for all three bands, with the brightness temperature difference of 0.54±0.36K for M14, 0.50±0.35K for M15, 0.46±0.34K for M16 (FTS minus VIIRS). The radiance ratio (FTS/VIIRS) is 1.011±0.007 for M14, 1.0080±0.006 for M15, 1.007±0.005 for M16. The radiance ratio has a weak positive dependency on the brightness temperature for all three band.

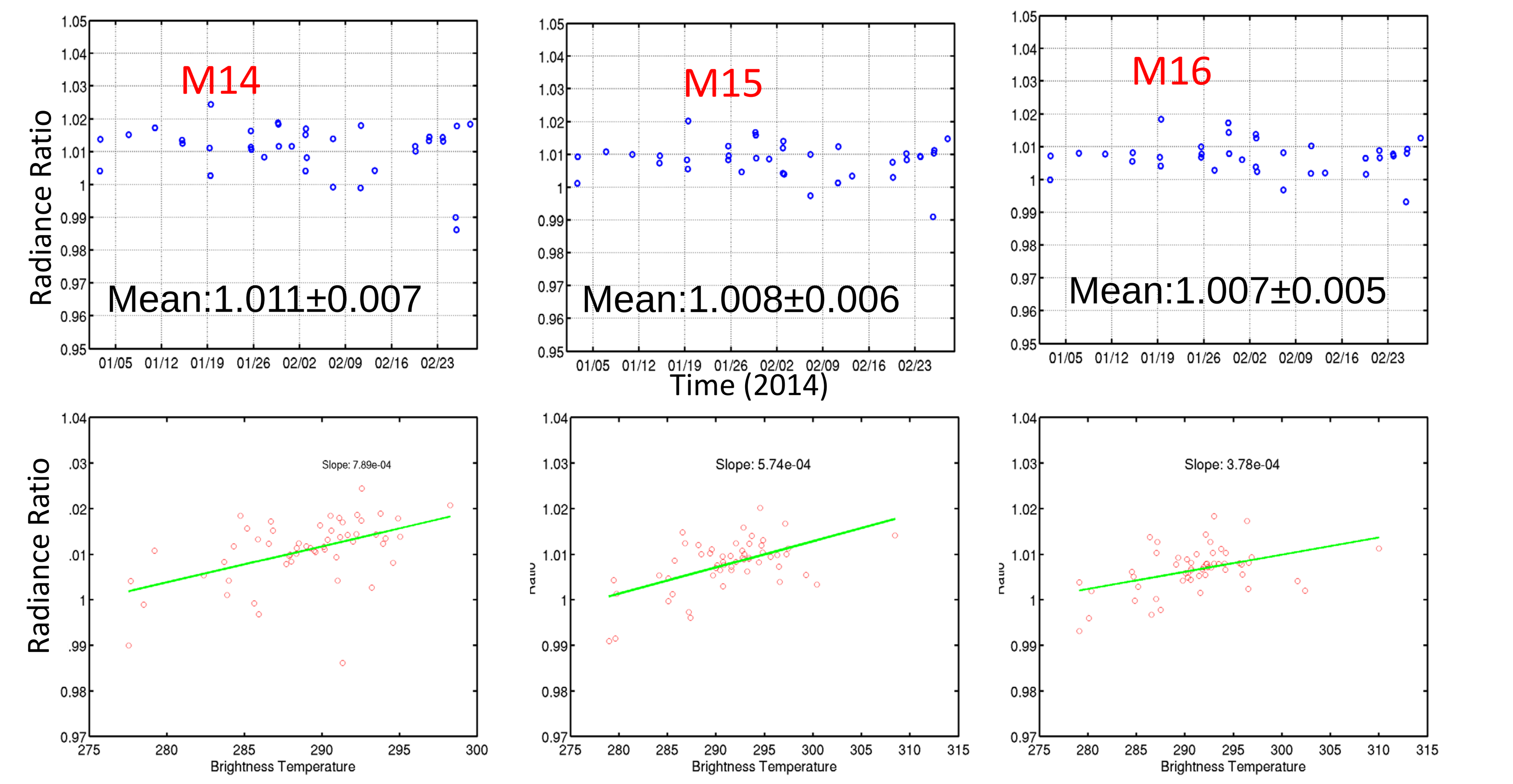

IASI/VIIRS: The brightness temperature difference (IASI-VIIRS) is 0.10±0.15K for M14, 0.02±0.15K for M15, -0.07±0.16K for M16. The radiance ratio is 1.003±0.004 for M14, 1.000±0.003 for M15 and 0.9985±0.004 for M16. Weak negative ratio dependency on scene temperature can be seen for M14, no clear ratio dependency for M15 and M16.

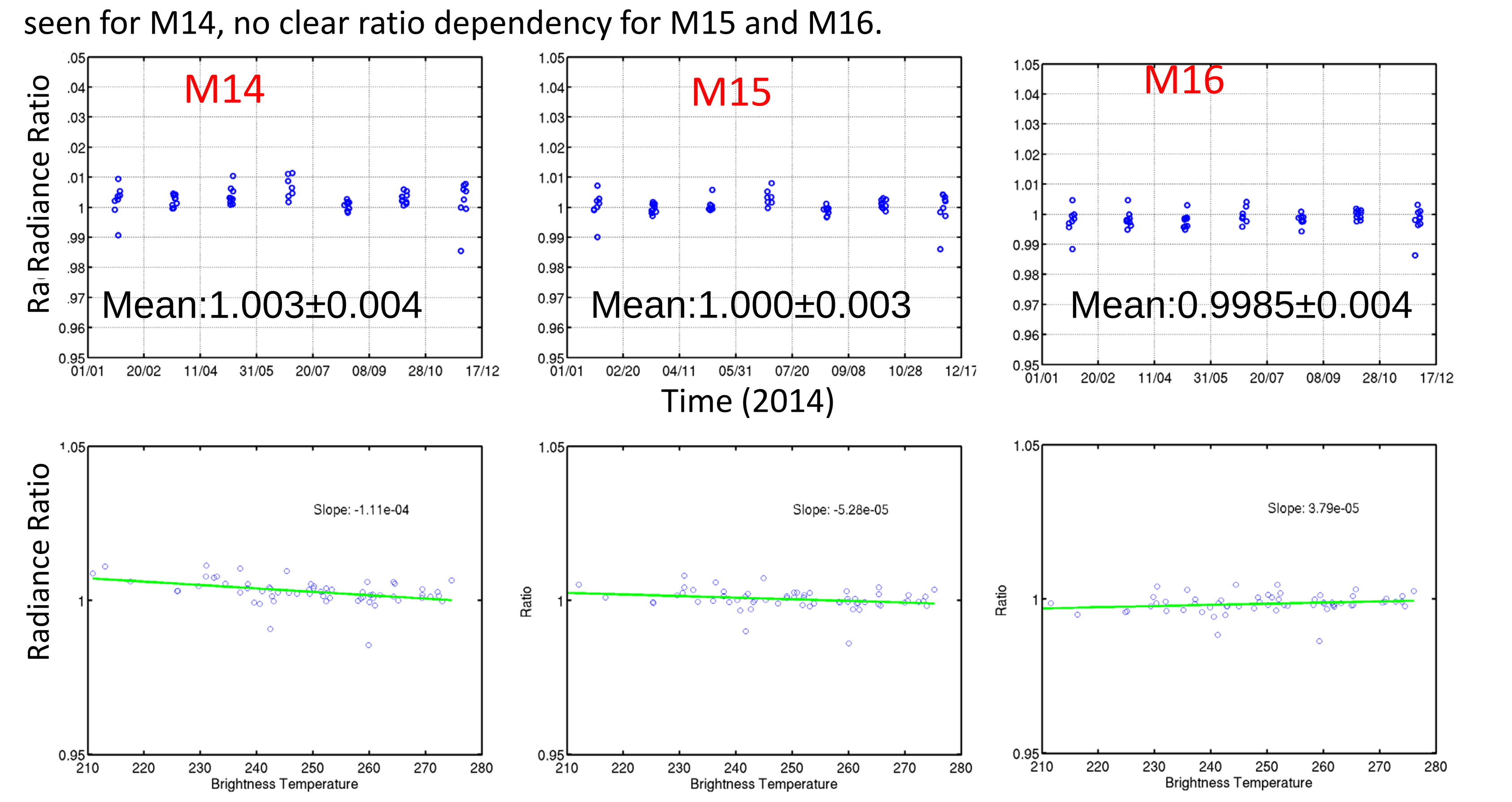

Summary:

- Both IASI and GoSAT FTS can be used to compare with the VIIRS M14-16, especially for M14 for which CrIS does not have coverage.
- For comparison between FTS and VIIRS, the brightness temperature of FTS has a higher bias of 0.54k for M14, 0.50K for M15 and 0.46K for M16.
- For comparison between IASI and VIIRS, the brightness temperature of IASI has a bias of 0.10K for M14,0.02K for M15 and -0.07K for M16.
- The higher bias between FTS and VIIRS may be due to the inclusion of FOVs within 5° scan angle of VIIRS since FTS has very low number of FOVs in each swath.

Acknowledgement:

The GoSAT/FTS dataset is from http://data.gosat.nies.go.jp/GosatUserInterfaceGateway/ guig/GuigPage/ open.do. The VIIRS/IASI data are from http://peate.ssec.wisc.edu/flo/search. This project is funded by NOAA/NEDIS/STAR.

Dark OMPS Generator Script (DOGS) for the Ozone Mapping and Profiler Suite (OMPS) Dark Table Production

Kristina Sprietzer[1] , Valerie Mikles[1], Bigyani Das[1], Walter Wolf[2], Marina Tsidulko[1], Weizhong Chen[1], Yunhui Zhao[1], Michael Wilson[1], Vipuli Dharmawardane[1], Qiang Zhao[1]

[1]IMSG, [2]NOAA/NESDIS/STAR

Summary

The Dark OMPS Generator Script (DOGS) is a Perl wrapper developed by the NOAA/NESDIS/STAR Algorithm Integration Team (AIT) to facilitate the Ozone Mapping and Profiler Suite (OMPS) Dark Table production process. Weekly Dark Table updates are important for correct radiance values and accuracy of other downstream ozone operational products which use either the OMPS Nadir Profiler (NP) or OMPS Nadir Mapper (NM) data.

What is DOGS?

DOGS is a wrapper script to run NASA program generated executables (PGEs). The wrapper script performs these major functions:

- Input and ancillary data are gathered and linked into processing directories.
- Program control files (PCF) are generated based on date.
- Environmental variables are sourced and setup.
- Output data are copied to directories specified by the user.

Purpose

Currently, Dark OMPS Tables are generated manually on the NASA PEATE system on a weekly basis. DOGS will automate the table production and allow the process to transition to NOAA's Government Resources for Algorithm Verification, Independent Test and Evaluation (GRAVITE) operational system.

STAR AIT

STAR AIT provides expertise on integration of JPSS algorithms into operational systems and performs the following tasks:

- Code Testing and Integration in Algorithm Development Library (ADL)
- Communication with Science Teams and DPES,
- Troubleshooting, Change Request Submission, Consultancy to Science Teams and DPES
- Facilitation of Lifecycle Reviews

Input Output Data Flow

Below is the process flow diagram showing the creation and organization directories needed to run DOGS and how input and output data are linked in the directory structures. This diagram is a visual aid to users of DOGS to understand how the different directories listed in their user configuration files are used.

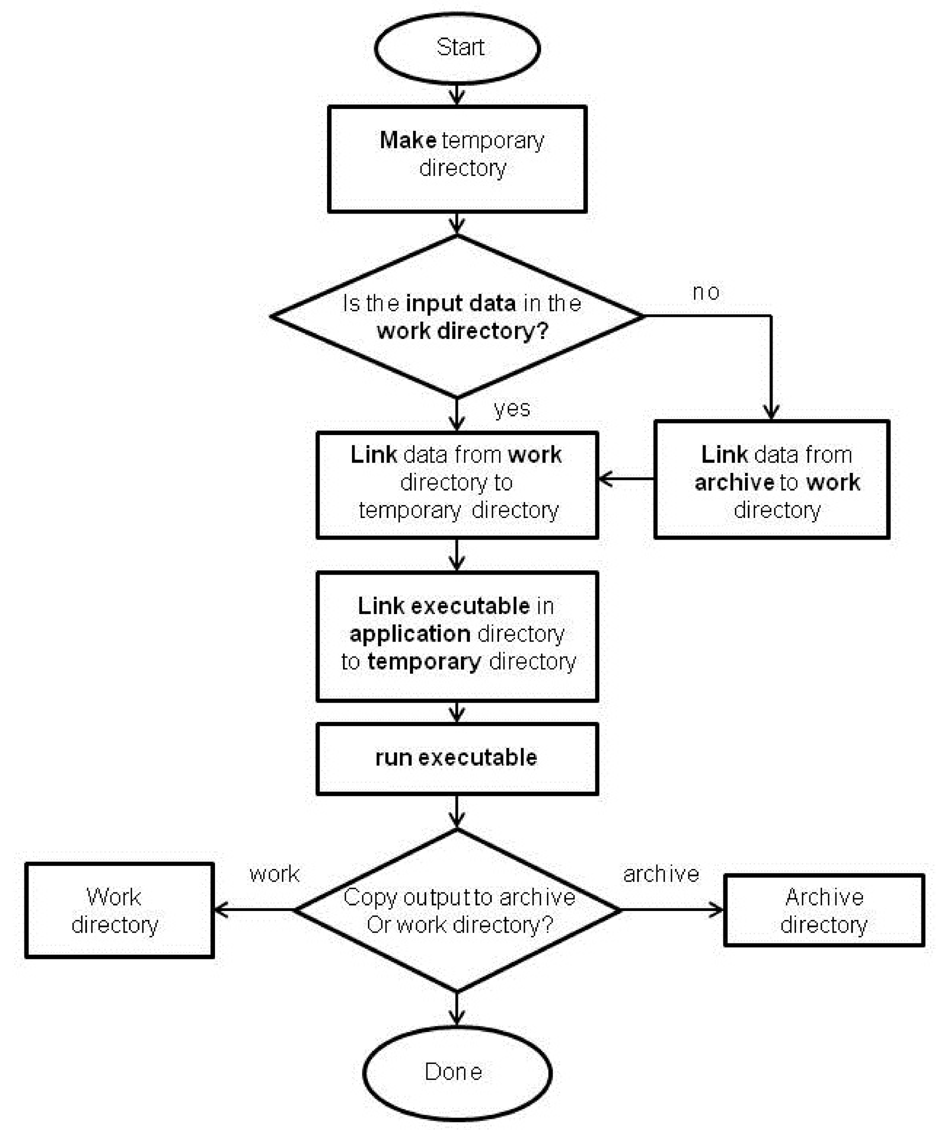

Wrapper Shell Script

GRAVITE_transition_dark_OMPS_processing.sh

This is a flow diagram of **the main executable** that creates the OMPS dark tables. Users only need to type this one executable command to generate the OMPS dark tables. This executable shell script sets up environmental variables and executes the Perl script shown on the right column of this poster.

This diagram shows how the program uses the file **user_list.list** which contains multiple **configuration files**.

This flow chart uses the example that each configuration file is dependent on date. The configuration file actually has many parameters, some of which are: date, output directories, and PGEs.

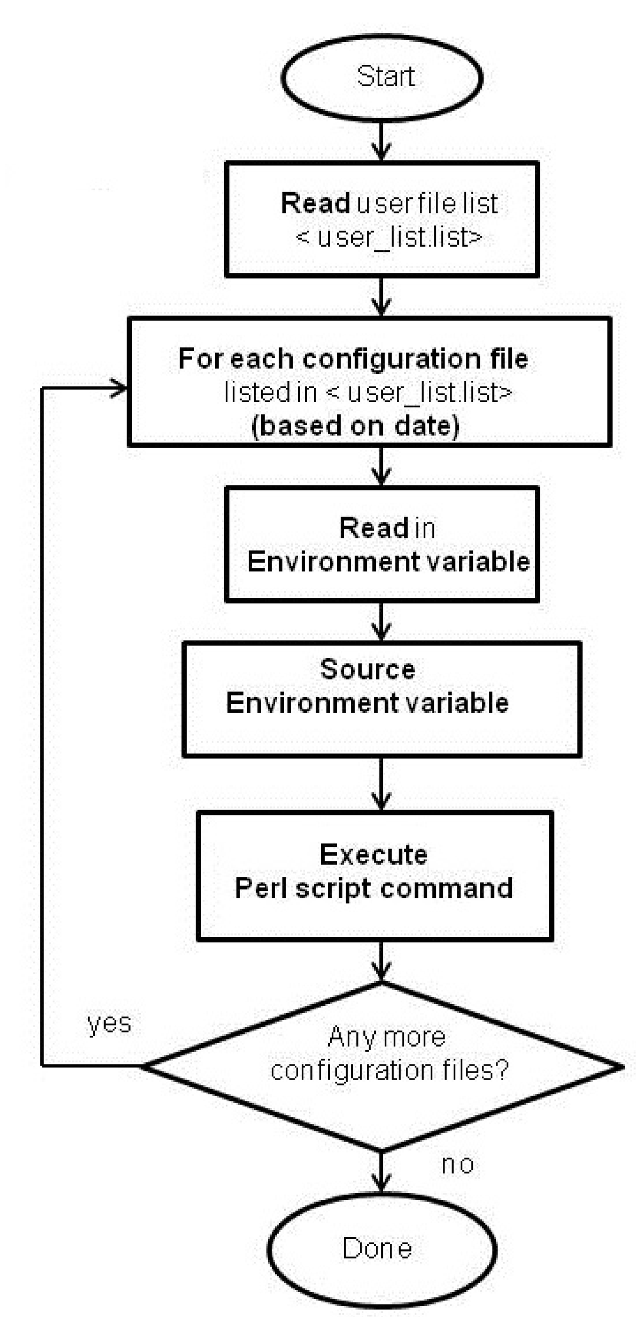

Perl Script

dark_OMPS_setup_and_execute_scripts.pl

This is the script that runs the PGEs. Based on parameters listed in the user configuration file (user_config.cfg), this script will set up input, execute PGEs, and copy output files to the appropriate directories.

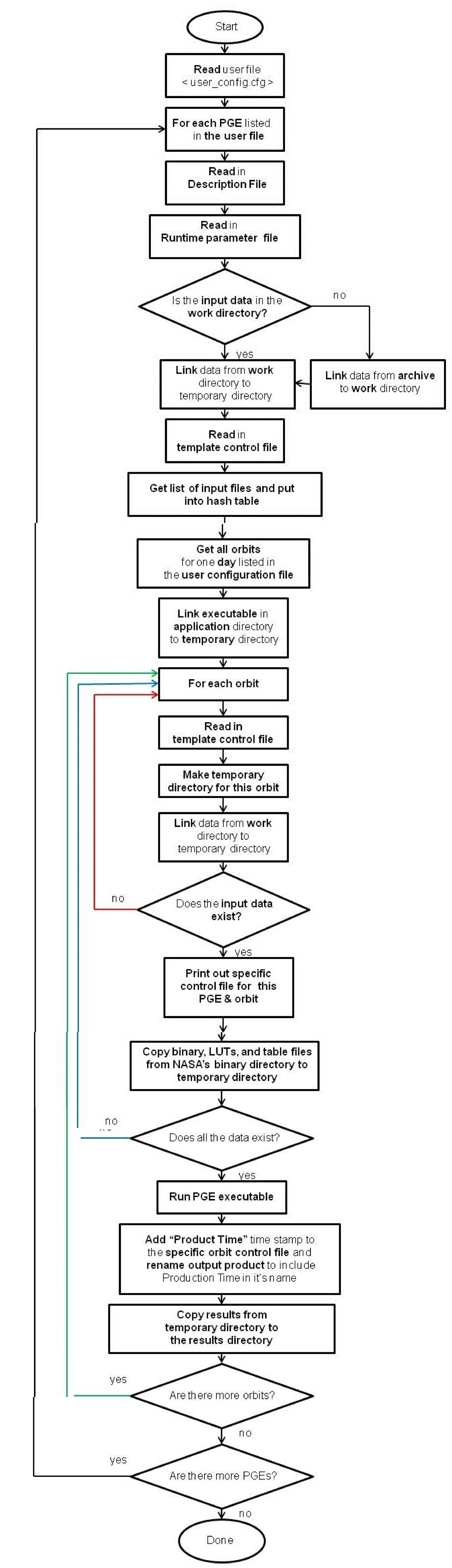

STAR Algorithm Integration Team: Configuration Management

Yunhui Zhao[1], Bigyani Das[1], Valerie Mikles[1], Weizhong Chen[1], Marina Tsidulko[1], Kristina Sprietzer[1], Qiang Zhao[1], Vipuli Dharmawardane[1], Xingpin Liu[1], Walter Wolf[2], Lihang Zhou[2]

[1]IMSG, College Park, MD 20740, USA; [2]NOAA/NESDIS/STAR, College Park, MD 20740 USA

Overview

Configuration Management supports routine algorithms integration work for the STAR Algorithm Integration Team (AIT) by identifying, controlling, maintaining and verifying all relevant versions of Configuration Items (CIs).

STAR AIT brings technical expertise and support to product algorithms, specifically in testing and validating science algorithms in the Algorithm Development Library (ADL) environment. STAR AIT assists JPSS science teams in implementing algorithm changes.

STAR AIT utilizes CM using IBM Rational ClearCase and ClearQuest and adopts ClearCase Unified Change Management (UCM) approach for JPSS related projects. Naming conventions are employed for the configuration identification process of ClearCase Streams, Views and Baselines. Streams are used to enable parallel development in projects. With appropriate branching strategy, developers from both AIT and science teams are able to create private development streams to access projects associated software, data and documentation. For science teams without access to ClearCase, AIT assists to integrate all corresponding algorithms updates into ClearCase and verify the changes. AIT is also responsible for design, development and implementation of the tools associated with tracking CIs and defining the change process.

Configuration Item and Identification

Configuration Items (CIs) are aggregations of data documentation, software and hardware that are designated for configuration management. CIs provide visibility during the lifecycle phases and are supported by the CM system. Items subject to configuration control within JPSS related projects include:

- ADL software
- IDPS Algorithm packages
- Science Teams Delivered Algorithms and Updates
- Acquired software (e.g. COTS)
- LUTs
- AIT Scripts (chain run scripts, CM related scripts, etc.)
- Tools (e.g. compilers, libraries)
- AIT Documents
- JPSS ATBDs

STAR AIT CM has the responsibility for identifying and selecting which elements and components can become CIs. Configuration Identification consist of setting and maintaining baselines that define the CIs at any point in time. Depending on the development lifecycle phase, different baselines are progressively established.

Ongoing Projects

JPSS ADL is created for the code testing and algorithm updates integration/validation within ADL3.x and ADL4.x environments.

JPSS ADL BLK2 is created for the code testing and algorithm updates integration/validation within ADL5.x environments.

NUCAPS is created for the code testing and algorithm updates integration/validation within NOAA Unique CrIS ATMS Processing System (NUCAPS).

JPSS ATBD is created for the CM of transferred JPSS ATBDs and the ATBD updates afterwards.

Branching Strategy for JPSS ADL project

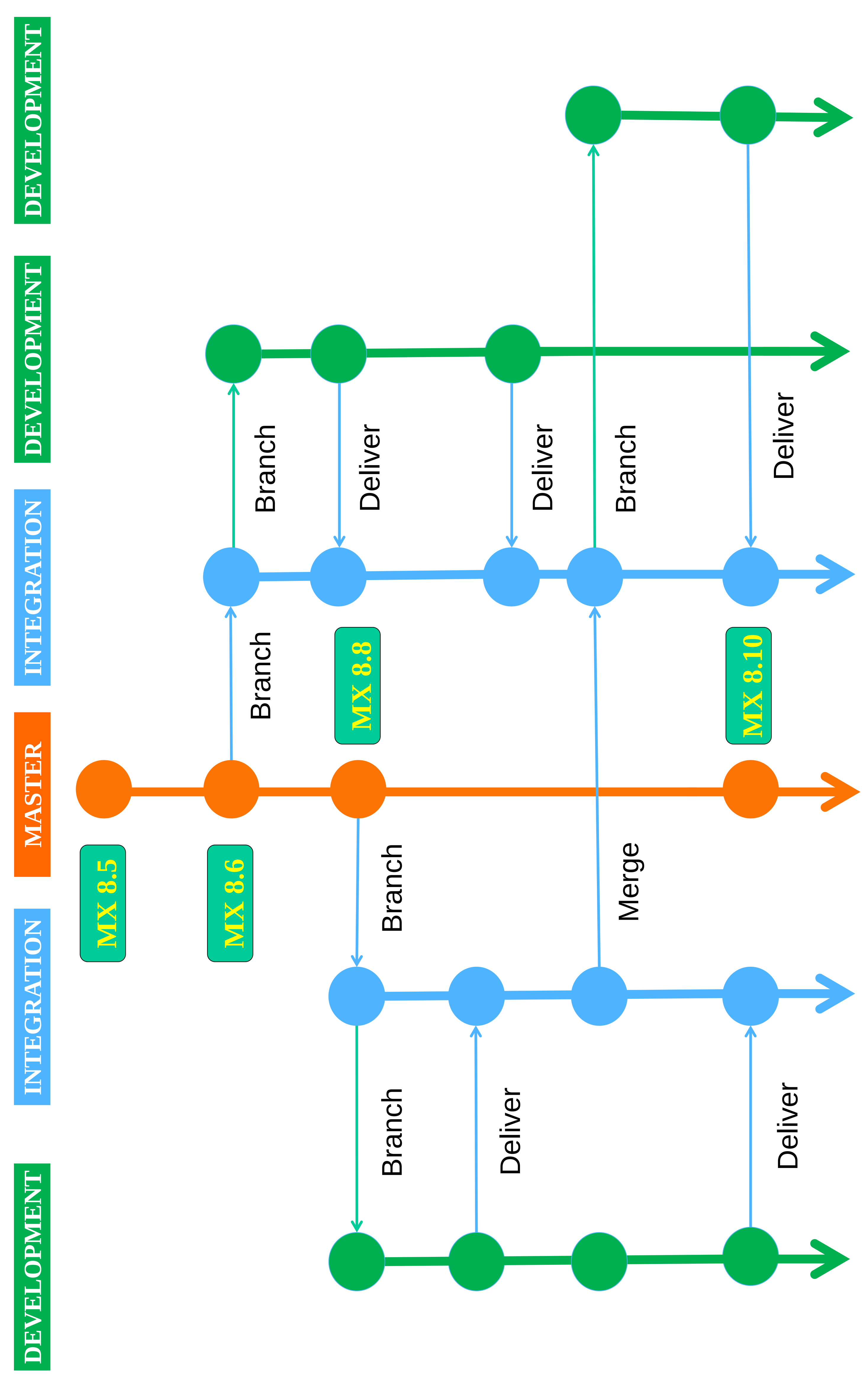

STAR AIT CM defines three different types of branches for project JPSS ADL:

The **MASTER** branch (ADL_MAJOR_INT stream in ClearCase UCM project) is used to reserve the operational code (MX Builds).

The **INTEGRATION** branch (ADL##_MX##_DEV_INT stream) is the integration branch used by developer from AIT or science teams to deliver their changes to or get other developers updates from.

The **DEVELOPMENT** branch is created by developers to implement updates, on which AIT developers can test and validate the algorithm updates.

Configuration Control

The monitoring of a change request from open to close is performed through the configuration control process. IBM Rational ClearQuest is used to initiate, track and report all STAR AIT change requests. A change request will be entered by generating one of the following forms in ClearQuest.

Development: a form used to propose a configuration change for development or enhancement. The change may be algorithm updates, LUT updates or AIT Scripts updates, etc.

Defect: a form used to record bugs and their resolutions. A defect kind change request can't be closed without the resolution state changed to "Fixed".

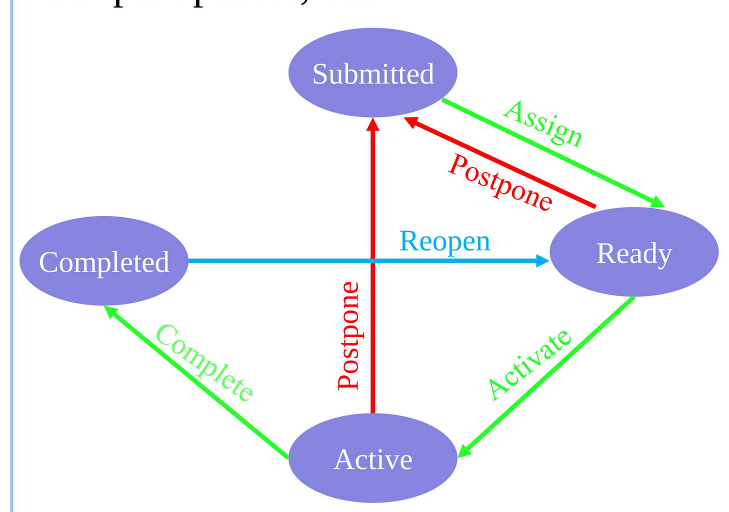

State map of BaseCMActivity

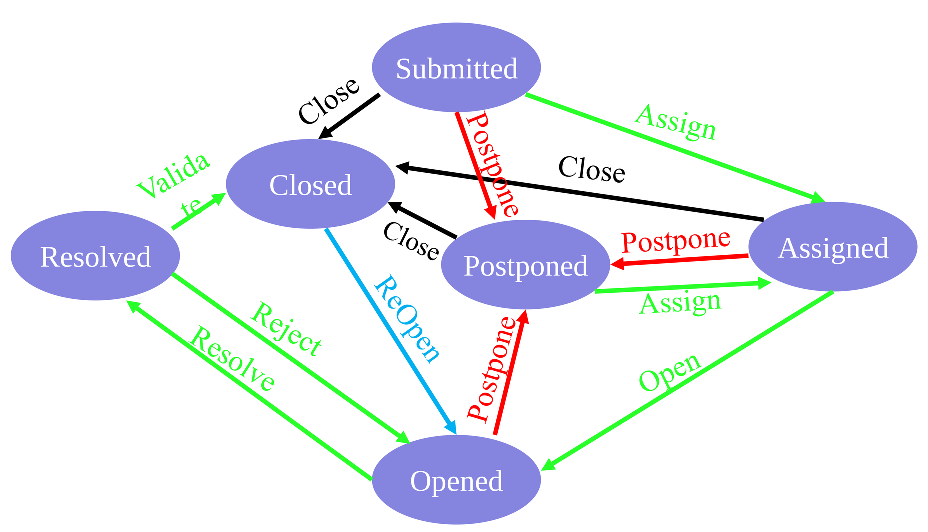

State map of Defect

Configuration Status Accounting is enabled to provides visibility into the states of activities and provides traceability for all changes of an evolving CI throughout the system lifecycle.

Configuration Management for JPSS ATBD

With the transition of JPSS ATBD to STAR, AIT CM is responsible to perform the configuration and change control through the ATBD documents development lifecycle after the transfer. All the transferred JPSS ATBDs (both WORD and PDF formats) are selected as CIs and labeled with appropriate baselines to establish revision history and maintain a definitive basis for control and status accounting.

STAR JPSS ATBD Naming Convention:

<Document ID>_<Mission ID>_<Satellite ID>_< Index>_JPSS_ATBD_<Product Name>_<Revision>

Document ID : STAR Document CM ID (distinguish document types)
Mission ID : Mission ID (distinguish different missions such as SNPP, J1, etc.)
Satellite ID : Satellite ID (distinguish different satellites)
Index : ATBD index (unique index for each product)
Product Name : Algorithm name
Revision : ATBD revision ID (distinguish different revision stages)

AIT CM Process

Once the ATBD updates are approved by Algorithm Engineering Review Board (AERB), a formal baseline will be established by STAR JPSS QA. The PDF format of the latest ATBD will be synchronized to the corresponding directory on STAR JPSS web server so the up-to-date content will be available immediately online.

Future Project and Planning

- STAR AIT is making CM plan for JPSS Cal/Val Maturity Documents.

Role of STAR Algorithm Integration Team (AIT) in the Algorithm Change Management Process for the JPSS Mission

Bigyani Das[1], Marina Tsidulko[1], Weizhong Chen[1], Qiang Zhao[1], Vipuli Dharmawardane[1], Valerie Mikles[1], Kristina Sprietzer[1], Yunhui Zhao[1], Michael Wilson[1], Walter Wolf[2]

[1]IMSG, Rockville, MD 20852, USA

[2]NOAA/NESDIS/STAR, College Park, MD 20740, USA

Abstract

The algorithm change management process is an important component towards the success of any satellite mission. For the Joint Polar Satellite System (JPSS) mission, this process becomes more significant as it involves management from two organizations (NOAA and NASA) and their associated organizational procedures for software standards and documentation standards. STAR's algorithm integration team (AIT) plays a key role in the algorithm change management process by contributing to algorithm integration, testing, evaluation, communication, documentation and life cycle reviews. In this presentation we describe in detail the contributions by STAR AIT in the algorithm change management process for the success of JPSS mission. We describe our current contributions for improving algorithms for both the Suomi NPP mission (launched October 28, 2011) and the upcoming JPSS 1 mission (planned for launch in 2017). We also discuss the procedures we follow for submitting algorithm change request packages to DPES and our interactions with various teams prior to approval by the AERB.

STAR AIT

STAR AIT provides expertise on integration of JPSS algorithms into operational systems and performs the following tasks:

- Code Testing in Algorithm Development Library (ADL) Framework
- Communication with Science Teams and Data Product and Engineering Services (DPES)
- Troubleshooting
- Change Request Submission
- Attending Team Meetings
- Reviewing Algorithm Theoretical Basis Documents (ATBD), Operational Algorithm Description (OAD) and other documents
- Consultancy to Science Teams
- Emulation of Various Operational Scenarios
- Code Analysis and Result Analysis
- Facilitation of Life Cycle Reviews

ADL Framework

- ADL is the Test System - Developed by Raytheon
- ADL mimics the Operational Interface Data Processing Segment (IDPS)
- ADL provides a Diagnostic Framework
- ADL provides one system to implement and test all the algorithms
- I-P-O Model (Input-Processing-Output)

STAR AIT Point of Contact (POC) for Different Algorithms

Algorithm	POC	Backup POCs
CrIS SDR	Vipuli Dharmawardane	Bigyani Das
ATMS SDR	Vipuli Dharmawardane	Bigyani Das
OMPS SDR – NM & NP	Bigyani Das	Vipuli Dharmawardane
OMPS EDR – NM & NP	Bigyani Das	Vipuli Dharmawardane
OMPS CAL SDR - DARKS	Bigyani Das	Weizhong Chen, Kristina Sprietzer
VIIRS SDR	Weizhong Chen	Qiang Zhao, Bigyani Das
VIIRS EDR - Cryosphere	Marina Tsidulko	Bigyani Das
VIIRS EDR - Imagery	Marina Tsidulko	Weizhong Chen
VIIRS EDR - AF	Marina Tsidulko	Weizhong Chen
VIIRS EDR – NDVI	Qiang Zhao	Bigyani Das
VIIRS EDR – Surface Reflectance	Qiang Zhao	Marina Tsidulko
VIIRS EDR – Cloud Mask	Weizhong Chen	Ruiyue Chen
VIIRS EDR – Cloud Products	Weizhong Chen	Ruiyue Chen
VIIRS EDR - Aerosol	Bigyani Das	Weizhong Chen
VIIRS EDR - LAND	Qiang Zhao	Marina Tsidulko
Requirements, Reviews, Quality Control	Valerie Mikles	Algorithm POCs
Documents	Valerie Mikles	Algorithm POCs
Scripts, Testing	Kristina Sprietzer	Algorithm POCs
Configuration Management	Yunhui Zhao	Algorithm POCs
CrIS, ATMS EDR - NUCAPS	Mike Wilson	Letitia Soulliard
Chain Runs	Weizhong Chen	Algorithm POCs
General Questions	Bigyani Das	Algorithm POCs
Management Meetings	Valerie Mikles	Bigyani Das
Software Installation/Maintenance	Weizhong Chen	Algorithm POCs

Algorithm Change Process

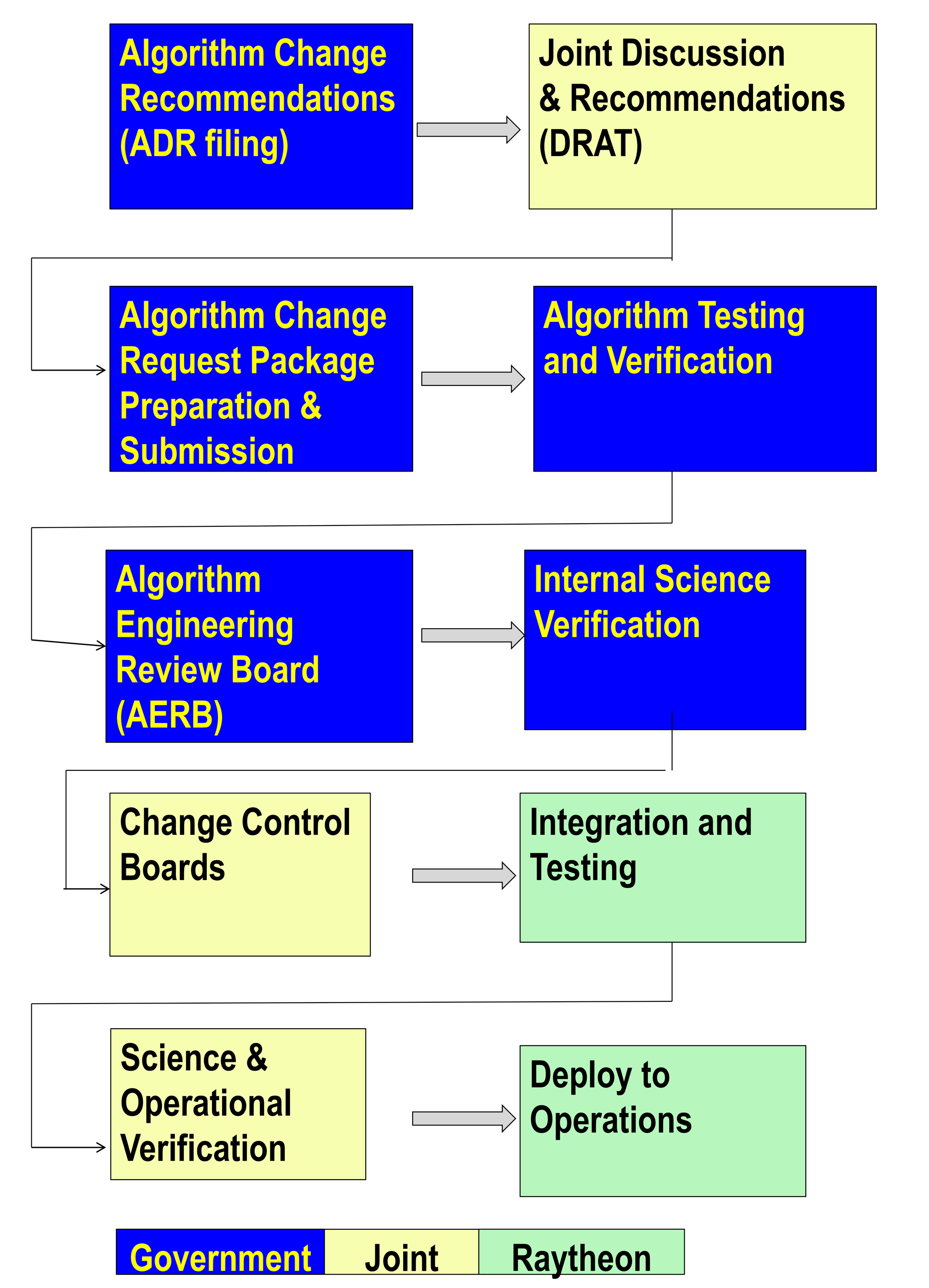

AIT Role

ADR Filing: Usually Algorithm Discrepancy Reports are filed by the scientists. At times the algorithm JAM or AIT POC files the ADR.

DRAT: The DRAT discussions are held to discuss the ADR and solution ideas. AIT POC participates in DRAT discussions.

TIM (Technical Interchange Meetings): Depending on the decision of the science team members, a TIM might be organized by the algorithm JAM. STAR AIT participates in TIM .

Algorithm Change Request Package Preparation and Submission: AIT's major contribution is focused on this task. This task includes testing, integration, document preparation, adding updates, preparing change request package and submitting to DPES.

DPES Testing: After AIT delivers the change request package, the testing and verification is being done by DPES and AIT is involved in this task by guiding the DPES in case of any discrepancy in the results, and supporting DPES with data and information when required.

AERB Review: This review is held to discuss and verify that the proposed solution for the respective discrepancy is being tested and verified and the results support that. AIT participates in the review.

Others: After AERB completes the review, AIT in general is out of the loop. However, AIT participates on occasions in "Science and Operational Verification" phase before the final deployment to operations.

Document Review and AIT

Document	Description	Review Board	Maintained By	STAR AIT
ATBD	Description of Science Theory	AERB	Science Teams	Currently ATBD changes are submitted by AIT
OAD	Description of Implementation of ATBD	AERB	CGS Contractor	OAD changes are communicated by AIT
AS Vol1 – SRS	Performance Requirements	Ground ERB	Ground Systems Engineering	
AS Vol2 Data Dictionary	Data Format for JPSS	Ground ERB	Ground System Engineering	AIT has been asked to make changes
AS Vol 3 Ref to OAD	Refers to OAD	Ground ERB	Ground System Engineering	
AS Vol 4 Parameter File	Quality Flag and Fill Condition Requirements	AERB	DPA	AIT has been asked to make changes
CDFCB (for S-NPP)	Data Format for S-NPP	Ground ERB	CGS Contractor	AIT has been asked to contribute

AIT Integration Process Flow

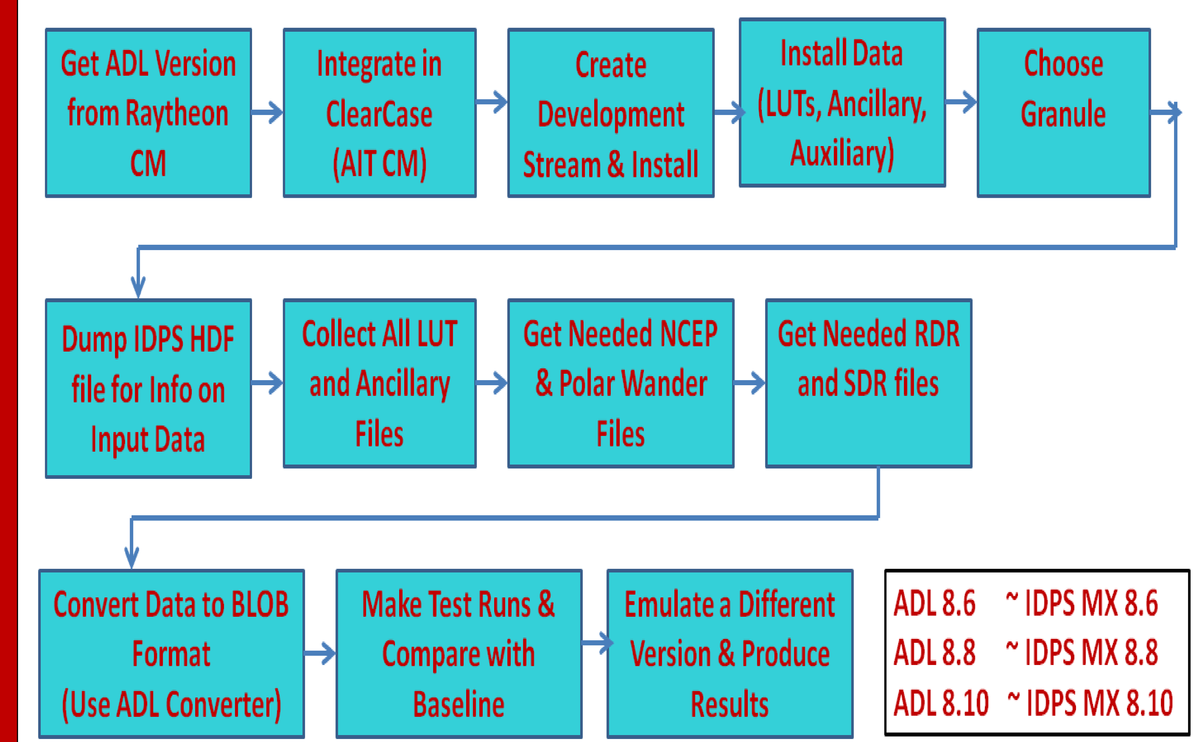

Contents of the Delivered Algorithm Package (DAP)

The Delivered Algorithm Package contains the following:

Original Code
Changed Code
Original LUT
Changed LUT
Baseline Results
Updated Results
Needed Input Tables
Ancillary Data
DPES Forms
Delivery Document with Test Instructions
Redlined ATBD (if needed)
Redlined OAD (if needed)
CDFCB Changes (if needed)
SRS Data Dictionary Document (if needed)
Other supplementary documents as needed

Ref: 474-00058_JPSS-Algorithm-Change-Mgmt-Plan_B.pdf

Example Contributions to S-NPP Algorithms

- OMPS NP V8 Pro Algorithm
- OMPC TC V8 Algorithm
- Aerosol EDR
- Land surface albedo LUT updating
- Adjust Quality Flag for Thin Cirrus in Land Surface Temperature (LST) and Update LUT
- Add Quality Check for Active Fire
- Updated PCT for CrIS SDR
- Updated PCT for ATMS SDR
- Equation Modification for Sea Surface Temperature and Evaluating Downstream Impact
- Roll Back LST LUT from Provisional to Beta Version
- OMPS Cal SDR Dark Table Creation
- VIIRS Surface Reflectance Algorithm Updates
- New Rain Algorithm for CrIMSS (Cross Track Infrared and Microwave Sounder Suite)
- Wavelength Shift and New Ozone Mixing Fraction for OMPS
- Implementing NOAA Global Multi-sensor Automated Snow/Ice Map (GMASI) Tile

Example Contributions to J1 Algorithms

- OMPS NM SDR Phase 1 and 2 J1 Uppers Deliveries with algorithm updates for de-aggregation and decompression criteria
- OMPS NP SDR J1-Uppers Package
- VIIRS NDVI Package
- VIIRS SDR Package
- VIIRS GEO Package
- CrIS SDR Package for Full Resolution and Normal Resolution Processing Capabilities
- CrIS SDR Package to correct Fringe Count Error
- VIIRS Active Fire DAP to NDE

Abbreviations

AS: Algorithm Specification
ATMS: Advanced Technology Microwave Sounder
CrIS: Cross-track Infrared Sounder
DRAT: Discrepancy Report Action Team
EDR: Environmental Data Record
JAM: JPSS Algorithm Manager
OMPS: Ozone Mapping and Profiler Suite
SDR: Sensor Data Record
SRS: Software Requirement Specification
VIIRS: Visible/Infrared Imager Radiometer Suite

STAR JPSS 2015 Annual Science Team Meeting – August 24-28, 2015, NCWCP, College Park, Maryland 20740

Corresponding Author: bigyani.das@noaa.gov

STAR Algorithm Integration Team

Tools, Processes, and Milestones

I.M. Systems Group, Inc.

Valerie Mikles, Bigyani Das, Walter Wolf, Kristina Sprietzer, Marina Tsidulko, Weizhong Chen, Qiang Zhao, Vipuli Dharmawardane, Yunhui Zhao

J1- Readiness

The JPSS Algorithm Integration Team (AIT) brings technical expertise and support to product algorithms, specifically in testing and validating science algorithms in the Algorithm Development Library (ADL) environment.

What we do:
- Assist teams with code updates, testing, and deliveries
- Provide technical support and expertise to teams
- Provide avenue for effective configuration management
- Facilitate a structured test and review process for new algorithms

We have developed a variety of in-house software for organizing, managing, and transitioning product algorithms. Additionally, we are taking leadership in the process of enhancing algorithms to meet upgraded requirements for J-1. Our involvement in the development and review process, in addition to our expertise in integrating the evolving algorithms into ADL, will make it possible to plug the new algorithms into the operational system with greater efficiency and ease.

Integration Specialists

AIT has five integration specialists each assigned to specific Sensor Data Record (SDR) and Environmental Data Record (EDR) teams based on expertise. Integration specialists:

- Interact directly with algorithm teams during development, testing, and integration
- Attend meetings with science teams to keep apprised of algorithm status
- Provide test results to algorithm team
- Provide chain run test results to all affected teams
- Prepare and deliver algorithm packages
- Maintain support through review and integration process

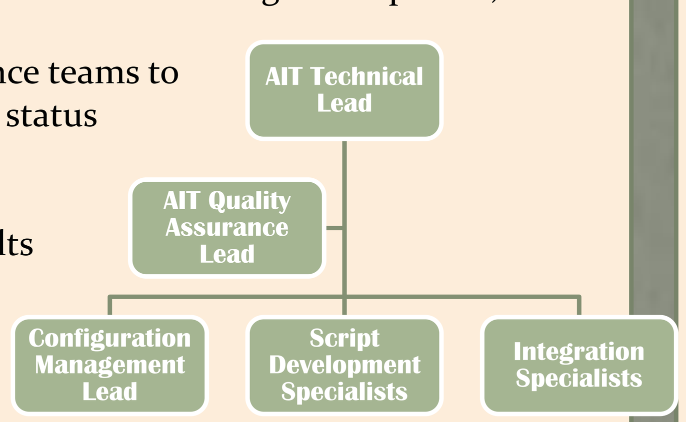

Quality Assurance

STAR AIT in conjunction with JPSS STAR Management (J-STAR) has developed a Quality Assurance Plan that describes the QA procedures for the STAR JPSS project. The AIT QA Lead is responsible for maintaining situational awareness of the JPSS project as a whole and coordinating with management and oversight teams.

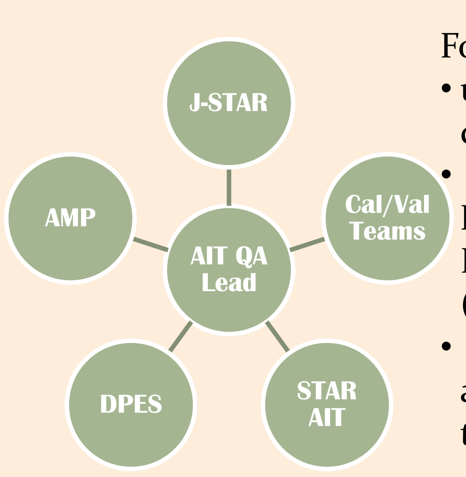

For QA purposes, AIT:
- uses Clearcase/Clearquest for algorithm configuration management
- complies with the Algorithm Change Management procedures put forth by Data Products Engineering & Services (DPES)
- assists algorithm teams in maintaining accurate and up-to-date documentation throughout the development process

J1 Algorithm Review Milestones

STAR AIT coordinates with science teams to present algorithm reviews in keeping with the SPSRB process. Algorithm Reviews have been completed for all major algorithm changes for J1. Completed review dates are listed in the table below. These algorithm changes include:
- Addition of Top-of-Canopy NDVI output to the Vegetation Index algorithm.
- Addition of high-resolution processing capabilities for CrIS SDR algorithm.
- Addition of high-resolution processing capabilities for the OMPS NP and NTC algorithm.
- Addition of the Fire Radiative Process and Fire Map to the Active Fire algorithm. Transition of algorithm to the NDE operational system.

Algorithm	Critical Design Review	Test Readiness Review	Algorithm Readiness Review
TOC NDVI EDR	5/22/14	11/6/14	4/24/15
CrIS SDR	8/21/14	X	5/12/15
Active Fire EDR	12/2/14	X	6/18/15
OMPS NP & NTC SDR	10/29/14	X	9/15

Algorithm Review Process

New algorithms developed for J1 are subject to the STAR Enterprise Lifecycle Review Process (EPL)
- consistent with the Satellite Product and Services Review Board (SPSRB) review process
- adds value to product development
- generates standard documentation covering
  - Requirements and Risks
  - Algorithm Theoretical Basis
  - Implementation Plan
  - Software Architecture
  - Quality Assurance
- process tailored based on implementation timescale and development progress
- tailored reviews mitigate risk by eliminating overhead of preparing multiple reviews
- technical risk is low because Level 1 and Level 2 requirements are handled by a separate review board and are already developed

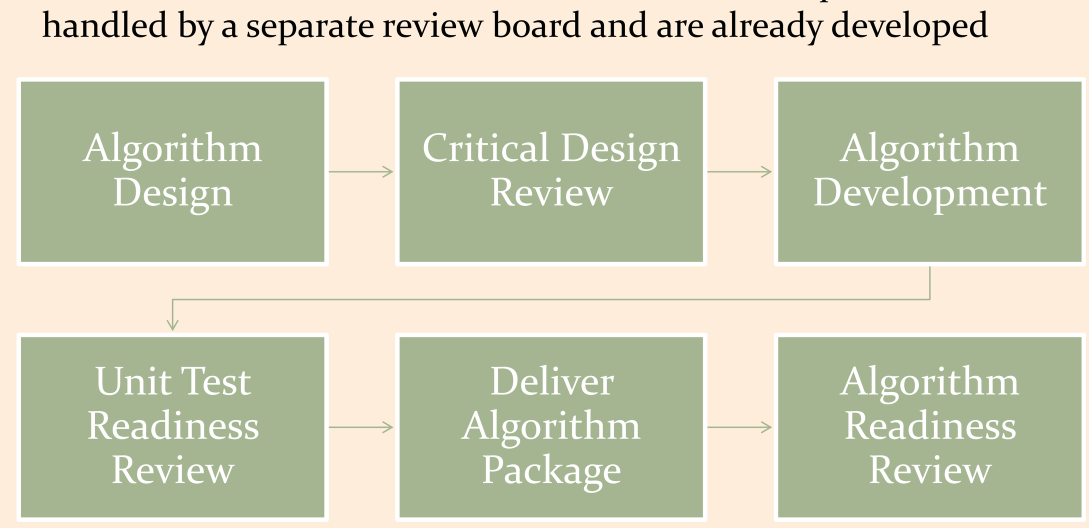

Requirements Tracking

- STAR AIT compiles Requirements Allocation Documents (RAD) for J1 Algorithms undergoing a review process.
- The RAD contains Level 3 and 4 requirements allocated to STAR.
- The RAD operates in parallel with the NASA Software Requirement Specification documents
- Requirements in the RAD are traced to Level 1 and Level 2 requirements documents
- The RAD is a standard deliverable and is made available at each review. Requirements and changes to requirements are discussed at each review.

Algorithm Change Process

The Algorithm Change Process is regulated to preserve the integrity and functionality of the operational system.

As we look toward J1 Readiness, many algorithm changes are not in response to discrepancies and errors in the code, but rather changing and updating the code to accommodate:
- New J1 Requirements
- The upgrade to the Block 2.0 operational system.

Algorithm upgrades follow the established change process documented in the Algorithm Change Management Plan. New algorithms (related to new J1 products) follow an additional review process prior to the submission of the change packaged to DPES.

File a Discrepancy Report
- Changes can be small or large
- Changes can be specific (e.g., this i+1 should be i+2) or general (e.g., the data for last Saturday is corrupted and I don't know what's going on)
- Changes can be against other teams (e.g., cloud mask is producing XYZ product for benefit of oceans team, but oceans team has no intention of using product in its delivered form)

DR Reviewed by DR Action Team
- The DRAT is an agent of the Algorithm Engineering Review Board. It is a discussion forum designed to vet issues and determine how to proceed.
- The DRAT will decide whether:
  - to schedule a Technical Interchange Meeting
  - ADL code is needed
  - test data is needed
  - the update affects requirements

Prepare Code Change Package
- STAR AIT is available to help at all stages of the development, testing, and submission process. Examples include:
  - integrating the algorithm into the current ADL build
  - running tests in ADL for both baseline and updated algorithm
  - troubleshooting code with the science team until the desired result is achieved
  - preparing a delivery package

Coordinate with DPES
- Once a delivery is made STAR AIT coordinates with DPES, responding to feedback during initial feasibility testing.
- STAR AIT continues to lend expertise both to DPES and science teams until the code change is approved by the AERB.

Recent DRs

STAR ASSISST regularly assists science teams with algorithm changes.
- We have generally worked on 30-40 DRs per FY.
- The current directive has emphasized KPPs. Most of our current work focuses on SDR algorithms and development and integration of J1 products. Past years have shown greater emphasis on Land, Aerosol, and Cryosphere EDRs.
- Integration and testing involves creating baseline and modified runs of test data. In cases for Cloud Mask and Aerosol changes, we diligently test the effect on downstream products using the Chainrun script.

The flow chart below shows an abbreviated version of the algorithm change process. AIT provides assistance to the science team's development of the product algorithms in the offline system. We will help science teams develop and integrate changes into ADL. We then aid in the submission process to DPES. When the updated operational algorithm is delivered, we can assist with merging the developing code with the new operational system.

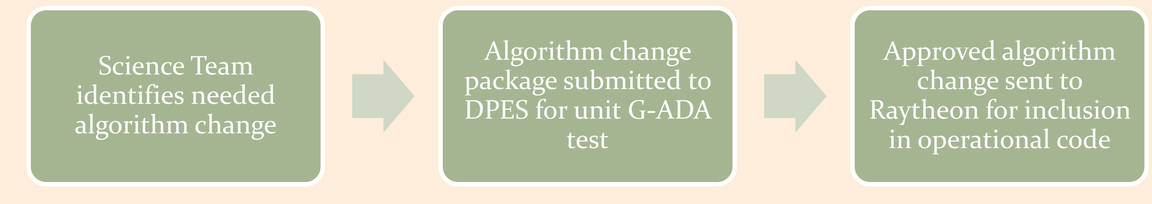

The table below shows a list of DRs we have worked on and/or submitted Algorithm Change Packages (ACP) for in the past fiscal year. ACP submission is an iterative process as we work with DPES to overcome the differences between the ADL and G-ADA systems.

Team	DRs	Summary of Work
Active Fires	7245	Implement J1 Upper – Integrate Fire Radiation Product and Fire Mask into code, delivery to NDE.
Aerosols	7723, 7786, 7787	Improve Aerosol algorithm Dust Model, Ephermeral Water, and Snow test products. Delivery to DPES.
ATMS	7879, 7941, 7954, 7966	Update PTCs, incorporate full radiance testing, perform integration and testing. Delivery to DPES.
Cloud Mask	7535, 7538	Integrate new Cloud Shadow calculation. Replace tiles with climatology input
Cloud Mask/ Aerosols	7437, 7438, 7408	Changes related to ephemeral water and cloud phase, integrated and tested in ADL.
CrIS SDR	7486, 7895, 7926, 4481	Implement J1 Upper - Modification of code for full spectral resolution.
Cryosphere	7791	Eliminate Ice surface Temperature algorithm dependency
OMPS EDR	4256	Improve OMPS NP Algorithm. Run baselines and tests on updated code.
OMPS SDR	7248, 7249, 7450, 7451, 7654, 7655, 7824, 7827, 7828, 7340, 7341, 7831	Implement J1 Upper - Modify wavelength scale, aggregation, and glueware features.
Surface Reflectance	7635, 7784, 7785, 7943	Update SRIP to handle changes in AOT input.
Vegetation Index	4376, 7216, 7697, 7039	Implement J1 Upper – Add TOC NDVI to the algorithm code.
VIIRS SDR	8036	Add new LUTs and RSB Autocal features.

AIT Tools

Chain run script

The Chain run script is a Perl script that automates the staging and processing of multiple JPSS SDR and EDR products. The tool, developed by STAR AIT facilitates efficient and consistent tests of interdependent algorithms.

Dark OMPS Generator Script (DOGS)

The Dark OMPS Generator Script (DOGS) is a Perl wrapper developed by the AIT to facilitate the OMPS Dark Table production process. Currently, Dark OMPS tables are generated by hand on the NASA PEATE system. DOGS will automate the table production and allow the process to transition to NOAA's GRAVITE system. Weekly dark table updates are important for correct radiance values and accuracy of other downstream ozone operational products which use either the OMPS Nadir Profiler (NP) or OMPS Nadir Mapper (NM).

SASQUATCH
Simplified And Streamlined QUality Assurance Through Coding Help

EPL Review documents include both Requirements Allocation Documents (RADs) and Requirements slides with identical content. Additionally, a spreadsheet is provided for review showing requirements tracing to Level 1 and Level 2 requirements. SASQUATCH is a perl script that reads requirements from a spreadsheet and generates both the RAD and Review slides, thus ensuring consistent content and formatting. EPL Review documents include a Review Item Disposition (RID) spreadsheet that tracks all risks and review items. For each review, the review items in the RID are presented. Building on the capability of SASQUATCH, Risk-QUATCH converts the RID spreadsheet into properly formatted presentation slides for the review.